nature neuroscience

Article

https://doi.org/10.1038/s41593-024-01724-1

A GnRH neuronal population in the olfactory bulb translates socially relevant odors into reproductive behavior in male mice

Received: 17 May 2023

Accepted: 3 July 2024

Published online: 2 August 2024



Laurine Decoster^{1,2,16}, Sara Trova © ^{1,2,14,16}, Stefano Zucca^{3,4}, Janice Bulk⁵, Ayden Gouveia⁵, Gaetan Ternier © ^{1,2}, Tori Lhomme^{1,2}, Amandine Legrand^{1,2}, Sarah Gallet © ^{1,2}, Ulrich Boehm © ⁶, Amanda Wyatt © ⁶, Vanessa Wahl © ⁶, Philipp Wartenberg ⁶, Erik Hrabovszky © ⁷, Gergely Rácz ⁸, Federico Luzzati^{3,4}, Giulia Nato ^{4,9}, Marco Fogli ^{3,4}, Paolo Peretto ^{3,4}, Sonja C. Schriever © ^{10,11}, Miriam Bernecker ^{10,11,12}, Paul T. Pfluger © ^{10,11,12}, Sophie M. Steculorum © ^{5,10,13}, Serena Bovetti ^{3,4}, Sowmyalakshmi Rasika © ^{1,2}, Vincent Prevot © ^{1,2}, Mauro S. B. Silva ^{1,2,15,16} & Paolo Giacobini © ^{1,2,16}

Hypothalamic gonadotropin-releasing hormone (GnRH) neurons regulate fertility and integrate hormonal status with environmental cues to ensure reproductive success. Here we show that GnRH neurons in the olfactory bulb (GnRH $^{\rm OB}$) of adult mice can mediate social recognition. Specifically, we show that GnRH $^{\rm OB}$ neurons extend neurites into the vomeronasal organ and olfactory epithelium and project to the median eminence. GnRH $^{\rm OB}$ neurons in males express vomeronasal and olfactory receptors, are activated by female odors and mediate gonadotropin release in response to female urine. Male preference for female odors required the presence and activation of GnRH $^{\rm OB}$ neurons, was impaired after genetic inhibition or ablation of these cells and relied on GnRH signaling in the posterodorsal medial amygdala. GnRH receptor expression in amygdala kisspeptin neurons appear to be required for GnRH $^{\rm OB}$ neurons' actions on male mounting behavior. Taken together, these results establish GnRH $^{\rm OB}$ neurons as regulating fertility, sex recognition and mating in male mice.

Successful reproduction relies on the integration of external and internal cues triggering appropriate behaviors and hormonal responses. In many animal species, the vomeronasal system mediates the detection of sex-specific and species-specific cues, called pheromones, involved in the control of social behaviors¹. Sensory neurons in the neuroepithelium of the vomeronasal organ (VNO) project to multiple glomeruli in the accessory olfactory bulb (AOB)^{2,3}. Mitral cells of the AOB in turn project to the medial amygdala (MeA), which is associated with sexual behavior in mammals⁴, including humans⁵, and to the bed nucleus of the stria terminalis, which contains specialized neurons governing key aspects of innate male sexual behavior⁶. It is now generally accepted

that the main olfactory system (MOS) plays an equally important role in the processing of pheromonal signals related to social attraction and recognition $^{7-9}$. These signals are detected by olfactory receptors located on ciliated olfactory sensory neurons in the main olfactory epithelium (MOE), which relay this information to the main olfactory bulb (MOB). Evidence from different species supports the role of the MOE in male preference for the opposite sex and mating initiation 8 . For instance, the targeted deletion of genes for the cyclic nucleotide-gated $\alpha 2$ channel (CNGA2, encoded by $Cnga2)^{10}$ or $G_{\rm olf}$ -activated adenylyl cyclase 3 (AC3, encoded by $Adcy3)^{11}$, which are expressed in the MOE but not in the VNO, disrupts the preference for female urine odors in

A full list of affiliations appears at the end of the paper. —e-mail: paolo.giacobini@inserm.fr

male mice and impairs male–female mating behavior, indicating that the MOS is essential for the initiation of pheromone-evoked mating behavior and preference for the opposite sex.

Gonadotropin-releasing hormone (GnRH) neurons originate in the olfactory placode, from which they migrate during early embryonic development toward the hypothalamus along axons that originate in the developing VNO¹². Hypothalamic GnRH neurons are pacemakers of reproduction, releasing GnRH in a rhythmic manner into the pituitary portal vasculature to regulate the synthesis and secretion of luteinizing hormone (LH) and follicle-stimulating hormone by the anterior pituitary gland¹³. In turn, LH and follicle-stimulating hormone control gonadal development and function and the production of sex steroid hormones.

The facilitation of sexual behaviors by pheromones has long been thought to be influenced by GnRH neurons since exposure to opposite-sex urine leads to a rapid LH surge in male and female rodents^{14,15}. In addition, seminal studies have shown that hypothalamic GnRH neurons receive signals from both nonsocial and social central olfactory pathways^{16,17}, and we have previously reported the presence of an extrahypothalamic population of GnRH neurons dispersed as a ring-like structure in the posterior part of each olfactory bulb (OB)¹⁸. Interestingly, both humans with Kallmann syndrome¹⁹ and GnRH-specific Dicer-deficient mice²⁰, in which GnRH neurons fail to secrete GnRH, also display olfactory impairment. Putting together these findings, it appears that GnRH neurons may link sexually relevant olfactory signals to neuroendocrine changes, which ultimately control reproductive success, through mechanisms that have yet to be elucidated.

Here, using several virogenetic approaches and genetic mouse models, we explored the occurrence, anatomy and connectivity of the population of olfactory bulb GnRH neurons (GnRH^{OB}), and its role in connecting olfactory and pheromonal cues with reproductive behavior.

Results

A significant proportion of GnRH cells is located in the OB

We coupled whole-mount immunolabeling with light-sheet imaging using iDISCO+technology (Extended Data Fig. 1a)^{18,21,22} on human postmortem OBs of men and women, and we observed that GnRH-positive cell bodies (Extended Data Fig. 1b) and fibers (Extended Data Fig. 1b) were present in the adult human OB and olfactory tubercle region. We then confirmed by whole-brain iDISCO+ immunolabeling and three-dimensional (3D)-reconstruction analysis of the GnRH^{OB} neuronal population the presence of GnRH neurons and fibers in the caudal region of the mouse OB (Fig. 1a), consistent with our previously reported results¹⁸. Depending on their location, these GnRH^{OB} neurons displayed heterogeneous morphologies. They mostly exhibited the classic bipolar shape of GnRH neurons in the granule cell layer and glomerular layer, a round shape in proximity to the olfactory nerve layer, and a multipolar shape in the mitral cell layer, from which long dendritic trees extended into the external plexiform layer (Fig. 1b). We found that the mouse GnRH^{OB} neuronal population consisted of about 200 neurons regardless of sex (Fig. 1c), representing $\sim\!20\%$ of the entire GnRH population in the mouse brain. In agreement with previous observations from our group 18 , the majority of GnRH OB neurons were located in the MOB in both males and females, with smaller populations within the AOB, the accessory olfactory nucleus (AON) and the ventral part of the tenia tecta, a component of the olfactory cortex (Fig. 1c). Further analyses in males showed that GnRH OB cell bodies were scattered across all layers of the MOB, with the great majority located in the olfactory nerve layer, glomerular layer and granule cell layer (Fig. 1d).

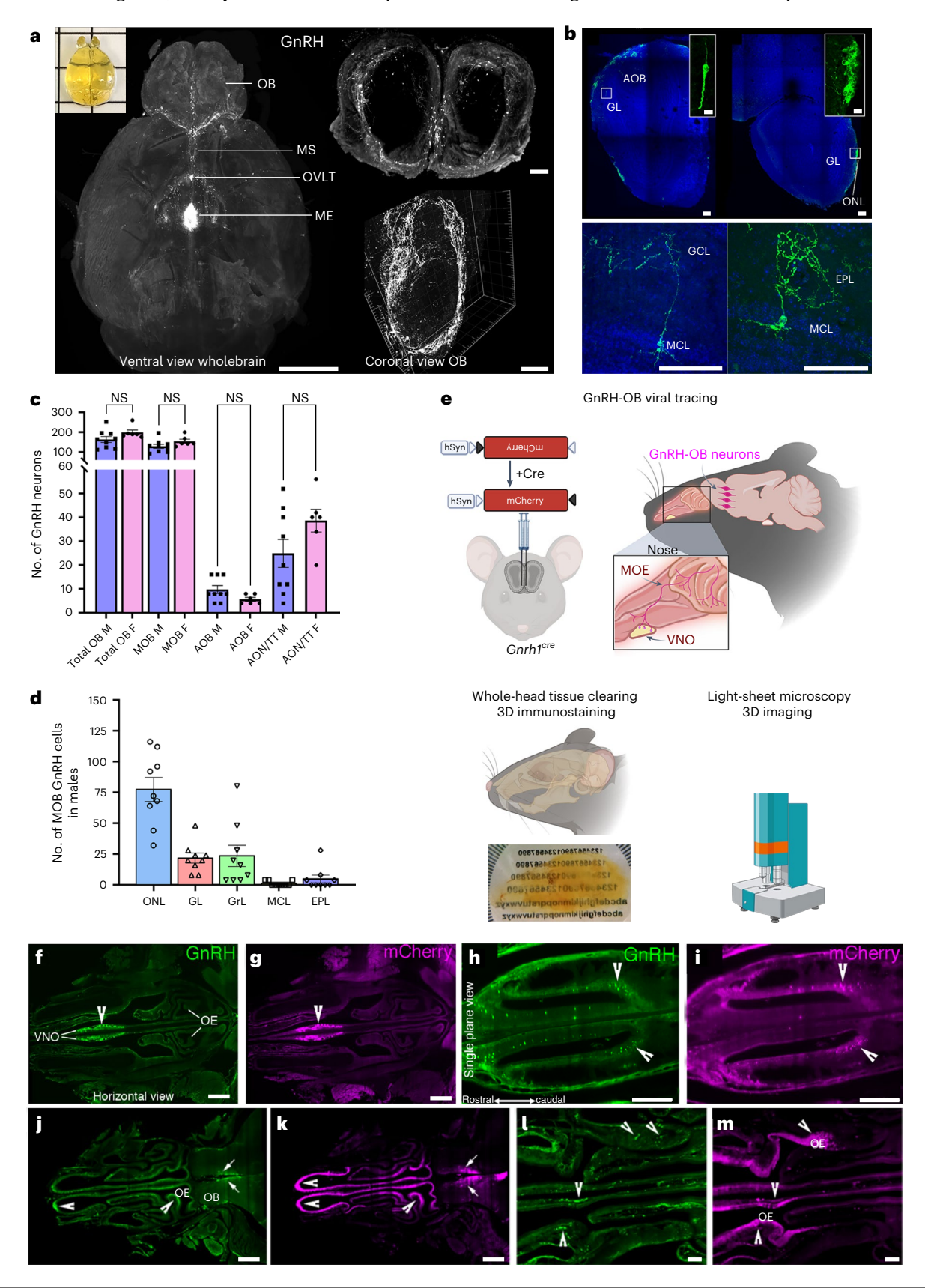
GnRH^{OB} cells project to olfactory and vomeronasal epithelia

We next investigated whether GnRH^{OB} neurons could sustain functional connections with olfactory structures. To address this question, we used iDISCO+ immunolabeling on entire decalcified adult mouse heads, in combination with viral tracing of GnRH^{OB} neuronal projections and volume imaging (Fig. 1e). Gnrh1^{cre/wt} male mice were injected with a Cre-dependent adeno-associated virus (AAV9) expressing mCherry under the control of the human synapsin (hSyn) promoter (Fig. 1e). We found that GnRH^{OB} neurons extend neurites into the VNO (Fig. 1f-i) and the MOE (Fig. 1j-m). Considering the anatomical connections between GnRH^{OB} neurons and the olfactory and pheromone-sensing structures, we next studied whether these neurons expressed receptors for olfactory and/or vomeronasal cues (Olfr and Vmnr genes). To this purpose, we performed single-nucleus RNA sequencing (snRNA-seq) on the male OBs. Of the 13,163 cells collected from the OBs of adult male mice (Extended Data Fig. 2a,b), we identified 54 Gnrh1-positive cells, corresponding to roughly 0.4% of the entire OB cell population (Extended Data Fig. 2c). Gnrh1-positive cells are not confined to a specific cluster but they are distributed across multiple clusters of the OB (Extended Data Fig. 2c). We generated heat maps showing the expression patterns of the top ten upregulated genes in Gnrh1-positive cells as compared to Gnrh1-negative cells (Extended Data Fig. 2d). Besides Gnrh1, the most highly enriched transcripts are a mixture of transcription factors (nuclear factor I/A, Nfia; AE binding protein 1, Aebp1), genes associated with neurite growth and/or cytoskeleton rearrangements (tetraspanin 9, Tspan9) and nuclear hormone receptors (RAR-related orphan receptor alpha, Rora). On examining our snRNA-seq dataset from Gnrh1-positive and Gnrh1-negative cells of the OB of male mice, we found the expression of several Olfr and Vmnr genes in the OB (Extended Data Fig. 2e.f). A fraction (2% to 12%) of GnRH^{OB} neurons express 30 olfactory receptor genes. Olfactory receptor family 11 subfamily L member 3 (Or1113, alias Olfr323) is the most abundant Olfr gene expressed by GnRH^{OB} neurons, detected in 12% of these cells but not in Gnrh1-negative cells (Extended Data Fig. 2g). Our investigation also revealed the presence of 11 Vmnr genes in GnRH^{OB} neurons (Extended Data Fig. 2f), with a predominant expression from the vomeronasal 2 receptor gene family. Vomeronasal 2, receptor 1, Vmn2r1, was expressed in 7% of GnRH^{OB} neurons and vomeronasal 2, receptor 2, Vmn2r2, in 5.6%, and Vmn2r87 in 5.6% (Extended Data Fig. 2f).

Fig. 1| A significant proportion of GnRH neurons is located in the OBs of mice and is connected with the OE and VNO. a, iDISCO+ and 3D imaging of an entire mouse brain (male) showing immunoreactive GnRH neurons and fibers in the OB (ventral view and frontal view), along the MS, the OVLT and reaching the ME; n=3, 12-16-week-old males. **b**, Representative confocal images (coronal sections) illustrating different morphologies of GnRH^{OB} neurons, performed in three biological replicates. **c**, Quantitative analysis of GnRH^{OB} neuronal distribution in the MOS and AOS in adult male and female mice (n=9, 16-20-week-old males; n=6, 16-week-old females). One-way analysis of variance (ANOVA) with Holm–Sidak's multiple-comparison test, 16, 160 male versus female 160 metronal distribution throughout different layers of the male MOB (160 metronal distribution throughout different layers of the male MOB (160 metronal workflow

We then isolated GnRH neurons from the OB and preoptic area (POA) of GnRH-green fluorescent protein (GFP) male mice²³ using fluorescence-activated cell sorting (FACS) and validated the expression of two *Olfr* and two *Vmnr* genes by quantitative PCR with reverse transcription (RT-qPCR) analysis in GFP-positive cells versus GFP-negative cells (Extended Data Fig. 3a,b). Finally, we validated the expression

of the two most frequent transcripts in GnRH^{OB} neurons, *Vmn2r1* and *Olfr323*, by single-molecule fluorescence in situ hybridization (smFISH), which confirmed the expression of *Vmn2r1* and *Olfr323*, respectively, in the basal layer of the adult mouse VNO (Extended Data Fig. 3c,d) and in the olfactory epithelium (OE; Extended Data Fig. 3e). In addition, in agreement with our snRNA-seq data, some *Gnrh1* neurons



located in the OB coexpressed Vmn2r1 and Olfr323 (Extended Data Fig. 3f-i), although the majority of GnRH neurons did not express these receptors (Extended Data Fig. 3j). Subsequently, we examined the transcript expression of mechanosensitive ion channels (Piezo1 and Piezo2) in GnRHOB neurons. This investigation was prompted by previous findings indicating Piezo2 channel expression in a subset of mouse mitral cells^{24,25}. In addition, a recent study demonstrated that pulsations of OB blood vessels induced by heartbeat can directly influence the neuronal activity of a subset of mitral cells through the activation of mechanosensitive channels²⁶, potentially in response to odors from the opposite sex. Our single-nucleus transcriptomic analysis indicated that *Piezo1* is expressed across the majority of OB cell clusters with the highest enrichment detected in the immune cells (Extended Data Fig. 3k.l). Piezo2 is highly expressed in periglomerular cells, mitral/ tufted cells, endothelial cells and oligodendrocytes (Extended Data Fig. 31). Further analysis showed *Piezo1* absence in *Gnrh1*-positive cells but presence in 1% of Gnrh1-negative cells, while Piezo2 was enriched in 5% of Gnrh1-positive cells (Extended Data Fig. 3m,n).

Together, these results suggest that $GnRH^{OB}$ neurons are both anatomically and molecularly equipped to sense social and nonsocial odors.

Male GnRH^{OB} neurons are activated by opposite-sex urine

Because the MOS plays an important role in sexual attraction⁸, we next asked whether GnRH^{OB} neurons of male mice responded to olfactory cues present in female urine by performing in vivo two-photon functional imaging of GnRH^{OB} neurons in males exposed to the urine of estrous females (Fig. 2a). Adult Gnrh1^{cre/wt} male mice were injected in the OB with Cre-dependent AAVs encoding the calcium indicators GCaMP6s and GCaMP7s, to selectively target GnRH^{OB} neurons $(GnRH^{GCaMP6s/GCaMP7s}). We confirmed the specific expression of GCaMP in \\$ GnRH-positive neurons by immunohistochemical analysis (Fig. 2b-e). Two weeks after viral injection, head-fixed mice were placed under the two-photon microscope. GnRH^{OB} neurons were identified by looking for GCaMP fluorescence, and responses to odors characterized by acute exposure to female urine or fresh air. We recorded from a total of 57 GnRH^{OB} neurons from 23 male GnRH^{GCaMP6s/GCaMP7s} mice (Fig. 2f) and classified their responses to female urine based on change in fluorescence within 10 s after stimulus onset²⁷. Among all recorded cells, 28% (16 of 57 cells) were activated by exposure to female urine, showing a significant increase in the relative change in fluorescence (dF/F_0) , compared with exposure to fresh air (Fig. 2g,h and Supplementary Video 1). Of the remaining recordings, 41 of 57 GnRH^{OB} neurons showed no response to female urine (Fig. 2i, j). We then performed similar experiments exposing the animals to saline, as an additional control, male urine or a nonsocial odor, methyl butyrate. All recorded GnRH^{OB} neurons did not show responses to those stimuli (Extended Data Fig. 4a-d).

These findings collectively suggest that a distinct population of male GnRH^{OB} neurons exhibits specific responsiveness to opposite-sex odor.

GnRH^{OB} neurons' hypophysiotropic response to opposite-sex odors

To determine whether GnRH^{OB} neurons also project to hypothalamic GnRH neurons (GnRH^{POA} cells) and/or directly to the median eminence (ME), we mapped their projections by bilaterally delivering a Cre-dependent AAV9 expressing mCherry under the control of the hSyn promoter into the OB (Fig. 3a) of male *Gnrh1*^{cre/uut} mice. AAV9-hSyn-DIO-mCherry viral tracers were used because they display anterograde and retrograde axonal transport capabilities²⁸. This approach yielded an average of 52% of GnRH^{OB} neurons coexpressing GnRH and mCherry in the MOB (Fig. 3b,c), 20% in the AOB and tenia tecta and 10% in the AON (Fig. 3b). We did not detect viral expression in GnRH neurons located in the rostral POA (rPOA; Fig. 3b,d,e), although GnRH^{OB} neurons extended discrete projections that crossed the rPOA and the

organum vasculosum of the lamina terminalis (OVLT; Fig. 3d-f). Many of these projections terminated in the ME (Fig. 3g). To estimate the fraction of GnRH^{OB} neurons projecting to the ME, we stereotaxically delivered a Cre-dependent AAV9 encoding an enhanced yellow fluorescent protein (eYFP) into the ME of Gnrh1^{cre/wt} male mice (Fig. 3h). We found the presence of GnRH-immunoreactive cells expressing eYFP in the OB (Fig. 3i) as well in the POA (Fig. 3j), with nearly 80 GnRH^{OB} neurons (~40%) being putative hypophysiotropic cells (Fig. 3k). Most of those neurons were located in the MOB (68.75 \pm 7.71), while a smaller fraction resided in the AOB (1.25 \pm 0.25), olfactory nerve layer (2.25 \pm 0.63) and AON/tenia tecta (TT) $(6.75 \pm 2.06; \text{Fig. 3k})$. Next, to investigate whether GnRH^{OB} neurons elicit a reproductive neuroendocrine response, we used Cre-dependent designer receptors exclusively activated by designer drugs (DREADDs) for bifunctional modulation of the activity of these GnRH neurons in vivo. We simultaneously introduced two Cre-dependent AAV vectors, encoding hM3Dq (AAV9-hSyn-DIO-hM3D_{Gq}-mCherry), an activator DREADD that utilizes clozapine N-oxide (CNO) as its ligand, and hKORD (AAV8-hSyn-DIO-hKORD-IRES-mCitrine), an inhibitory G_i-coupled kappa-opioid receptor DREADD using salvinorin B (SALB)²⁹ as a ligand, into the OB of *Gnrh1*^{cre/wt} male mice (GnRH^{hM3Dq/hKORD}; Fig. 3I). Approximately 80% of GnRH $^{hM3Dq/hKORD}$ in the OB expressed both mCherry and mCitrine (Fig. 3m), whereas hypothalamic GnRH neurons did not express the DREADDs reporters (Fig. 3n and Extended Data Fig. 5).

After assessing the infection efficiency of the GnRHOB neuronal population using the chemogenetic approach, we measured serum LH pulsatility by serial tail blood sampling in these male mice following CNO administration. The chemogenetic activation of GnRH^{OB} neurons with 1 mg per kg body weight CNO intraperitoneal injection triggered a fourfold increase in LH secretion compared with baseline levels, whereas we did not observe any changes when the same group was injected with the vehicle (saline) or when wild-type (WT) animals were injected with CNO (Fig. 30). The LH surge reached its peak approximately 12 min after the administration of CNO, maintaining a plateau throughout the remaining hormonal assessment period. This resulted in a significant $rise in circulating testosterone \, levels \, 1.5 \, h \, later \, in \, male \, GnRH^{h\overline{M}3Dq} \, mice$ administered with CNO compared to either WT mice injected with CNO or GnRH^{hM3Dq} mice injected with saline (Fig. 3p). Together, these findings show that GnRH^{OB} neurons, when activated, trigger a typical gonadotropic effect and modulate testosterone levels in males.

Previous results indicate that urinary compounds from the opposite sex influence the secretion of gonadotropins and sex hormones in both males and females 17,30,31 . Conversely, male mice exposed to the scent of the same sex do not exhibit significant alterations in circulating LH levels (Extended Data Fig. 6). Thus, to test the requirement of GnRH^{OB} neurons for the pheromone-mediated LH response, GnRH^{hKORD} male mice were treated with SALB or vehicle, and the same animals were exposed either to urine collected from novel estrous females or to saline (Fig. 3q). While female pheromones elicited a sharp increase in LH release over nearly 1 h following vehicle administration, chemogenetic silencing of GnRH^{OB} neurons with SALB completely blunted this gonadotropic response (Fig. 3q).

Altogether, these results demonstrate that GnRH^{OB} neurons are mostly hypophysiotropic and mediate LH and T secretion in male mice following exposure to opposite-sex odors.

GnRH^{OB} neurons modulate the firing rate of GnRH^{POA} neurons

Considering that projections from GnRH^{OB} neurons traverse the rPOA, we wondered whether these neurons could establish communication with the GnRH neuronal population situated in the hypothalamus, thereby influencing their neuroendocrine effects. To test this hypothesis, we bilaterally delivered the Cre-dependent AAV9-hM3D_{Gq}-mCherry into the OB of *Gnrh1*^{cre/wt}::*Gnrh1*^{g/p} male mice and established the anatomical and functional connectivity between these neuronal populations using immunofluorescence and electrophysiological recordings (Fig. 4a). Histological evaluation of brain slice preparations containing

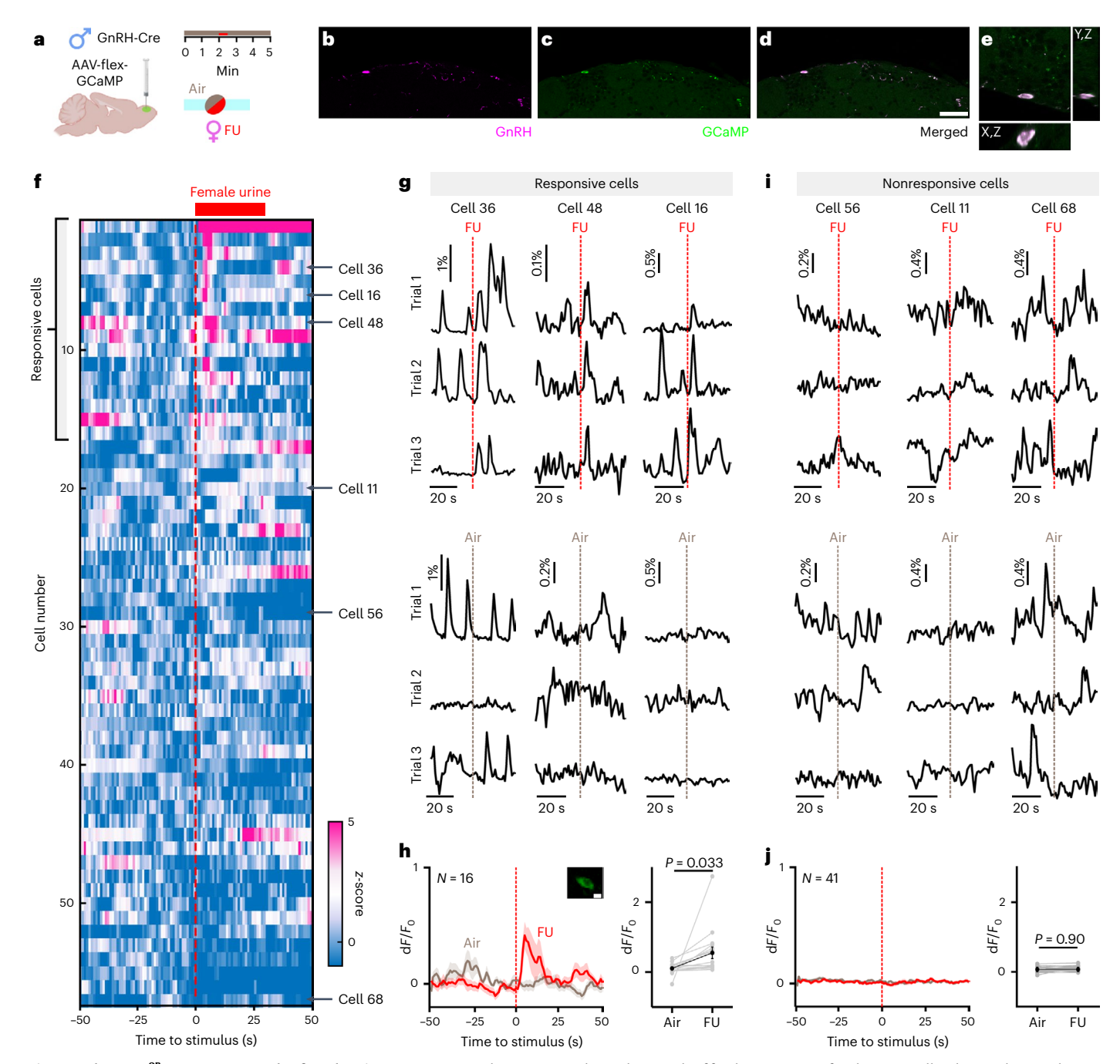


Fig. 2 | Male GnRH 08 neurons respond to female urine. a, In vivo two-photon imaging of GnRH-positive neurons was performed during exposure to female urine (FU) in 23 male mice, 12–16 weeks old. b, Representative confocal image (coronal section) illustrating GnRH immunoreactivity in a neuron after coinjecting AAVRg FLEX-jGCaMP7s and AAV9-FLEX-GCaMP6s. The infection efficiency was assessed in three animals. c, GCaMP expression in the same neuron shown in a. d, GnRH and GCaMP colocalization (merge of two colors). Single-plane confocal images show a GCaMP-expressing neuron stained for GnRH. Scale bars, 50 μ m. e, Higher-magnification confocal image and resliced section of the neuron depicted in b. Scale bar inset, 10 μ m. f, Average fluorescence profile of 57 recorded cells in response to FU. The red dashed line marks stimulus onset; red top line marks stimulus duration (30 s). Data are shown as z-score of the average trace for each neuron. Black arrows identify cells in g and h with their cell IDs. g, Representative traces from three responsive cells aligned to stimulus onset (FU or air). Upper part shows three consecutive trials of FU exposure. Lower part

shows three trials of fresh air exposure for the same cells. The gray line marks stimulus onset. **h**, Quantification of the overall response to FU for all responsive cells (n=16). Left: average fluorescence profile of all responsive cells to either FU (in red) or fresh air (in gray). The dashed line indicates stimulus onset of either FU or air. Inset shows a representative image of GCaMP-expressing GnRH cells imaged with the two-photon microscope. Scale bar, 10 μ m. The solid line indicates the average signal, while the shaded area indicates the standard error calculated across all cells. Right: quantification of the peak d F/F_0 calculated in the 10 s after stimulus onset for all responsive cells to either air or FU. Gray dots and lines indicate single cells. Black dots and lines represent the mean and the associated standard error. P value for statistical comparison is shown in the graph (two-sided paired t-test, P = 0.033, n = 16 cells). **i.j**, Same as **g** (**i**) and **h** (**j**) but for nonresponsive cells (two-sided paired t-test, P = 0.9, n = 41 cells). All experiments were performed in three biological replicates.

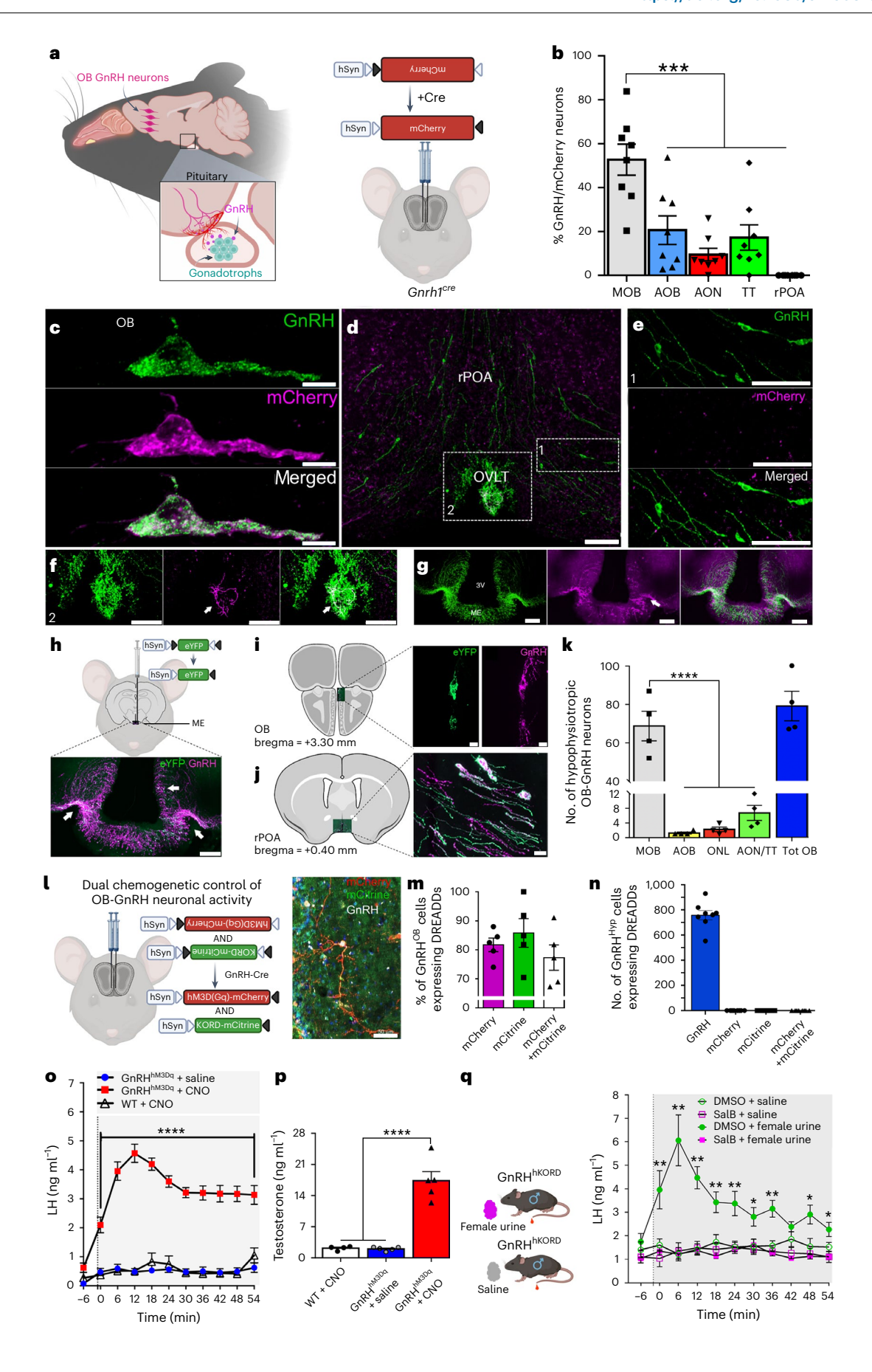


Fig. 3 | **GnRH**^{oB} **neurons mediate LH secretion in response to opposite-sex odors. a**, Experimental strategy for expression of AAV9-mCherry in GnRH^{oB} neurons in *Gnrh1*^{cre/uxt} male mice. **b**, Quantification of viral tracer-infected GnRH^{oB} neurons in the OB and rPOA (n = 8, P90); one-way ANOVA with Tukey's multiple-comparison test, $F_{4,35} = 14.89$, ****P = 0.0002. **c**-**g**, Representative images of GnRH and mCherry in the OB (**c**), rPOA (**d** and **e**), OVLT (**f**) and ME (**g**). High-power images show views of white boxes 1 (**e**) and 2 (**f**) from **d**. **h**, Schematic and coronal section of the ME showing GnRH and eYFP expression. **i, j**, Representative coronal sections of the OB (**i**) and the rPOA (**j**) depicting the expression of GnRH and eYFP. **k**, Number and distribution of hypophysiotropic GnRH^{oB} neurons (n = 4, 12-week-old males); one-way ANOVA and Tukey's multiple-comparison test ($F_{4,15} = 5.24$, *****P < 0.0001). Tot, total. **1**, Schematic of the experimental design of the chemogenetic control of GnRH^{oB} neuronal activity. Photomicrograph shows a GnRH^{oB} neuron coexpressing mCherry and mCitrine. **m**, Percentage of

mCherry- and mCitrine-expressing cells in GnRH^{OB} neurons (n=5,16-20-week-old males). $\bf n$, Number of hypothalamic GnRH neurons expressing mCherry and mCitrine or both from two independent biological replicates (n=8). $\bf o$, LH levels after chemogenetic GnRH^{OB} activation (n=8 GnRH^{hM3Dq} + saline; n=8 GnRH^{hM3Dq} + CNO; n=5 WT + CNO; 16-20-week-old males). Two-way ANOVA with Tukey's multiple-comparison test ($F_{10,70}=23.46$). $\bf p$, Testosterone levels after chemogenetic GnRH^{OB} activation (n=5 GnRH^{hM3Dq} + saline; n=5 GnRH^{hM3Dq} + CNO; n=4 WT + CNO; 16-20-week-old males); two-way ANOVA with Tukey's multiple-comparison test ($F_{2,11}=47.45$). $\bf q$, LH levels after chemogenetic GnRH^{OB} inhibition, n=12,16-20-week-old males; two-way ANOVA with Tukey's multiple-comparison test ($F_{33,165}=5.43$, time versus treatment, *P<0.05; **P<0.01). At least three experimental replicates were performed for each experiment. Scale bars, 100 µm ($\bf c-h$), 10 µm ($\bf i$ and $\bf j$) and 50 µm ($\bf i$). All values are the mean $\bf t$ s.e.m. Created with BioRender.com.

the rPOA confirmed that hypothalamic GnRH cell bodies do not express mCherry (Fig. 4b). However, we observed mCherry-immunoreactive fibers crossing this territory in close proximity to GnRH cell bodies and dendrites (Fig. 4b). Using confocal microscopy, we identified contact spots (Fig. 4c) between mCherry-positive fibers from GnRHOB $neurons\,on\,both\,the\,soma\,and\,primary\,dendrites\,of\,GnRH^{POA}\,neurons$ (Fig. 4c,d). We next isolated GnRH neurons from the OB and POA of *Gnrh1*^{gfp} male mice²³ using FACS and performed RT-qPCR experiments on GFP-positive and GFP-negative sorted cells (Fig. 4f). These mice express GFP under the control of GnRH promoter. Consequently, both populations of GnRH neurons, situated in both the OB and the hypothalamus, respectively, maintain GFP expression. As expected, we found enrichment of the Gnrh1 transcript in GFP-positive cells isolated from the OB and POA as compared with the GFP-negative cells (Fig. 4f). We then evaluated the expression of genes that are critical for fertility and pubertal onset such as KiSS-1 metastasis suppressor, Kiss1, and its receptor Kiss1r and the GnRH receptor (Gnrhr). GnRH neurons from both populations expressed Kiss1r but neither Kiss1 nor Gnrhr (Fig. 4g). In addition, we found that GnRH^{OB} cells did not express sexual steroid receptors (that is, estrogen receptor alpha (ERα), progesterone receptor (PR) or androgen receptor (AR); Extended Data Fig. 7). Profiling of $neurotran smitter\, expression\, revealed\, that\, GnRH^{OB}\, neurons\, expressed$ significantly higher transcript levels of glutamatergic markers such as glutamate ionotropic receptor NMDA type subunit 1, Grin1, and glutamate ionotropic receptor NMDA type subunit 2B, Grin2b, and solute carrier family 17 member 7. Slc17a7, which encodes the vesicular glutamate transporter type 1, as compared to GnRHPOA neurons (Fig. 4h). We also found a significantly higher expression of GABAergic (glutamate decarboxylase 1 and 2, Gad1, and Gad2) transcripts in GnRH^{OB} as compared to GnRHPOA neurons (Fig. 4h).

We then performed whole-cell current-clamp recordings of hypothalamic GnRH-GFP neurons in rPOA slice preparations containing GnRH $^{\rm POA}$ GFP-positive cell bodies and the mCherry-positive fibers of GnRH $^{\rm hM3Dq}$ OB neurons, before, during and after bath application of $1\,\mu\rm M$ CNO. In the absence of CNO, most GnRH $^{\rm POA}$ neurons exhibited

typical tonic firing (Fig. 4i). Bath application of 1 µM CNO triggered a robust and sustained increase in the spontaneous action potential firing rate of GnRHPOA neurons as compared with basal conditions (Fig. 4j,k). This was accompanied by an increase in the resting membrane potential of GnRH^{POA} neurons compared with basal conditions (Fig. 4k). Considering the glutamatergic and GABAergic properties of GnRH^{OB} neurons, and noting the absence of *Gnrhr* expression in both GnRH neuronal populations, we were prompted to investigate whether the communication between GnRH^{OB} and GnRH^{POA} neurons relied on glutamatergic, GABAergic transmission, or both. To clarify this question, whole-cell voltage-clamp recordings were performed on GFP-identified neurons under conditions to enhance and isolate GABAergic and glutamatergic currents (Fig. 41). As standard in the field³², to isolate GABAergic currents, glutamatergic currents were blocked with a combination of 6-cyano-7-nitroquinoxaline-2,3-dione and D-2-amino-5-phosphonovaleric acid, and the membrane potential of GnRH neurons was held at -60 mV. To isolate glutamatergic currents, GABAergic currents were blocked with a combination of gabazine and CGP35348 and the membrane potential of GnRH neurons was held at -70 mV. As illustrated in Fig. 4l-n, chemogenetic activation of GnRH^{OB} neurons resulted in a significant suppression of the mean GABAergic postsynaptic current firing in hypothalamic GnRH neurons and a significant increase in glutamatergic postsynaptic transmission.

Together, these data suggest that the stimulation of GnRH^{oB} neurons can influence the firing frequency of GnRH^{POA} neurons, primarily by amplifying glutamatergic signaling to hypothalamic GnRH neurons.

GnRH^{OB} neurons govern preference for opposite-sex odors

We next investigated whether $GnRH^{OB}$ neuronal activation could influence social preferences. To this aim, we reciprocally modulated $GnRH^{OB}$ neuronal activity by co-infecting $GnRH^{OB}$ neurons of $Gnrh1^{cre/wt}$ male mice with both AAV9- $hM3D_{Gq}$ -mCherry and AAV8-KORD-mCitrine DREADDs (Fig. 5a). Four weeks after viral delivery, we subjected these animals to an olfactory preference test in which we evaluated their response to urine from isolated stud male or estrous female mice while

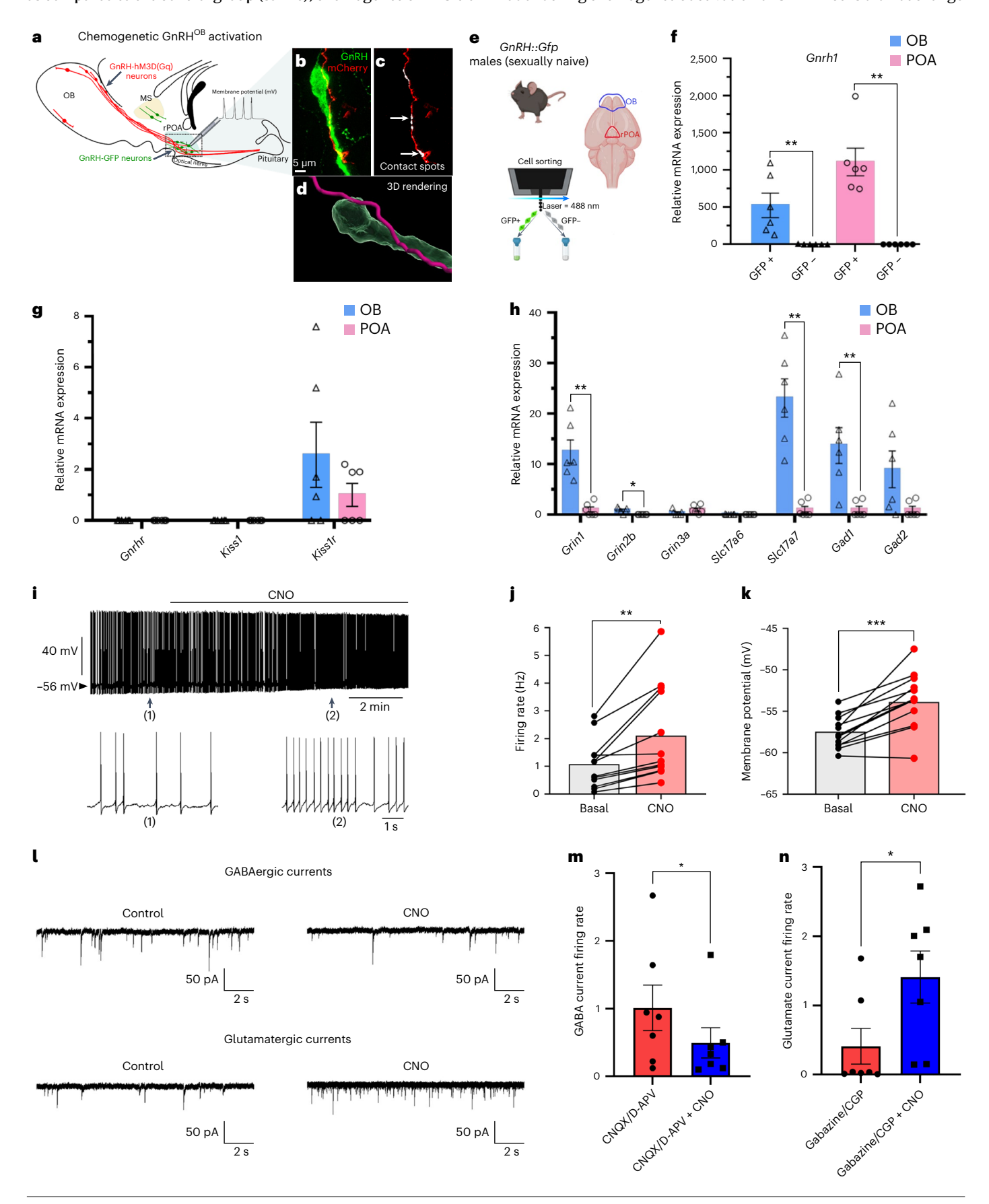
Fig. 4 \mid Connectivity between GnRH $^{\text{OB}}$ and GnRH $^{\text{POA}}$ neurons.

- **a**, Electrophysiology setup to activate $GnRH^{OB}$ neurons using 1 μ M CNO while recording $GnRH^{POA}$ neuronal activity via the patch-clamp technique. **b**, Confocal images showing GnRH and mCherry labeling; n=3 biological replicates.
- **c**, White arrows indicate contact points between GnRH^{OB} and GnRH^{POA} neurons.
- ${f d}$, 3D rendering of a GnRH^{POA} cell body and GnRH^{OB} neurites shown in ${f b}$.
- **e**, Schematic of FACS used to isolate GFP+ and GFP- cells from the OB and POA of GnRH::Gfp sexually naive male mice. **f**, Relative expression of Gnrh1 in sorted cells (n=6 animals, 12-week-old males, one-way ANOVA with Holm-Sidak's multiple-comparison test; OB, **P=0.0022; POA, **P=0.0039). **g**, Relative mRNA expression of Kiss1r, Kiss1 and Gnrhr in OB^{GFP+} and POA^{GFP+} sorted cells (n=6 animals, 12-week-old males; P>0.05 two-way ANOVA with Holm-Sidak's multiple-comparison test). **h**, mRNA expression level of Grin1, Grin2b, Grin3a, Slc17a6, Slc17a7, Gad1 and Gad2 in Gnrh-positive cells isolated from the OB and

the POA (n=6 animals, 12-week-old males; two-way ANOVA with Holm–Sidak's multiple-comparison test; Grin1, **P=0.0004; Grin2b, *P=0.0210; Grin3a, P>0.99; Slc17a6, P>0.99; Slc17a7, P<0.0001; Gad1, **P=0.0001; Gad2, P=0.99). i, Whole-cell current-clamp recording showing the spontaneous burst firing of a GnRH^{POA} neuron before and during bath application of CNO. Bottom traces show expansions of the recording at the indicated time points 1 and 2. j, k, Firing rate (Hz) (j) and membrane potential (mV) (k) of GnRH^{POA} neurons (n=12 recorded cells from 6 mice, 12–16-week-old males; **P=0.0094; ***P=0.0007; two-sided paired t-test). I, Representative GABAergic and glutamatergic currents of GnRH^{POA} neurons with or without CNO. m,n, GnRH^{POA} mean GABAergic (m) and glutamatergic (n) current firing (n=7 recorded cells from two mice, 16–20-week-old males; *P=0.0313 (m); *P=0.0156 (n); two-sided paired Wilcoxon signed-rank test). Data are represented as the mean \pm s.e.m. Created with BioRender.com.

activating or inhibiting the activity of GnRH^{OB} neurons in the same animals (Fig. 5b). We found that while chemogenetic activation of GnRH^{OB} neurons did not change the preference for opposite-sex odors as compared to the control group (saline), chemogenetic inhibition

of GnRH^{OB} neurons with SALB robustly shifted olfactory preferences toward the male odor as compared to vehicle-treated males (Fig. 5c). The number of explorations of male mice inspecting both sources of odor during chemogenetic activation of GnRH^{OB} cells did not change



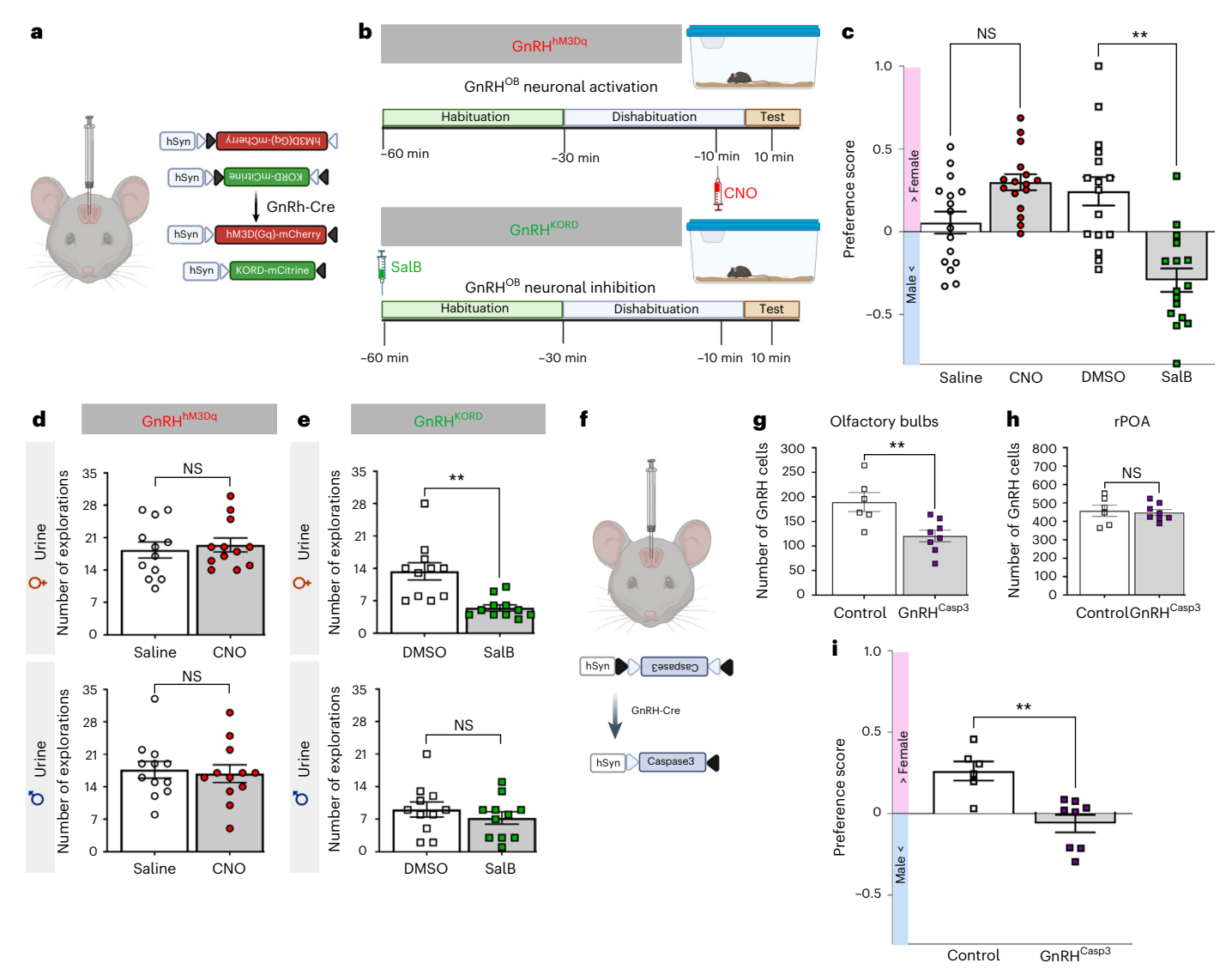


Fig. 5 \mid GnRH 0B neurons drive olfactory preference in male mice.

a, Schematic of the experimental design of the dual chemogenetic control of GnRH^{OB} neuronal activity. **b**, Schematic of the experimental workflow. CNO injection was performed 10 min before the test and salvinorin B injection 1 h before. **c**, Male mice injected with CNO display a preference for the female odor (urine) comparable to control males (injected with saline), whereas male mice injected with SalB do not show a female-directed preference and actually show a preference for the male odor. Chemogenetic activation n = 16, chemogenetic inhibition n = 16, 16 - 20-week-old males; two-way ANOVA with Holm–Sidak's multiple-comparison test (16 - 20-week-old males; two-way ANOVA with Holm–Sidak's multiple-comparison test (16 - 20-week-old males; two-way AnovA with Holm–Sidak's multiple-comparison test (16 - 20-week-old males; two-way AnovA with Holm–Sidak's multiple-comparison test (16 - 20-week-old males; two-way AnovA with Holm–Sidak's multiple-comparison test (16 - 20-week-old males; two-way AnovA with Holm–Sidak's multiple-comparison test (16 - 20-week-old males; two-way AnovA with Holm–Sidak's multiple-comparison test (16 - 20-week-old males; two-way AnovA with Holm–Sidak's multiple-comparison test (16 - 20-week-old males; two-way AnovA with Holm–Sidak's multiple-comparison test (16 - 20-week-old males; two-way AnovA with Holm–Sidak's multiple-comparison test (16 - 20-week-old males; two-way AnovA with Holm–Sidak's multiple-comparison test (16 - 20-week-old males; two-way AnovA with Holm–Sidak's multiple-comparison test (16 - 20-week-old males; two-way AnovA with Holm–Sidak's multiple-comparison test (16 - 20-week-old males; two-way AnovA with Holm–Sidak's multiple-comparison test (16 - 20-week-old males; two-way AnovA with Holm–Sidak's multiple-comparison test (16 - 20-week-old males; two-way AnovA with Holm–Sidak's multiple-comparison test (16 - 20-week-old males; two-way AnovA with Holm–Sidak's multiple-comparison test (16 - 20-week-old males; two-way AnovA with H

inhibition n=11,16-20-week-old males; two-sided paired Wilcoxon signed-rank test (**P=0.0031). \mathbf{f} , Schematic of the bilateral AAV9-hSyn-DIO-Caspase-3 stereotaxic injection in the OB. \mathbf{g} , \mathbf{h} , Number of GnRH neurons in the OB (\mathbf{g}) and in the rPOA (\mathbf{h}) of control and GnRH^{Casp3} male mice. \mathbf{i} , GnRH^{Casp3} male mice do not show a female-directed preference as compared with controls. For all experiments described in \mathbf{g} - \mathbf{i} , the total number of animals was n=6 control mice (n=3 $Gnrh1^{cre/uvt}$ injected with an AAV9-eYFP virus in the OB; n=3 $Gnrh1^{uvt/vt}$ injected with an AAV9-hSyn-DIO-Caspase-3 virus in the OB); n=8 GnRH^{Casp3} male mice, 16-20-week-old males. Statistical analysis was performed using a two-sided unpaired t-test in \mathbf{g} (**t) = 0.0074) and \mathbf{h} (t) = 0.7788) and an unpaired two-sided Mann–Whitney t0 test in t1 (**t2 = 0.006). All graphs show values as the mean t3.e.m. DMSO, dimethylsulfoxide. Created with BioRender.com.

(Fig. 5d). Instead, we observed a significant decrease in the number of explorations of female urine but not of male urine during chemogenetic inhibition (Fig. 5e), suggesting changes in olfactory exploratory drive with the inhibition of GnRH^{OB} neurons. We next used a genetic strategy to specifically ablate GnRH^{OB} neurons in a Cre-dependent manner taking advantage of an AAV9-flex-taCasp3-TEVp virus³³. We stereotaxically targeted the virus to the OB of adult *Gnrh1^{cre/wt}* male mice (Fig. 5f). GnRH^{OB} neurons were unaffected in control animals but significantly reduced by 40% in GnRH^{Casp3} mice 3 weeks following viral delivery (Fig. 5g). GnRH neurons in the rPOA were unaffected between control and virus-injected animals (Fig. 5h), indicating that the taCasp3-mediated ablation was restricted to the proximity of the

injection site. The partial ablation of GnRH^{OB} neurons was sufficient to alter olfactory preference in adult GnRH^{Casp3} male mice, which failed to show female-odor-directed preferences (Fig. 5i).

$GnRH^{OB}$ neurons drive opposite-sex odor preference and copulation through the pdMeA

We next mapped the potential targets of GnRH action by analyzing the distribution of the GnRH receptor (GnRHR) across the main and accessory olfactory areas and associated central brain structures. We took advantage of the GRIC/R26-tau-GFP (τ GFP) mouse line ^{34,35} in which GnRHR cells express the τ GFP protein (Fig. 6a) ³⁵. Immunohistochemical analyses revealed GFP expression in cells of both the MOS and

accessory olfactory system (AOS; Fig. 6b,c) as well as along the central downstream pathways (olfactory pathway: MOB, piriform cortex (PC). olfactory tract (OT), entorhinal cortex (EC); vomeronasal pathway: bed nucleus of the stria terminalis, anterior part of the medial amygdala (aMeA), posterodorsal medial amygdala (pdMeA) and posteromedial cortical nucleus (PMCN); Fig. 6d and Extended Data Fig. 8a-j). We also assessed whether exposure to female urine could induce cFos expression in GnRHR neurons located along these pathways in GRIC/R26-τGFP male mice (Fig. 6e-g). Stimulated animals showed increased percentages of GnRHR cells expressing cFos in the OB, aMeA, pdMeA and PC (Fig. 6f,g). Among these regions, the pdMeA is widely recognized as the 'vomeronasal amygdala' due to its role as the neuroanatomical bridge connecting the VNO-AOB pathway to the hypothalamic nuclei that regulate reproductive behaviors in mammals^{36,37}. We therefore asked whether GnRH^{OB} neuronal inputs to the pdMeA may be required to drive opposite-sex odor preference and sexual behavior. Neuroanatomical observations in male mice revealed that GnRH-immunoreactive fibers ran close to GnRHR-GFP+ cells located in the pdMeA (Fig. 6h,i).

To determine whether pdMeA neurons receive inputs from GnRH^{OB} and/or from GnRHPOA neurons, we injected RetroBeads into the pdMeA (Fig. 6j). Consistent with previous tracing studies in rodents³⁸, the RetroBeads labeled the mitral cell layer of the AOB but not the MOB (Fig. 6k), demonstrating high reliability of retrograde labeling. Importantly, we found a few scattered GnRH^{OB} neurons co-labeled with the RetroBeads (Fig. 61-0). Because AAV9 have been reported to display anterograde and retrograde axonal transport capabilities²⁸, we next targeted the inhibitory DREADD AAV9-hM4D_{Gi}-mCherry to the pdMeA of Gnrh1^{cre/wt} male mice (Fig. 6p) with the aim of infecting GnRH^{OB} neurons sending projections to this region. Quantitative analysis revealed that 60% of GnRH neurons located in the AOB and 10% of GnRH neurons located in the MOB and in the AON were infected with the inhibitory DREADD (Extended Data Fig. 9a,b). Importantly, there was no infection observed in GnRHPOA neurons (Extended Data Fig. 9b), indicating that the pdMeA receives inputs from a subset of GnRH^{OB} neurons but not from GnRHPOA neurons. Chemogenetic inhibition of the GnRHOB cell population targeting the pdMeA significantly decreased the olfactory attraction to female urine in sexually inexperienced GnRHhM4Di male mice, whereas it increased their preference for same-sex odors compared to controls (GnRH^{Cre/wt;hM4Di} male mice injected with saline; GnRHwt/wt;hM4Di mice injected with CNO; Fig. 6q). Because we did not detect any difference in the number of explorations and in the latency to explore female or male odors in the two groups of animals (Extended Data Fig. 9c), our data suggest that the inhibition of GnRH^{OB} neurons does not impact the motivation of these animals to seek novel odors.

In addition, the copulatory behavior of sexually naive $GnRH^{hM4Di}$ male mice was impaired as shown by a significant decrease in the number of mounts of $GnRH^{hM4Di}$ male mice after CNO injection compared to

controls (Fig. 6r). There were no discernible differences between the two groups of mice in investigation duration, latency to first mount, intromission latency and number of intromissions (Extended Data Fig. 9d). Moreover, anxiety and locomotor behaviors showed no alteration (Extended Data Fig. 9e), ruling out the possibility that the alterations in mating behavior of GnRH^{hM4Di} male mice are due to stress.

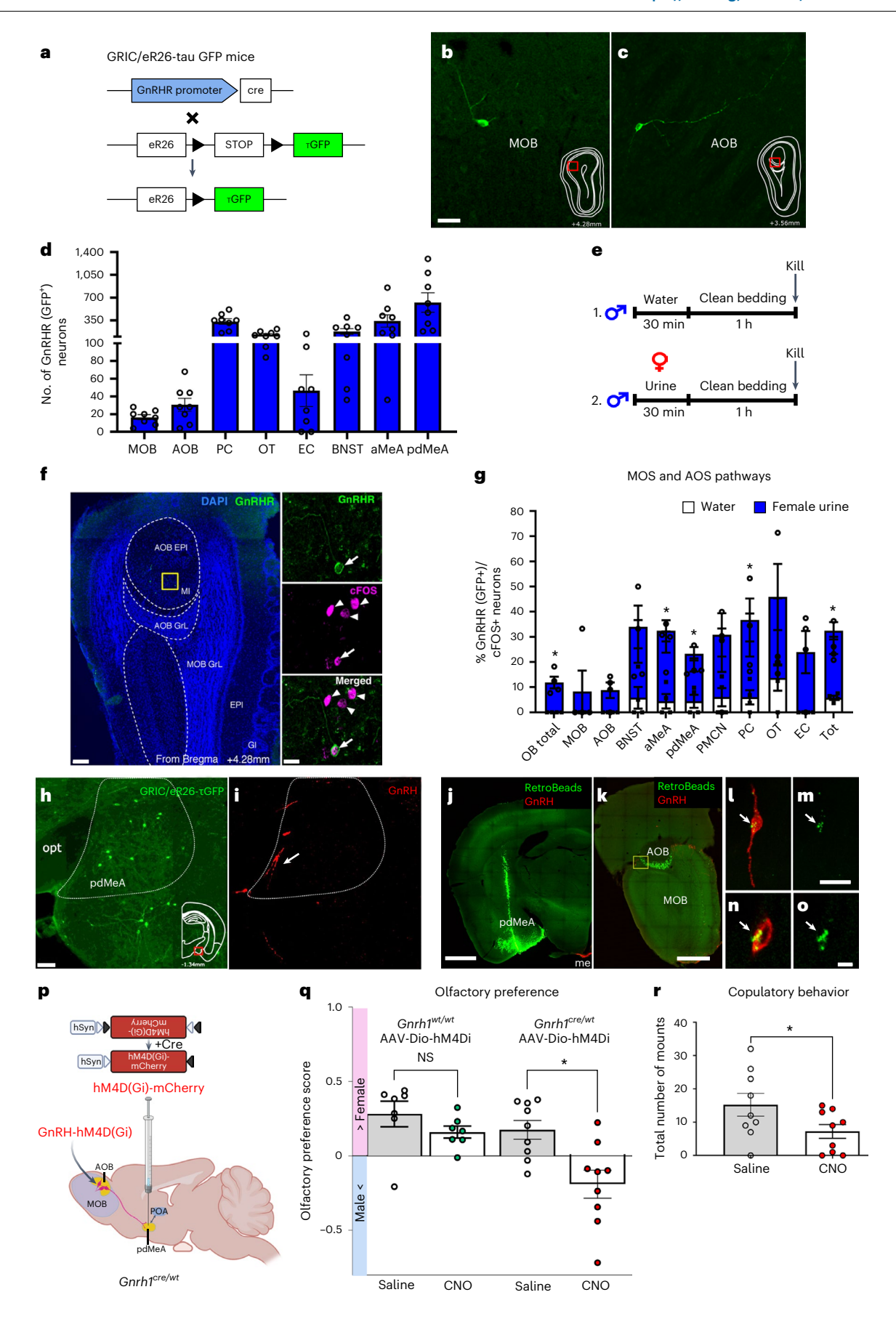
Collectively, these results indicate that GnRH^{OB} neurons play a crucial role in enabling male mice to identify scents of the opposite sex and initiate mating through a cross-talk with the pdMeA.

pdMeA^{Kiss1} neurons mediate male copulatory behavior via GnRHR Kisspeptin, derived from the *Kiss1* gene, is crucial for reproduction. Deficiencies in *Kiss1* or its receptor, *Kiss1r*, in both humans and mice lead to delayed puberty, hormonal imbalances and decreased fertility³⁹⁻⁴¹. The main areas where kisspeptin-synthesizing neurons are found are the anteroventral periventricular (AVPV) and the arcuate nucleus (ARC) within the hypothalamus, with smaller populations found in extrahypothalamic areas like the MeA⁴². Previous tracing studies in male rats have revealed that pdMeA kisspeptin (Kiss1) neurons receive projections from the AOB³⁸, suggesting a potential role in regulating pheromone-mediated sexual behavior. To investigate this further, we examined the expression of Kiss1 and Gnrhr transcripts using RNAscope in situ hybridization in the pdMeA, AVPV and ARC regions of sexually inexperienced and experienced male mice (Fig. 7a,b). Our findings indicate that approximately 60% of Kiss1-expressing neurons in the pdMeA express Gnrhr in both groups of animals, while AVPVKiss1 and ARCKiss1 neurons do not express Gnrhr (Fig. 7b). Extending upon this data, we next undertook a genetic manipulation approach through CRISPR genome editing in pdMeA^{Kiss1} neurons in vivo to unravel the functional relevance of Gnrhr in sexual preference and mating behavior. This was achieved using a virogenetic-driven RNA guide, which leads to changes within the Gnrhr sequence. The AAV-mCherry-Gnrhr guide RNA (gRNA) vector was bilaterally stereotaxically injected into the pdMeA of Kiss1-IRES-Cre/ R26-CAG-LSL-Cas9-P2A-GFP male mice as well as in control animals (R26-CAG-LSL-Cas9-P2A-GFP; Fig. 7c). Immunofluorescence was used to validate the specificity of the mouse line. In CRISPRKiss1-Gnrhr mice, the two populations of ARC^{Kiss1} and pdMeA^{Kiss1} neurons were identified by GFP labeling, while no GFP expression was observed in these regions in control mice (Fig. 7d,e). Additionally, injection site specificity was confirmed by mCherry expression in the pdMeA of both control and Kiss1-IRES-Cre/R26-CAG-LSL-Cas9-P2A-GFP male mice (Fig. 7d.e). Notably, double-labeled cells (mCherry/GFP) were detected only in the pdMeA of CRISPRKissi-Gnrhr mice, and our quantitative analysis revealed an infection rate of nearly 65% (Fig. 7f). Subsequently, we assessed the olfactory and copulatory behaviors in both sets of AAV-injected animals. Our findings revealed that CRISPR-mediated genome editing of Gnrhr in $pdMeA^{\textit{Kiss1}}\,neurons\,in\,vivo\,had\,no\,discernible\,effect\,on\,the\,preference\,for\,all the preference\,for\,all the$

Fig. 6 | GnRH^{OB} neurons recognize opposite-sex odors and initiate mating via the pdMeA. a, Genetic strategy to label GnRHR-expressing neurons. b,c, Coronal sections of the MOB (b) and AOB (c) display GnRHR-expressing neurons stained for GFP in GRIC/eR26-cGFP mouse line. White drawings and red boxes indicate OB sections, bregma coordinates and regions of image capture. d, GFP+ cell counts across brain regions involved in olfactory processing (n = 8). e, Schematic of the experimental protocol performed in f and g. f, Coronal section of OB labeled for GnRHR and DAPI. Yellow inset corresponds to high-magnification images in the right-hand pictures depicting a double-labeled GnRHR-cFOS+ cell in the AOB mitral layer (MI; arrow); n = 3 biological replicates. **g**, Percentage of GnRHR cells coexpressing cFOS in MOS and AOS pathways after exposure to water or female urine in GRIC/eR26- τ GFP male mice (n = 4, 12-week-old males). Two-sided paired Mann-Whitney U test (OB total, *P = 0.0286; aMeA, *P = 0.0376; pdMeA, *P = 0.0426; PC, *P = 0.0238; Tot, *P = 0.0321). **h,i**, pdMeA section labeling: immunoreactivity for GRIC/eR26- τ GFP (**h**) and GnRH (**i**) in coronal sections (n = 2biological replicates). **j-o**, Retrograde labeling of GnRH^{OB} neurons projecting to the pdMeA.j, RetroBeads injection site.k, Representative confocal image

 $(coronal\ section)\ of\ an\ olfactory\ bulb\ illustrating\ RetroBeads-labeled\ neurons\ (green)\ and\ GnRH-immunoreactive\ neurons\ (red)\ in\ the\ AOB.$

I, High-magnification photomicrograph of the region shown within the yellow box in **k** and illustrating a GnRH⁰⁸ neuron expressing the RetroBeads (arrow). **m**, Photomicrograph of the same neuron shown in I highlighting the RetroBeads labeling (arrow). **n**, Confocal image illustrating a GnRH⁰⁸ neuron expressing the RetroBeads (arrow). **o**, Photomicrograph of the same neuron shown in **n** highlighting the RetroBeads labeling (arrow). **p**, Stereotaxic injection schematic depicting bilateral AAV-hSyn-DIO-hM4D(Gi)-mCherry injection in the MeA. **q**, **r**, Olfactory preference (**q**) and copulatory behavior (**r**) in GnRH^{hM4Di} male mice injected with CNO or saline. **q**, n = 7 and 9, 16-24-week-old males; two-way ANOVA with Holm–Sidak's multiple-comparison test ($F_{1.14} = 11.27$; *P = 0.0293; n = 3 biological replicates). **r**, n = 9, 16-24-week-old males; two-sided Mann–Whitney U test, *P = 0.0424. Scale bars, $20 \mu m$ (**b** and **c**); $100 \mu m$ (**f**, left image) and $20 \mu m$ (**f**; right images); $40 \mu m$ (**h** and **i**); 1 mm (**j**); $500 \mu m$ (**k**); $5 \mu m$ (1-o). Data are the mean ± s.e.m. Created with BioRender.com.



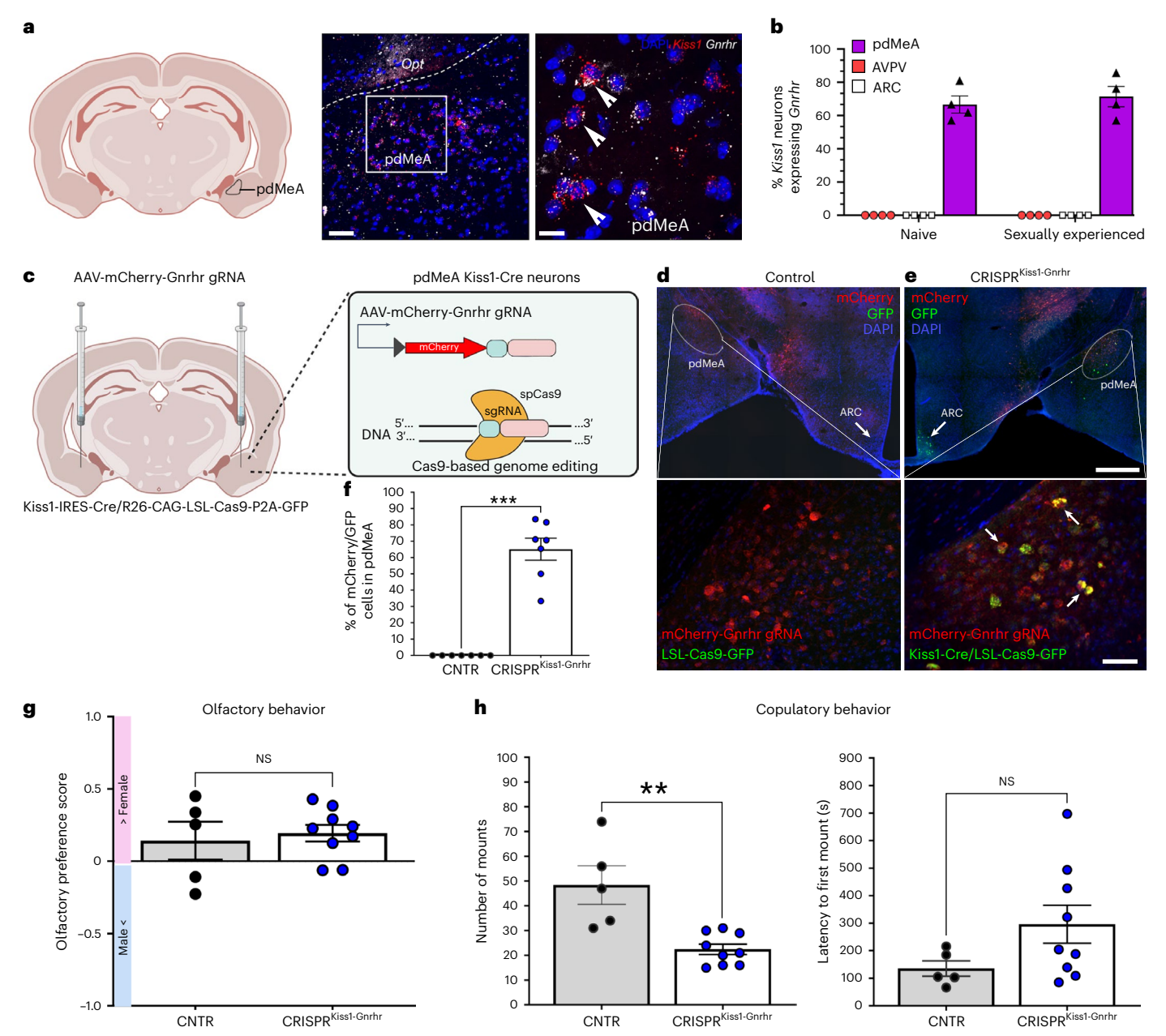


Fig. 7 | **GnRHR** expression on kisspeptin neurons in the pdMeA mediates mating behavior in male mice. **a**, Coronal section of pdMeA in an adult male mouse (P90) showing *KissI* and *Gnrhr* transcripts; n = 4 replicates. Arrows indicate kisspeptin neurons coexpressing *Gnrhr*. The white dashed line indicates the optic tract (Opt). **b**, Percentage of kisspeptin neurons coexpressing the *Gnrhr* in the pdMeA, the AVPV and the ARC in sexually inexperienced and experienced males (n = 4 naive males, n = 4 sexually experienced males). **c**, Bilateral AAV-mCherry-Gnrhr gRNA vector injection in the pdMeA of KissI-IRES-Cre/R26-CAG-LSL-Cas9-P2A-GFP male mice. **d**, Coronal section of a control mouse brain (AAV-mCherry-sg-RNA-Gnrhr injected), showing the pdMeA and ARC immunolabeled for mCherry and GFP, and counterstained with DAPI. High magnification of pdMeA shown below; n = 3 biological replicates. **e**, Coronal section of a CRISPR^{KissI-Gnrhr} male mouse, showing the pdMeA and ARC immunolabeled

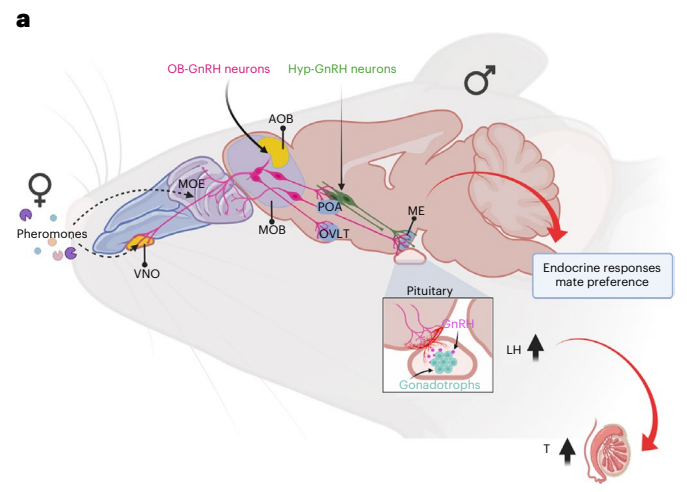
for mCherry and GFP, and counterstained with DAPI. High magnification of pdMeA shown below. Arrows indicate double-labeled neurons; n=3 biological replicates. **f**, Percentage of mCherry/GFP cells in the pdMeA of control (n=7) and CRISPR^{Kissl-Gnrhr} (n=7) male mice (16-20-week-old; ****P<0.001; two-sided Mann–Whitney U test). **g**, Olfactory behavior in male mice (n=5 control; n=9 CRISPR^{Kissl-Gnrhr}; 16-20-week-old males; NS P>0.05; two-sided Mann–Whitney U test (P=0.1265). **h**, Total number of mounts and latency to first mount during the copulatory behavior test in sexually naive AAV-mCherry-sg-RNA-Gnrhr control and CRISPR^{Kissl-Gnrhr} males; n=5 control; n=9 CRISPR^{Kissl-Gnrhr}; 16-20-week-old males; two-sided Mann–Whitney U test, **P=0.0015, NS P>0.05. Scale bars, 50 μ m (left) and 20 μ m (right) (**a**); 500 μ m (top) and 50 μ m (bottom) (**d** and **e**). Data are represented as the mean \pm s.e.m. Created with BioRender.com.

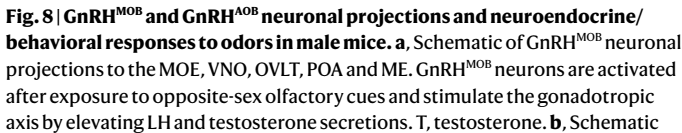
opposite-sex odors compared to the control group (Fig. 7g). However, sexually naive CRISPR-edited pdMeA^{Kiss1-Gnrhr} mice exhibited a significant decrease in the number of mounts as compared to controls (Fig. 7h), while the latency to the first mount remained unaffected (Fig. 7h). Additionally, there were no alterations observed in the number of intromissions or ejaculation latency (Extended Data Fig. 10a,b), thus suggesting

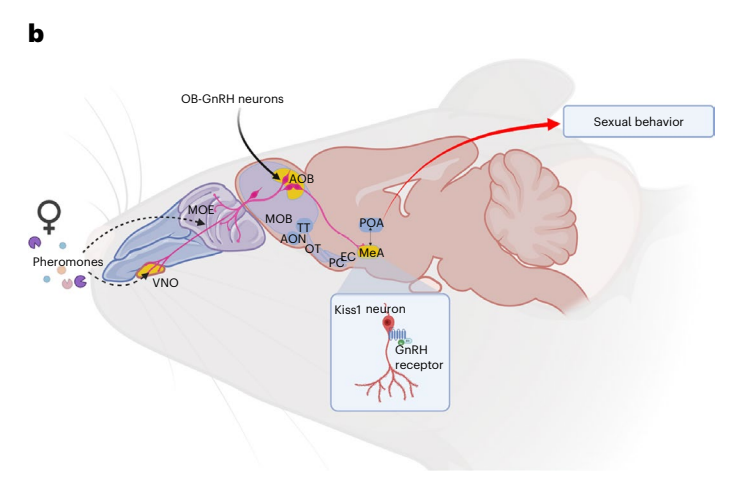
that $pdMeA^{Kiss1}$ neurons potentially exert a significant influence on driving the initiation of copulatory behavior via GnRHR.

Discussion

Our study identified a role of an extrahypothalamic population of GnRH neurons located in the OB as a specialized hub uniting chemosensory







of GnRH AOB neuronal projections to the MOE, VNO and MeA. When exposed to the scent of the opposite sex, GnRH AOB neurons stimulate the onset of copulatory behavior in inexperienced male mice via the expression of GnRHR in the kisspeptin neurons of the pdMeA. Created with BioRender.com.

cues with opposite-sex attraction, sexual behavior and corresponding endocrine changes in male mice. Chemosensory signals are recognized as triggers for male sexual arousal and behavior. The primary olfactory system plays a crucial role in drawing males toward females in estrus, while the vomeronasal receptors activate supplementary olfactory pathways that initiate mating behavior through their connections with the hypothalamus⁸. Consistently, targeted deletion of the olfactory sensory transduction molecules downstream of odorant receptors encoded by $Cnga2^{10}$ or $Ac3^{11}$, which are expressed in the MOE but not in the VNO, disrupts the preference for female urine odors in male mice and impairs male–female mating behavior.

In this work, we showed that one-fourth of the entire brain population of GnRH neurons is located in the OB with the majority of GnRH^{OB} cell bodies located within the MOB. Using whole-head immunostaining and GnRH^{OB} viral tracing, we provide evidence of anatomical connectivity between GnRH^{OB} neurons and the MOE and VNO. In addition, our transcriptomic data highlight the expression of 11 *Vmnr* genes in up to 7% of GnRH^{OB} neurons and 30 Olfr genes in up to 12% of GnRH^{OB} neurons, suggesting that a subset of these cells may directly detect odorant and pheromonal molecules. An alternative and/complementary scenario is also possible since a recent study²⁶ has identified a subpopulation of 'heartbeat sentinel neurons' located in the OB, which senses, through excitatory mechanosensitive ion channels, the vascular blood pressure pulsations associated with the heartbeat. Notably, despite not relying on synaptic transmission, the fast transduction pathway still managed to synchronize the intrinsic spiking patterns of mitral cells with the vascular pressure pulsation rhythm²⁶. That study²⁶ proposed that this interoceptive mechanism could enhance appropriate responses triggered by arousal linked to the onset of social interactions. Hence, it is plausible that encountering scents from individuals of the opposite sex might cause changes in breathing patterns, thereby affecting the heartbeat, which in turn could influence the rhythmic pulsation of vascular pressure in the OB. Consequently, this vascular pressure rhythm might also impact on the spiking activity of GnRH^{OB} neurons, which we found to express the fast excitatory mechanosensitive ion channel Piezo2. Indeed, our in vivo two-photon functional imaging of GnRH^{OB} neurons of males exposed to female estrous urine revealed that one-third of the GnRH^{OB} neuronal population is selectively activated in response to the odor of the opposite sex. However, GnRHOB neuronal responses were overall smaller compared to those previously characterized in other OB cells in response to urine^{43,44}. This is probably attributable to the fact these cells could represent a distinctive OB neuronal population never characterized before, with unknown electrophysiological properties, which might result in a different activation profile. Importantly, none of the recorded GnRH cells responded to the same-sex odor, or to nonsocial odors. This in vivo evidence that mammalian GnRH neurons show odorant-driven activity provides a missing piece in the puzzle of olfactory-mediated sex behaviors.

We also found by virally mediated circuit connectivity analysis that GnRH^{OB} cells project to the POA and to the ME. Previous studies have demonstrated that both the vomeronasal and main olfactory subsystems send projections to the hypothalamic GnRH neurons ^{16,17}. Here, we found that GnRH^{OB} neurons projecting to the POA and ME are mostly located in the MOB and that chemogenetic activation of these $cells \, results \, in \, a \, significant \, increase \, of \, the \, GnRH^{POA} \, neuronal \, activity \, following the energy in the energy of the$ lowed by LH and testosterone secretion. Our data showed that GnRH^{OB} neurons express high levels of GABAergic and glutamatergic markers, and the electrophysiology experiments revealed that stimulation of GnRH^{OB} neurons influences the firing frequency of GnRH^{POA} neurons primarily by amplifying postsynaptic AMPA/kainate receptor-mediated currents. Viral expression was never detected in GnRH neurons located in the rPOA after infection of GnRH^{OB} neurons in *Gnrh1*^{cre/wt} male mice. Hence, GnRH^{OB} and GnRH^{POA} neurons most likely communicate indirectly through a multisynaptic network converging onto GnRHPOA neurons, ultimately resulting in increased LH secretion. Altogether, these approaches show that GnRH^{OB} neurons can decode the opposite-sex chemosensory cues into activation of GnRH^{POA} neurons, thus triggering fertility-related neuroendocrine changes (Fig. 8a). In line with this hypothesis, the sharp increase in LH release induced by the exposure to intact estrous female urine, consistent with previous studies 14,15, was completely eliminated after chemogenetic silencing of GnRH^{OB} neurons.

A previous work showed that $Gnrh1^{cre/wt}$; $Dicer1^{loxP/loxP}$ females, which are incapable of synthesizing and secreting GnRH in adulthood 20 , failed to show male-directed preferences 45 . Here, we identified the $GnRH^{OB}$ neurons as the cellular component responsible for the opposite-sex attraction since our experiments showed that chemogenetic inhibition or ablation of $GnRH^{OB}$ neurons disrupts the olfactory preference of adult males toward the female odor.

Consistent with the expression of GnRH and its cognate receptor GnRHR in several extrahypothalamic areas in mice and humans $^{18,46-48}$, our mapping experiments highlighted a wide distribution of $\it Gnrhr$ -positive cells in the main and accessory olfactory systems as well

as along all cortical and hypothalamic recipients of the MOB and AOB. Notably, adult mice demonstrate a preference for the opposite-sex smell through a cross-talk between the main and accessory olfactory systems⁴⁹. The MOE plays a more significant role in driving the preference for the opposite sex and initiating sexual behavior, while signaling from the VNO is implicated in sex identification^{8,10,50}.

In this study, we found a significant increase in the activation of *Gnrhr*-positive cells, after stimulation with female urine, in the OB, as well as in brain regions downstream of the main and accessory olfactory systems. Among these areas, the pdMeA, a limbic center interpreting olfactory cues and mediating partner preference partly via extrahypothalamic kisspeptin neurons, is crucial in the neural network governing sexual behavior ^{38,51-53}. A certain degree of convergence exists between the MOS and the AOS at the level of the corticomedial amvgdala^{37,54,55}. However, the identity of cells relaying signals from the olfactory system to the MeA to finally modulate sex recognition and mating behavior remains poorly defined. Here, we provide evidence that 60% of GnRH neurons located in the AOB project to the pdMeA and that chemogenetic inhibition of these neurons abrogated the olfactory preference of Gnrh1^{cre/wt} male mice toward the female urine and impacted their copulatory behavior, thus suggesting that GnRHOB neurons projecting to the pdMeA are essential for both sex recognition and the initiation of mating behavior in males. As there was no infection observed in GnRHPOA cell bodies, hypothalamic GnRH neurons most likely do not send direct projections to the pdMeA.

Previous investigations in male rats have demonstrated that pdMeA kisspeptin neurons receive input from the AOB³⁸, indicating a potential involvement in modulating pheromone-induced sexual behavior. This is further supported by findings showing that chemogenetic stimulation of MeA kisspeptin neurons in male mice enhances their preference for estrous females⁵¹. We showed that the pdMeA^{Kiss1} neuronal population differs from the AVPV and ARC kisspeptin populations in *Gnrhr* expression. Nearly 60% of pdMeA^{Kiss1} cells express the GnRH receptor in sexually naive and sexually experienced males, whereas there is no expression in the other two hypothalamic regions.

Our findings revealed that CRISPR-mediated genome editing of Gnrhr in pdMeA^{Kiss1} neurons in vivo significantly reduced the number of mounts of male mice. Because the levels of male sexual behavior were equivalent in the two animal groups, it is plausible to attribute a limited role for GnRHR in pdMeA^{Kiss1} neurons on male coital behavior and to assume that pdMeA^{Kiss1} neurons potentially influence the initiation of copulatory behavior via GnRHR signaling (Fig. 8b). Unlike the chemogenetic inhibition experiments directed at the GnRHOB neurons projecting to the pdMeA, which lead to significant changes of both olfactory preference and copulatory behavior, CRISPR^{Kiss1-Gnrhr} mice do not exhibit alterations in their preference for the opposite-sex smell. These findings suggest that either the infection efficiency (\sim 60%) of the AAV-mCherry-Gnrhr gRNA in the pdMeA^{Kiss1} neurons is insufficient to observe changes in olfactory preference, or non-kisspeptin GnRHR-expressing neurons may contribute to this innate behavior.

This study provides insights into the biology and homeostasis of reproduction in mammals. The mechanism we observed in mice likely operates in other species as well, and a strong human relevance is suggested by the presence of GnRH neurons in the OB of human postmortem brains. Quite convincing pheromonal effects have been demonstrated in humans who do not have a functional vomeronasal system ⁵⁶. However, the issue of whether these responses are mediated by a functional VNO in humans is still controversial, although previous studies have demonstrated the existence of a distinguishable VNO in a substantial proportion of adult humans ⁵⁷ as well as in human fetuses ¹⁸.

During the last few years, we and others have started to shed light on the extra-reproductive roles of GnRH neurons, associated with cognitive functions 46 and programming of systemic aging 58 . The current study expands those findings, highlighting a role for GnRH 08 neurons in the processing of chemo-social cues responsible for opposite-sex attraction.

Online content

Any methods, additional references, Nature Portfolio reporting summaries, source data, extended data, supplementary information, acknowledgements, peer review information; details of author contributions and competing interests; and statements of data and code availability are available at https://doi.org/10.1038/s41593-024-01724-1.

References

- Dulac, C. & Torello, A. T. Molecular detection of pheromone signals in mammals: from genes to behaviour. *Nat. Rev. Neurosci.* 4. 551–562 (2003).
- Belluscio, L., Koentges, G., Axel, R. & Dulac, C. A map of pheromone receptor activation in the mammalian brain. Cell 97, 209–220 (1999).
- Rodriguez, I., Feinstein, P. & Mombaerts, P. Variable patterns of axonal projections of sensory neurons in the mouse vomeronasal system. Cell 97, 199–208 (1999).
- Lehman, M. N., Winans, S. S. & Powers, J. B. Medial nucleus of the amygdala mediates chemosensory control of male hamster sexual behavior. Science 210, 557–560 (1980).
- Baird, A. D., Wilson, S. J., Bladin, P. F., Saling, M. M. & Reutens, D. C. The amygdala and sexual drive: insights from temporal lobe epilepsy surgery. *Ann. Neurol.* 55, 87–96 (2004).
- 6. Bayless, D. W. et al. A neural circuit for male sexual behavior and reward. *Cell* **186**, 3862–3881 (2023).
- Keller, M., Pillon, D. & Bakker, J. Olfactory systems in mate recognition and sexual behavior. Vitam. Horm. 83, 331–350 (2010).
- 8. Keverne, E. B. Importance of olfactory and vomeronasal systems for male sexual function. *Physiol. Behav.* **83**, 177–187 (2004).
- Aoki, M. et al. Prolactin-sensitive olfactory sensory neurons regulate male preference in female mice by modulating responses to chemosensory cues. Sci. Adv. 7, eabg4074 (2021).
- Mandiyan, V. S., Coats, J. K. & Shah, N. M. Deficits in sexual and aggressive behaviors in *Cnga2* mutant mice. *Nat. Neurosci.* 8, 1660–1662 (2005).
- Wang, Z. et al. Pheromone detection in male mice depends on signaling through the type 3 adenylyl cyclase in the main olfactory epithelium. J. Neurosci. 26, 7375–7379 (2006).
- Duittoz, A. H. et al. Development of the gonadotropin-releasing hormone system. J. Neuroendocrinol. 34, e13087 (2022).
- Herbison, A. E. Control of puberty onset and fertility by gonadotropin-releasing hormone neurons. *Nat. Rev. Endocrinol.* 12, 452–466 (2016).
- Bronson, F. H. The regulation of luteinizing hormone secretion by estrogen: relationships among negative feedback, surge potential, and male stimulation in juvenile, peripubertal, and adult female mice. *Endocrinology* 108, 506–516 (1981).
- Dluzen, D. E., Ramirez, V. D., Carter, C. S. & Getz, L. L. Male vole urine changes luteinizing hormone-releasing hormone and norepinephrine in female olfactory bulb. Science 212, 573–575 (1981).
- Boehm, U., Zou, Z. & Buck, L. B. Feedback loops link odor and pheromone signaling with reproduction. Cell 123, 683–695 (2005).
- Yoon, H., Enquist, L. W. & Dulac, C. Olfactory inputs to hypothalamic neurons controlling reproduction and fertility. *Cell* 123, 669–682 (2005).
- 18. Casoni, F. et al. Development of the neurons controlling fertility in humans: new insights from 3D imaging and transparent fetal brains. *Development* **143**, 3969–3981 (2016).
- Boehm, U. et al. Expert consensus document: European Consensus Statement on congenital hypogonadotropic hypogonadism-pathogenesis, diagnosis and treatment. *Nat. Rev. Endocrinol.* 11, 547–564 (2015).
- Messina, A. et al. A microRNA switch regulates the rise in hypothalamic GnRH production before puberty. Nat. Neurosci. 19, 835–844 (2016).

- Belle, M. et al. Tridimensional visualization and analysis of early human development. Cell 169, 161–173 (2017).
- Renier, N. et al. iDISCO: a simple, rapid method to immunolabel large tissue samples for volume imaging. Cell 159, 896–910 (2014).
- Spergel, D. J., Kruth, U., Hanley, D. F., Sprengel, R. & Seeburg, P. H. GABA- and glutamate-activated channels in green fluorescent protein-tagged gonadotropin-releasing hormone neurons in transgenic mice. J. Neurosci. 19, 2037–2050 (1999).
- Wang, J. & Hamill, O. P. Piezo2-peripheral baroreceptor channel expressed in select neurons of the mouse brain: a putative mechanism for synchronizing neural networks by transducing intracranial pressure pulses. J. Integr. Neurosci. 20, 825–837 (2021).
- Zeppilli, S. et al. Molecular characterization of projection neuron subtypes in the mouse olfactory bulb. eLife 10, e65445 (2021).
- Jammal Salameh, L., Bitzenhofer, S. H., Hanganu-Opatz, I. L., Dutschmann, M. & Egger, V. Blood pressure pulsations modulate central neuronal activity via mechanosensitive ion channels. Science 383, eadk8511 (2024).
- Galliano, E. et al. Embryonic and postnatal neurogenesis produce functionally distinct subclasses of dopaminergic neuron. eLife 7, e32373 (2018).
- Castle, M. J., Gershenson, Z. T., Giles, A. R., Holzbaur, E. L. & Wolfe, J. H. Adeno-associated virus serotypes 1, 8, and 9 share conserved mechanisms for anterograde and retrograde axonal transport. *Hum. Gene Ther.* 25, 705–720 (2014).
- Vardy, E. et al. A new DREADD facilitates the multiplexed chemogenetic interrogation of behavior. *Neuron* 86, 936–946 (2015).
- Johnston, R. E. & Bronson, F. Endocrine control of female mouse odors that elicit luteinizing hormone surges and attraction in males. *Biol. Reprod.* 27, 1174–1180 (1982).
- Maruniak, J. A. & Bronson, F. H. Gonadotropic responses of male mice to female urine. *Endocrinology* 99, 963–969 (1976).
- Chu, Z. & Moenter, S. M. Endogenous activation of metabotropic glutamate receptors modulates GABAergic transmission to gonadotropin-releasing hormone neurons and alters their firing rate: a possible local feedback circuit. J. Neurosci. 25, 5740–5749 (2005).
- 33. Yang, C. F. et al. Sexually dimorphic neurons in the ventromedial hypothalamus govern mating in both sexes and aggression in males. *Cell* **153**, 896–909 (2013).
- Wen, S. et al. Genetic identification of GnRH receptor neurons: a new model for studying neural circuits underlying reproductive physiology in the mouse brain. *Endocrinology* 152, 1515–1526 (2011).
- 35. Wen, S. et al. Functional characterization of genetically labeled gonadotropes. *Endocrinology* **149**, 2701–2711 (2008).
- Kang, N., Baum, M. J. & Cherry, J. A. A direct main olfactory bulb projection to the 'vomeronasal' amygdala in female mice selectively responds to volatile pheromones from males. Eur. J. Neurosci. 29, 624–634 (2009).
- Kevetter, G. A. & Winans, S. S. Connections of the corticomedial amygdala in the golden hamster. II. Efferents of the "olfactory amygdala". J. Comp. Neurol. 197, 99–111 (1981).
- 38. Pineda, R., Plaisier, F., Millar, R. P. & Ludwig, M. Amygdala kisspeptin neurons: putative mediators of olfactory control of the gonadotropic axis. *Neuroendocrinology* **104**, 223–238 (2017).
- Seminara, S. B. et al. The GPR54 gene as a regulator of puberty.
 N. Engl. J. Med. 349, 1614–1627 (2003).
- Topaloglu, A. K. et al. Inactivating KISS1 mutation and hypogonadotropic hypogonadism. N. Engl. J. Med. 366, 629–635 (2012).
- de Roux, N. et al. Hypogonadotropic hypogonadism due to loss of function of the KiSS1-derived peptide receptor GPR54. Proc. Natl Acad. Sci. USA 100, 10972–10976 (2003).

- 42. Stephens, S. B. Z. & Kauffman, A. S. Regulation and possible functions of kisspeptin in the medial amygdala. *Front. Endocrinol.* **8.** 191 (2017).
- Lin, D. Y., Zhang, S. Z., Block, E. & Katz, L. C. Encoding social signals in the mouse main olfactory bulb. *Nature* 434, 470–477 (2005).
- 44. Shani-Narkiss, H. et al. Young adult-born neurons improve odor coding by mitral cells. *Nat. Commun.* **11**, 5867 (2020).
- 45. Hellier, V. et al. Female sexual behavior in mice is controlled by kisspeptin neurons. *Nat. Commun.* **9**, 400 (2018).
- Manfredi-Lozano, M. et al. GnRH replacement rescues cognition in Down syndrome. Science 377, eabq4515 (2022).
- Schang, A. L. et al. GnRH receptor gene expression in the developing rat hippocampus: transcriptional regulation and potential roles in neuronal plasticity. *Endocrinology* **152**, 568–580 (2011).
- Skrapits, K. et al. The cryptic gonadotropin-releasing hormone neuronal system of human basal ganglia. *eLife* 10, e67714 (2021).
- 49. Hurst, J. L. Female recognition and assessment of males through scent. *Behav. Brain Res* **200**, 295–303 (2009).
- Choi, J. M. et al. Development of the main olfactory system and main olfactory epithelium-dependent male mating behavior are altered in Go-deficient mice. *Proc. Natl Acad. Sci. USA* 113, 10974–10979 (2016).
- 51. Adekunbi, D. A. et al. Kisspeptin neurones in the posterodorsal medial amygdala modulate sexual partner preference and anxiety in male mice. *J. Neuroendocrinol.* **30**, e12572 (2018).
- 52. Lehman, M. N. & Winans, S. S. Vomeronasal and olfactory pathways to the amygdala controlling male hamster sexual behavior: autoradiographic and behavioral analyses. *Brain Res.* **240**, 27–41 (1982).
- 53. Wood, R. I. & Newman, S. W. Integration of chemosensory and hormonal cues is essential for mating in the male Syrian hamster. *J. Neurosci.* **15**, 7261–7269 (1995).
- 54. Gomez, D. M. & Newman, S. W. Differential projections of the anterior and posterior regions of the medial amygdaloid nucleus in the Syrian hamster. *J. Comp. Neurol.* **317**, 195–218 (1992).
- Kevetter, G. A. & Winans, S. S. Connections of the corticomedial amygdala in the golden hamster. I. Efferents of the "vomeronasal amygdala". J. Comp. Neurol. 197, 81–98 (1981).
- Meredith, M. Human vomeronasal organ function: a critical review of best and worst cases. *Chem. Senses* 26, 433–445 (2001).
- 57. Frasnelli, J., Lundstrom, J. N., Boyle, J. A., Katsarkas, A. & Jones-Gotman, M. The vomeronasal organ is not involved in the perception of endogenous odors. *Hum. Brain Mapp.* **32**, 450–460 (2011).
- Zhang, G. et al. Hypothalamic programming of systemic ageing involving IKK-β, NF-κB and GnRH. Nature 497, 211–216 (2013).

Publisher's note Springer Nature remains neutral with regard to jurisdictional claims in published maps and institutional affiliations.

Springer Nature or its licensor (e.g. a society or other partner) holds exclusive rights to this article under a publishing agreement with the author(s) or other rightsholder(s); author self-archiving of the accepted manuscript version of this article is solely governed by the terms of such publishing agreement and applicable law.

© The Author(s), under exclusive licence to Springer Nature America, Inc. 2024

¹Laboratory of Development and Plasticity of the Neuroendocrine Brain, FHU 1000 Days for Health, School of Medicine, Lille, France. ²Univ. Lille, Inserm, CHU Lille, Lille Neuroscience & Cognition, UMR-S 1172, Labex DistAlz, Lille, France. ³Department of Life Sciences and Systems Biology, University of Torino, Torino, Italy. ⁴Neuroscience Institute Cavalieri Ottolenghi, Orbassano, Italy. ⁵Max Planck Institute for Metabolism Research, Max Planck Research Group Neurocircuit Wiring and Function, Cologne, Germany. ⁵Experimental Pharmacology, Center for Molecular Signaling (PZMS), Center for Genderspecific Biology and Medicine (CGBM), Saarland University School of Medicine, Homburg, Germany. ¹Laboratory of Reproductive Neurobiology, Hun-Ren Institute of Experimental Medicine, Budapest, Hungary. ⁵Department of Pathology and Experimental Cancer Research, Semmelweis University, Budapest, Hungary. ⁵Department of Neuroscience "Rita Levi Montalcini", University of Turin, Turin, Italy. ¹¹German Center for Diabetes Research (DZD), Neuherberg, Germany. ¹¹Research Unit Neurobiology of Diabetes, Institute for Diabetes and Obesity, Helmholtz Munich, Neuherberg, Germany. ¹²Division of Neurobiology of Diabetes, TUM School of Medicine, Technical University of Munich, Munich, Germany. ¹³Excellence Cluster on Cellular Stress Responses in Aging-Associated Diseases (CECAD), University of Cologne, Cologne, Germany. ¹⁴Present address: Centro CMP3VdA, Istituto Italiano di Tecnologia (IIT), Aosta, Italy. ¹⁵Present address: Division of Endocrinology, Diabetes and Hypertension, Department of Medicine, Brigham and Women's Hospital and Harvard Medical School, Boston, MA, USA. ¹⁶These authors contributed equally: Laurine Decoster, Sara Trova, Mauro S. B. Silva, Paolo Giacobini. ⊠e-mail: paolo.giacobini@inserm.fr

Methods

Humans

Autopsies were carried out at the Department of Pathology and Experimental Cancer Research, Semmelweis University, Budapest, Hungary, less than 24 h after death. The OBs were dissected from the brains of three individuals (37-year-old male, 64-year-old male and 77-year-old female) who had no neurological or endocrine disorders in their medical history. The tissues were immersion-fixed with ice-cold 4% formal-dehyde for 24 h and then placed in PBS with 0.1% sodium azide and stored at 4 °C until processed for GnRH immunolabeling.

Animals

Mice were group housed under specific pathogen-free conditions in a temperature-controlled (21–22 °C) and humidity-controlled (30–60%) environment, with a 12-h light-dark cycle and ad libitum access to food and water. They were housed in individually ventilated cages, with a maximum of six mice per cage. Animal studies were approved by the Institutional Ethics Committees for the Care and Use of Experimental Animals of the University of Lille and the French Ministry of National Education, Higher Education and Research (APAFIS number 2617-2015110517317420 v5 and APAFIS number 13387-2017122712209790 v9), the Universities of Turin and Saarland and by the National Council on Animal Care of the Italian Ministry of Health (authorization number 813/2018-PR) and the Department for Environment and Consumer Protection - Veterinary Section, Cologne, North Rhine-Westphalia, Germany. All experiments were performed in accordance with the guidelines for animal use specified by the European Union Council Directive of 22 September 2010 (2010/63/EU).

The sex, age and number of the animals used are specified. Most male and female mice used in this study were sexually naive; however, for the female-odor-mediated LH-release protocol, all male mice were sexually experienced following three confirmed successful breeding sessions. Investigators were blind to the genotype or treatment group of animals. Experiments were designed to minimize the number of animals used. C57BL/6J GnRH::Cre (Tg(Gnrh1::cre)1Dlc)¹⁷, *Gnrh::gfp* mice¹⁷ and C57BL/6J GnRHR::IRES-Cre (GRIC)/eR26-τGFP³⁵ and the Kiss1-IRES-Cre⁵⁹ mouse lines were generous gifts from C. Dulac (Howard Hughes Medical Institute) and U.B. (University of Saarland School of Medicine, D-66421 Homburg, Germany).

iDISCO+

Head decalcification. When iDISCO+ was performed on intact mouse heads, decalcification of the samples was required before the pretreatment step. Decalcification was achieved by immersion of the heads in a solution of 20% disodium EDTA in PBS, for 2–3 days at room temperature (RT) with rotation. Samples were then rinsed in PBS and kept at $4\,^{\circ}\text{C}$ until further processing.

Sample pretreatment with methanol. Samples were dehydrated in a gradient of 40%, 60%, 80% and 100% methanol and 100% methanol in PBS for 1 h each at RT on a rotating wheel, before overnight delipidation in a solution of 33% methanol/66% dichloromethane (DCM; Sigma-Aldrich) at 4 °C. Next, samples were rinsed twice in 100% methanol for 1 h and bleached in 5% hydrogen peroxide in methanol at 4 °C overnight. Finally, samples were washed in 100% methanol for 1 h and gradually rehydrated in 80%, 60% and 40% methanol (1 h each) and PBS (twice for 1 h).

Whole-mount immunolabeling. Samples were incubated at RT on an adjustable rotator in a blocking solution of PBS containing 0.2% gelatin (Sigma), 0.5% Triton X-100 (Sigma-Aldrich) and 0.05% sodium azide (PBS-GT) for 4 days. Samples were transferred to a PBS-GT solution containing the primary antibodies anti-GnRH (rat number EH1044; dilution 1:10,000; produced by E.H., Laboratory of Reproductive Neurobiology, Institute of Experimental Medicine, Budapest, Hungary),

anti-GFP (chicken, dilution 1:5,000, Aves Labs GFP-1020, GFP3717982) and anti-RFP (rabbit, dilution 1:1,000, Rockland 600-401-379, 46510) and placed at 37 °C in rotation for 3 weeks. This was followed by several washes of 1.5 h in PBS-GT at RT over 2 days. Next, samples were incubated with secondary antibodies (goat anti-rabbit Alexa Fluor 488, Invitrogen A11008, 2284594; goat anti-chicken Alexa Fluor 568, Invitrogen A11041, 1383072; goat anti-rat Alexa Fluor 647, Invitrogen A21247, 2089926; dilution 1:1,000) in PBS-GT and placed at 37 °C in rotation for 10 days. Finally, samples were washed several times in 2 days for 1.5 h each.

Tissue clearing. Samples were dehydrated in a gradient of 40%, 60%, 80% and 100% methanol and 100% methanol in PBS for 1 h each at RT on a rotating wheel and protected from the light. Delipidation was achieved with an overnight incubation in 33% methanol/66% DCM, and followed by two washes of 2 h with 100% DCM. Samples were cleared in dibenzyl ether (DBE; Sigma-Aldrich) for 2 h at RT with rotation and protected from the light. Finally, samples were moved into fresh DBE and stored in glass tubes in the dark and at RT until imaging.

3D imaging and analysis. 3D imaging was performed on the Ultramicroscope I (LaVision BioTec) equipped with $\times 1.1/0.1$ -NA and $\times 4/0.3$ -NA objectives and an Andor Neo 5.5 sCMOS camera. The light sheet was generated by a laser (wavelength 488 nm, 568 nm or 647 nm, Coherent Sapphire Laser, LaVision BioTec) and two cylindrical lenses. Samples were placed in an imaging reservoir made of 100% quartz (LaVision BioTec) filled with DBE and illuminated from the side by the laser light. InspectorPro v5.1.363 software (LaVision BioTec) was used for image acquisition: the z-step between each image was fixed at 4 μ m, and for tile imaging the overlap was set to 10%. The resulting sequences of TIFF files were processed with Imaris Converter and Imaris Stitcher (Oxford Instruments), and Imaris (Oxford Instruments), all v9.8, for visualization and analysis.

Tissue preparation for immunohistochemistry

Mice were deeply anesthetized via an intraperitoneal injection of a 3:1 ketamine (50–100 mg per kg body weight) and xylazine (5–10 mg per kg body weight) solution. All the animals were transcardially perfused with a 0.9% saline solution followed by cold 4% paraformaldehyde in 0.05 M Tris-buffered saline (TBS), pH7.6. Brains were removed from the skull and post-fixed for 4–6 h in 4% paraformaldehyde at 4 °C. Post-fixing was followed by a cryopreservation step with a 30% sucrose solution in 0.05 M TBS pH7.6 at 4 °C. Brains were sectioned by a microtome (Leica). Free-floating coronal sections (35 μ m) were collected in multi-well dishes to provide representative series of the brain. The sections were stored at –20 °C in an antifreeze solution (30% ethylene glycol, 20% glycerol, 50% 0.05 M TBS; pH7.6) until use.

Immunohistochemistry

Sections were rinsed in 0.05 M TBS, pH 7.6, to remove the antifreeze solution and incubated in a blocking solution (0.05 M TBS; 0.3% Triton X-100; 0.25% BSA; 2% normal donkey serum for 1 h at RT. Then sections were incubated in a solution containing 0.05 M TBS, 0.3% Triton X-100, 1:100 of normal donkey serum and primary antibodies for 48 h at 4 °C. Sections were rinsed in 0.05 M TBS, pH 7.6, and then incubated in the incubation solution with appropriate fluorochrome-conjugated secondary antibodies, for 2 hat RT. The primary antibodies used were anti-GnRH (rat; dilution 1:10,000; produced by E.H., Laboratory of Endocrine Neurobiology, Institute of Experimental Medicine, Budapest, Hungary; 1044), anti-GnRH (rabbit polyclonal antibody; dilution 1:2,000; Proteintech 26950-1-AP, 49588), anti-RFP (rabbit; dilution 1:1,000; Rockland 600-401-379, 46510), anti-GFP (chicken; dilution 1:1,000; Aves Labs GFP-1020, GFP3717982), anti-cFos (mouse; dilution 1:500; GeneTex GTX 60996, 822002386), anti-ERα (rabbit polyclonal; dilution 1:1,000; Millipore 06-935, 3586856), anti-AR (rabbit; dilution

1:500; Millipore 06-680, 3811357) and anti-PR (rabbit; dilution 1:500; Sigma SAB4502184, 210558). Secondary antibodies used were donkey anti-rabbit Alexa Fluor 488 (Invitrogen A21206, 2668665), donkey anti-rabbit Alexa Fluor 568 (Invitrogen A10042, 2540901), donkey anti-chicken Alexa Fluor 488 (Jackson ImmunoResearch 703-545-155, 1649925), donkey anti-rat Alexa Fluor 488 (Invitrogen A21208, 1979698), donkey anti-rat Alexa Fluor 594 (Invitrogen A21209, 2400917), donkey anti-rat Alexa Fluor 647 (Invitrogen A78947, 2497480) and diluted at 1:500. Finally, sections were coverslipped with Fluoromount-G with DAPI (Invitrogen 00-4959-52), as an antifade mounting medium.

Serial section GnRH^{OB} 3D reconstruction

The brains of two female mice, of CD1 and C57BL/6J strains, were cut on a cryostat in 40- and 50-mm-thick floating sections, respectively, and labeled with anti-GnRH. For both specimens, 35 sections spanning the caudal part of the OB were acquired on a Leica TCS SP5 confocal microscope (Leica, Germany) using a $\times 40/1.25$ oil objective (NA 0.16) with a $0.75 \times 0.75 \times 3$ mm voxel size for CD1 and a $0.75 \times 0.75 \times 2.5$ mm voxel size for C57BL/6J specimens. Confocal stacks of subsequent sections were aligned. Stitched tiles were imported in TrackEM2, and corresponding points were identified among corresponding superficial focal planes and subsequently aligned applying a rigid-body transformation. The aligned sequences of 355 and 461 focal planes were exported for analysis using ImageJ or Imaris 9.8 (Oxford Instruments). For 3D rendering, the z-axis was scaled relative to the x-y plane to match the expected length of the reconstructed volume from cryostat sectioning (1,400 mm and 1,750 mm, respectively.)

Cell counting

GnRH cell counting through the rostrocaudal extent of the OBs was performed from 35 μ m coronal sections by an investigator who was blind to the genotype of the animals. For each mouse, cell numbers were obtained using one of four series of sections and multiplied by four. GnRH neurons were visualized using an Axio Imager Z2 ApoTome microscope equipped with a motorized stage (Zeiss) and an ORCA-Flash 4.0 V2 camera (Hamamatsu) driven by the ZEN 2.3 Blue edition imaging software (Zeiss) to account for the deepness of the tissue. Cell counting was performed by an investigator who was blind to the genotype of the animals.

Image acquisition and analysis

ImageJ (National Institutes of Health) and Adobe Photoshop 22.1.0 (Adobe Systems) were used to process, quantify, adjust and merge the photomontages. Figures were prepared using Adobe Photoshop (Adobe Systems, RRID SCR_014199).

snRNA-seq

Tissue collection. The OBs of 18-week-old male C57BL/6N mice (Charles River) were microdissected and immediately frozen in liquid nitrogen. Two biological replicates were analyzed, and each replicate comprised three OBs.

Tissue homogenization and FACS-snRNA-seq. Tissue homogenization was carried out in a 7 ml Dounce tissue grinder. Frozen OBs were transferred into 1 ml of ice-cold homogenization buffer (NIM 2, 0.4% IGEPAL (vol/vol), 0.4 U μl^{-1} RNasin, 0.2 U μl^{-1} Superasin, 0.15 mM spermine and 0.5 mM spermidine). Homogenization was carried out by 10 strokes of loose pestle 'A' followed by 20 strokes of tight pestle 'B' after a 5-min incubation on ice. Homogenates were filtered through 20- μ m cell strainers and centrifuged at 1,000g for 10 min at 4 °C. Supernatant was removed by decanting and the nuclei pellets were resuspended in 1 ml FACS buffer (0.15 mM spermine, 0.5 mM spermidine, 0.2 U μl^{-1} protector RNase inhibitor, 0.4% IGEPAL (vol/vol), 1% BSA (wt/vol) and 1 μ M DAPI in RNAase-free PBS). Next, 300 μ l of suspension from each of three individual nuclear isolations was combined for one replicate

and subjected to FACS. Cell sorting was performed with a FACSAria III system (BD Biosciences) using a 70- μm nozzle. Gating for forward and side scatter was used for doublet discrimination, and sorting was performed selecting singlets in the DAPI+ population. In total, 100,000 events were directly sorted into 10 μl of diluted nuclei buffer reaching a final concentration of -1% BSA (wt/vol) and 0.2 U μl^{-1} protector RNase inhibitor

snRNA-seq: RNA preparation, library generation, sequencing and analysis. Libraries were prepared using the Chromium Next GEM Automated Single Cell 3' Reagent Kit v3.1 (10x Genomics, 1000268) following the manufacturer's instructions. Libraries were sequenced on a HiSeq 4000 (Illumina) with 150-bp paired-end sequencing of read 2.

A total of 13.163 cells from two different sequencing runs were analyzed, comprising 1.02 billion total reads for an average read count of 77,489 per cell. Raw reads were processed with Cell Ranger (v.6.1.2) and aligned to Ensembl genome GRCm39 (release 105 cr6.1.2)⁶⁰. Approximately 92.4% of reads mapped confidently to the genome. All cells with at least 200 detected genes and 500 unique molecular identifiers were retained. Datasets were further merged and analyzed with Seurat (v4.1.1), and cells with mitochondrial genes greater than 5% were discarded. Cells with at least one read for Gnrh1 were annotated as Gnrh-positive cells, which totaled 54 cells or about 0.4% of total cells. Read counts were normalized by a scaling factor of 10,000 followed by log transformation. The data were then scaled and centered using the ScaleData function with default parameters. A principal component analysis was performed, and all dimensions where the percentage change in variation against the next subsequent principal component was greater than 0.1% were used to construct a nearest-neighbor graph using the Find-Neighbors function. Cells were clustered with a resolution of 0.2 and visualized by uniform manifold approximation and projection. Clusters $were \, manually \, annotated \, using \, Find All Markers \, functions \, to \, determine \, and \, to \, determine \, and$ each cluster's significant marker genes. Markers were used to annotate clusters by matching them to known features of OB populations^{61,62}. Some clusters were further subclustered using the FindSubCluster function if their expression profile matched known neuronal subtypes from the literature. One cluster containing a small amount of contaminating olfactory sensory neurons was manually removed as a quality-control measure. Gene Ontology term analysis was performed using enrichGO for all sub-ontologies. All visualizations were created using the Seurat package with modifications performed using ggplot2 (v.3.3.6).

Isolation of OB and rPOA GnRH neurons using FACS

The OBs and the preoptic area of *Gnrh::Gfp* mice were microdissected and enzymatically dissociated using a papain dissociation system (Worthington Biochemical Corporation, LK003150) to obtain single-cell suspensions. Enzymatic dissociation was carried out by an incubation with papain at 37 °C for 30 min with 300 rpm agitation. Homogenization was carried out by mechanical dissociation with a pipette followed by a centrifugation during 5 min at 1,000g at 4 °C to remove supernatant and resuspension with ovomucoid solution. Another centrifugation was carried out to remove and resuspend the pellet of cells with 300 ml FACS buffer (10% HBSS (vol/vol), 5% glucose). FACS was performed using a SONY SH800 Sorter Cytometer device using a 70-µm sorting chip. The sort decision was based on measurements of GFP fluorescence (excitation 488 nm, 50 mW detection: GFP bandpass 530/30 nm, autofluorescence bandpass 695/40 nm) by comparing cell suspensions from Gnrh::Gfp cortex. For each animal, 100 to 300 cells were sorted directly into 10 μ l of extraction buffer (0.1% Triton X-100 (Sigma-Aldrich) and 0.4 U μl⁻¹RNAase OUT (Life Technologies). Gating strategy diagrams are shown in Supplementary Fig. 1.

FACS data analysis

FACS data were acquired and analyzed using BD FACSDiva 8.0 (BD Biosciences) and Kaluza 2.0 (Beckman Coulter) software.

RT-qPCR analyses

The OBs and the POA of *Gnrh::Gfp* mice were microdissected and enzymatically dissociated using papain to obtain single-cell suspensions. FACS was performed using a SONY SH800 Sorter Cytometer device. The sort decision was based on measurements of GFP fluorescence (excitation 488 nm, 50 mW detection: GFP bandpass 530/30 nm, autofluorescence bandpass 695/40 nm) by comparing cell suspensions from *Gnrh::Gfp* cortex. For each animal, 100 to 300 cells were sorted directly into 10 μ l of extraction buffer (0.1% Triton X-100 (Sigma-Aldrich) and 0.4 U μ l⁻¹ RNase OUT (Life Technologies).

For gene expression analyses, mRNAs obtained from FACS-sorted GnRH neurons were reverse transcribed using SuperScript III Reverse Transcriptase (Life Technologies) and a linear pre-amplification step was performed using the TagMan PreAmp Master Mix Kit protocol (P/N 4366128, Applied Biosystems). Real-time PCR was carried out on the Applied Biosystems 7900HT Fast Real-Time PCR System using exon-boundary-specific TagMan gene expression assays (Applied Biosystems) as follows: Gad1 (Gad1-Mm04207432 g1), Gad2 (Gad2-Mm00484623_m1), Gnrh1 (Gnrh1-Mm01315605_m1), Gnrhr (Gnrhr-Mm00439143_m1), Grin1 (Grin1-Mm00433790_m1), Grin2b (Grin2b-Mm00433820_m1), Grin3a (Grin3a-Mm01341723_m1), Kiss1 (Kiss1-Mm03058560_m1), Kiss1r (Kiss1r-Mm00475046_m1), Slc17a6 (Slc17a6-Mm00499876 m1), Slc17a7 (Slc17a7-Mm00812886 m1), Or14j2 (Olfr113-Mm00836606_s1), Or11l3 (Olfr323-Mm00526507_ s1), Vmn1r209 (Vmn1r209-Mm02393496_s1) and Vmn2r1 (Vmn2r1-Mm00498222 m1). Control housekeeping genes were r18S (r18S-Mm3928990 g1) and Actb (Actb-Mm00607939 s1). Gene expression data were analyzed using SDS 2.4.1 and Data Assist 3.0.1 software with R18S and actin as control housekeeping mRNAs.

RNAscope FISH

FISH was performed on 14-µm fresh frozen sections of the OB and the VNO of adult male mice using the RNAscope Multiplex Fluorescent Kit v2 according to the manufacturer's protocol (Advanced Cell Diagnostics). Specific probes were used to detect *Gnrh1* (476281, XM_006518564.3, target region 81–914), *Vmn2r1* (1218801, NM_001384924.1, target region 150–2,986) and *Olfr323* (1218821, NM_146376.2, target region 2–958) mRNAs. Hybridization with a probe against the *Bacillus subtilis* dihydrodipicolinate reductase (*dapB*) gene (320871) was used as a negative control.

Electrophysiology

Brain slice preparation. Electrophysiological recordings were performed on living brain slices from 8- to 12-week-old mice. Mice were exposed to isoflurane anesthesia and killed by decapitation. The brain was dissected and rapidly placed in ice-cold artificial cerebrospinal fluid (aCSF) containing: 120 mM NaCl, 3.2 mM KCl, 1 mM NaH₂PO₄, 26 mM NaHCO₃, 1 mM MgCl₂, 2 mM CaCl₂, 10 mM glucose (300 mOsm, pH7.4) and bubbled with 95% O₂ to 5% CO₂. Then, 200- μ m sagittal slices containing the OBs and the rPOA were cut using a VT1200 vibratome (Leica). Slices were incubated at 34 °C in oxygenated aCSF for a recovery period of 1 h and then placed at RT until patch-clamp recording.

Patch-clamp recording

Individual brain slices were placed in a submerged recording chamber (Warner Instruments) and continuously perfused at a rate of 3 ml min with oxygenated a CSF maintained at 32.8 °C by a heater controller (TC-344C-Warner Instrument). GnRH neurons were visualized under ×10 and ×40 magnification using an upright fluorescence microscope with infrared differential interference contrast (DM-LFSA, Leica) and an ORCA-Flash4.0 digital CMOS camera (Hamamatsu). Recording pipettes were pulled from borosilicate glass capillaries (1.5-mm outer diameter, 1.12-mm inner diameter; World Precision Instruments) using a P1000 Flaming Brown puller (Sutter Instruments) and had a resistance of 6 M Ω . Whole-cell patch-clamp recordings were performed using a

MultiClamp 700B Amplifier, digitized with the Digidata 1322A interface and acquired with pClamp 10.2 software (Molecular Devices).

For whole-cell current-clamp recording, pipettes were filled with an internal solution containing 140 mM potassium gluconate, 10 mM potassium chloride, 1 mM EGTA, 2 mM $\rm Na_2$ -ATP and 10 mM HEPES, pH7.3, with potassium hydroxide.

For whole-cell voltage-clamp recording of GABAergic currents, pipettes were filled with high-chloride solution containing 140 mM potassium chloride, 10 mM HEPES, 5 mM EGTA, 4.0 mM Mg-ATP, 0.4 mM Na-GTP and 0.1 mM calcium chloride, with pH adjusted to 7.3 by sodium hydroxide. To isolate GABAergic currents, glutamatergic currents were blocked with a combination of 20 μ M 6-cyano-7-nitroquinoxaline-2,3 -dione and 100 μ M D-2-amino-5-phosphonovaleric acid. Membrane potential of GnRH neurons was held at –60 mV.

For whole-cell voltage-clamp recording of glutamate currents, pipettes were filled with solution containing 125 mM D-gluconic acid, 80 mM cesium chloride, 10 mM HEPES, 5 mM EGTA, 4 mM Mg-ATP, 0.4 mM Na-GTP and 0.1 mM calcium chloride, with pH adjusted to 7.4 by cesium hydroxide. To isolate glutamatergic currents, GABAergic currents were blocked with a combination of 5 μ M gabazine and 2 μ M CGP35348. Membrane potential of GnRH neurons was held at –70 mV. Under these experimental conditions, NMDA receptors are blocked by Mg $^{2^+}$; thus, only AMPA/kainate receptor-mediated currents are recorded.

For hM3Dq-expressing GnRH neurons, 1 μ M CNO was added in the aCSF bathing medium by the use of the perfusion system after stable baseline recording. Recordings were analyzed using Clampfit 10.2 pClamp software (Molecular Devices). The membrane potential and mean firing rate for spontaneous activity and amplitude and mean firing rate for currents were determined before and during the bath application of drugs. Neurons were considered responsive if there was a >20% change in firing rate during CNO activation. Only cells that showed less than 20% change in access resistance throughout the recording were included in this study. Junction potential was corrected in the data analysis.

Stereotaxic surgeries for AAV injections

Adult mice were anesthetized with 2% isoflurane and placed in a stere-otaxic apparatus (Stoelting) with head and nose fixed. All experiments were performed with sterile instruments and aseptic conditions. Mice were maintained on a warm platform at 37 °C during anesthesia. A small skin incision was performed to expose the animal skull and two injection sites were drilled across the skull to allow injection of AAVs. The skin was then sutured, and animals were allowed to recover for at least 2 weeks.

In vivo calcium imaging

Experimental procedures involving animals have been approved by the University of Turin Ethical Committee and by the National Council on Animal Care of the Italian Ministry of Health (authorization number 813/2018-PR). All experiments were carried out according to the guidelines of the European Communities Council Directive. All animals were housed under a 12-h light-dark cycle in individually ventilated cages, with a maximum of five animals per cage. Experiments were performed on adult (12-16-week-old) GnRH::Cre male mice. The AAVs pGP-AAV-CAG-FLEX-jGCaMP7s-WPRE (AAV Retrograde, 104405-AAVRg) and pAAV.CAG.Flex.GCaMP6s.WPRE.SV40 (AAV9, 100842-AAV9) were purchased from Addgene. Briefly, mice were anesthetized by isoflurane inhalation and placed into a stereotaxic apparatus (Stoelting). Mice were maintained on a warm platform at 37 °C during anesthesia. A small skin incision was performed to expose the animal skull, and two injection sites were drilled across the skull to allow injection of AAVs. GnRH-positive neurons in the MOB were targeted by using the following stereotaxic coordinates: 6.4 mm anterior and 1.2 mm lateral to bregma, z = 1 mm for the first injection

site, and 3.9 mm anterior and 1.8 mm lateral to bregma, z=1.5 mm for the second injection site. In total, 500 nl of a mixture of pAAV.CAG. Flex.GCaMP6s and pGP-AAV-CAG-FLEX-jGCaMP7 (1:4 and 1:2 in 0.9% saline, respectively) were slowly injected in each injection site over a period of 30 min. The skin was then sutured, and animals were allowed to recover for at least 2 weeks.

Two-photon functional imaging and odor delivery

Responses of GnRH-positive neurons to odors were recorded and characterized by performing in vivo two-photon functional imaging on GCaMP-injected mice under anesthesia. Animals received a mixture of ketamine (50 mg per kg body weight) and xylazine (4 mg per kg body weight) by intraperitoneal injection for anesthesia. The skin was then removed to expose the skull and a metal head-plate was attached to the animal skull and centered over the MOB. A small craniotomy $(-300\times300~\mu\text{m}^2)$ was opened on top of the most lateral-posterior part of the MOB carefully maintaining the dura intact. The surface of the brain was kept moist with normal HEPES-buffered aCSF. Body temperature was maintained at 37 °C with a heating pad. The depth of anesthesia was assured by monitoring respiration rate, eyelid reflex, vibrissae movements and reactions to pinching the tail and toe. All incisions were infiltrated with lidocaine.

Animals were placed under a standard two-photon laser-scanning microscope (Nikon A1RMP) coupled to a Chameleon Ultra II (Coherent; excitation wavelength, 920 nm). The activity of GnRH-positive neurons was monitored by imaging GCaMP fluorescence, collected via a ×16 objective (Nikon CFI75 LWD 16xW NIR, 0.80 NA, 3.0 mm WD). Signals were acquired by collecting temporal series (t-series) of images at an acquisition frame rate of 1.1-3 Hz at laser power between 20 and 40 mW. To test for odor responses in GnRH-positive neurons, a custom-made olfactometer was used for odor delivery. The system was equipped with a common source of fresh air which was split into two parallel tubing systems to deliver either air only or a single odor. The airflow was kept constant throughout the entire recording and odors were delivered by quickly switching between the two parallel ways. The tubing system reached the animal nose at about 0.5 cm. Each odor was delivered by loading 50 µl of odor solution in the olfactometer. Stimuli consisted of fresh urine from female mice in estrous phase, fresh urine from male mice, saline solution (0.9% NaCl in distilled water) and methyl butyrate (Sigma, 246093; 10 ppm in mineral oil). For each recorded cell, at least two control (no odor) and two odor trials were run. For experiments in Fig. 2, the odor trial consisted of 120 s of fresh air, 30 s of odor exposure and 150 s of fresh air. For experiments shown in Extended Data Fig. 4, each trial consisted of 90 s of fresh air, 30 s of odor exposure and 90 s of fresh air. At the end of each experiment, animals were perfused, and the brains collected for histological analysis.

Two-photon data analysis

Temporal series recorded by two-photon imaging were first imported into the open-source ImageJ/Fiji software and preprocessed to extract the fluorescence signal. A region of interest was drawn following the cell profile, and the average fluorescence intensity in the defined region was evaluated for each frame. The temporal profile of cell fluorescence was extracted for all trials from each recorded cell and analyzed using MATLAB software (TheMathWorks, R2021B). Fluorescence signals were first downsampled at 1 Hz to allow comparison between different neurons acquired at different acquisition frequency and then computed as $dF/F_0 = (F(t) - F_0)/F_0$, where F(t) is the fluorescence value at time t, and F_0 is the fluorescence baseline which was calculated as the average intensity across the whole t-series. Only cells with at least two odor trials were considered to evaluate odor responses. For each neuron, traces were aligned with the stimulus onset and averaged. The maximum dF/F_0 within 10 s after the stimulus onset was calculated on the averaged trace. To classify responsive cells, a threshold was set as the baseline fluorescence value +3 standard deviations (calculated in the 20 s before the stimulus onset). Neurons with a maximum dF/F_0 exceeding the threshold were classified as responsive; otherwise, they were classified as not responsive. To test if odors evoked a significant response compared to fresh air presentation, statistical analysis was performed comparing responses to odors and to fresh air only, using the parametric paired t-test. Values are expressed as the mean \pm s.e.m.; P values from statistical comparisons are shown in the graphs. To evaluate response latency for positively modulated cells, we fitted the calcium trace with a straight line considering the stimulus onset and the peak of response. The intersection between the straight line and the line at zero value of dF/F_0 was considered as response latency.

In vivo chemogenetic manipulation

Stereotaxic coordinates according to the Paxinos mouse brain atlas were ± 3.4 mm anteroposterior, ± 0.3 mm mediolateral and ± 2.6 mm dorsoventral to target the olfactory GnRH neurons (glomerular and olfactory nerve layer). Syringes were left in situ for 5 min before and 10 min following injection. For chemogenetic activation and inhibition studies, GnRH::Cre mice received simultaneous bilateral injection of 250 nl (50 nl min $^{-1}$ rate) of a solution mix into the OBs containing both AAV9-hSyn-DIO-hM3D(Gq)-mCherry (Addgene, 44361-AAV9; activator DREADD) and KORD (k-opioid receptor p.Asp138Asn mutant; inhibitor DREADD; AAV8-hSyn-dF-HA-KORD-IRES-mCitrine; Addgene, 65417-AAV8). pAAV-hSyn-dF-HA-KORD-IRES-mCitrine was a gift from B. Roth (Addgene, 65417).

Stereotaxic coordinates according to the Paxinos mouse brain atlas were -1.9 mm anteroposterior; ± 2.0 mm mediolateral and -5.0 mm dorsoventral to target the olfactory GnRH neurons sending projections to the MeA. Syringes were left in situ for 5 min before and 10 min following injection. For chemogenetic inhibition studies, mice received simultaneous bilateral injection of 300 nl (50 nl min $^{-1}$) of AAV-hSyn-DIO-hM4D(Gi)-mCherry (Addgene, 44362).

pAAV-hSyn-DIO-hM4D(Gi)-mCherry (Addgene, 44362) was a gift from B. Roth. Bilateral injections were performed using a 2 μ l Hamilton syringe (7000 series; Hamilton Company).

Cell-specific genetic ablation

For Caspase-3 studies, mice received simultaneous bilateral injection of 500 nl (50 nl min⁻¹) of AAV9-flex-taCasp3-TEVp. pAAV-kex-taCasp3-TEVp was a gift from N. Shah and J. Wells (Addgene, 45580). Viral preparations (AAV9 packaging) were performed by E. Turco at the University of Turin, Italy.

Retrograde tracing with RetroBeads

Adult male C57BL/6J mice (12–16 weeks old) were anesthetized with 0.3 ml per kg body weight ketamine (Ketavet, Gellini) and 0.2 ml per kg body weight xylazine (Rompun, Bayer), positioned in a stereotaxic apparatus (Stoelting) and injected with a pneumatic pressure injection apparatus (Picospritzer II, General Valve Corporation). Then, 500 nl of carboxylate-modified 0.03 μm FluoSpheres (EUGENE, L-5500; 'Retro-Beads') conjugated with a 490/520 nm fluorophore were injected in each site over a period of 10 min. Injection coordinates were 1.6 mm posterior and 2.7 mm lateral to bregma, z = 4.8 mm and 1.6 mm posterior and 4.8 mm lateral to bregma, z = 4.0 mm with a 30° inclination. The skin was then sutured, and animals were analyzed 2 weeks later.

MeA Kiss neuron-specific Gnrhr knock down

Male Kiss1-IRES-Cre(het)/R26-CAG-LSL-Cas9-P2A-GFP(het) (experimental) and R26-CAG-LSL-Cas9-P2A-GFP(hom) (Jackson strain number 026175; control) mice were bilaterally injected with 1 μ l (100 nl min⁻¹) of AAV2/5-CAG-mCherry_U6-Gnrhr gRNA (1.09 × 10¹³ genome copies per ml) into the MeA. Stereotaxic coordinates according to the Paxinos mouse brain atlas were –1.9 mm anteroposterior, \pm 2.0 mm mediolateral

and –5.0 mm dorsoventral to target the Kiss neurons within this region. The syringe was left in place for 5 min before and 10 min after each injection before withdrawal. The AAV expresses both a guide RNA targeting Gnrhr (ggaagaaagtcacggtcact) and mCherry and was packaged using standard triple-transfection methods in HEK293T cells.

LH and testosterone ELISA

Following behavioral experiments, serial blood samples were collected at baseline, -6 min, considering time -1 min as the start of saline (vehicle solution) or CNO (1 mg per kg body weight) injections or female smell exposure. Briefly, 4 μ l of full blood was collected from the tail every 6 min over 1 h. Samples were collected in 50 μ l of 0.01 M PBS-0.05% Tween (PBS-T) and immediately snap frozen in dry ice. Blood samples were stored at $-80\,^{\circ}\text{C}$ until being processed for the LH ELISA (described below). Regarding the testosterone ELISA, blood samples were collected 1.5 h after saline (vehicle solution) or CNO (1 mg per kg body weight) injections or after female smell exposure. Blood was collected from the cheek. Then, samples were centrifuged for 15 min at 4,100 g at 4 $^{\circ}\text{C}$. The supernatant was pipetted and stored at $-80\,^{\circ}\text{C}$ until processing for the testosterone ELISA (described below). Male mice were sexually experienced and trained at least thrice before blood collection.

An ultrasensitive and in-house ELISA was used to measure circulating LH levels as previously reported⁶³. Firstly, 96-well high-affinity binding microplates (9018; Corning) were coated with a bovine LHβ518B7 monoclonal antibody (1:1,000 dilution in 0.01 MPBS) provided by L. E. Sibley (UC Davis). Circulating hormone levels were determined using a mouse LH-RP reference provided by A. F. Parlow (National Hormone & Pituitary Program, USA). A rabbit polyclonal primary antibody for LH (1:10,000 dilution; rabbit anti-serum AFP240580Rb; National Hormone and Peptide Program, USA) and a polyclonal goat anti-rabbit IgG secondary antibody (1:1,000 dilution; DAKO) were also used for this assay. Absorbance was read at a wavelength of 490 nm (Multiskan Ascent Thermo Labsystems, Ascent Software). The concentration of LH in serum samples was determined by interpolating the OD values of unknowns against a nonlinear regression of the LH standard curve. The sensitivity of this routine LH ELISA assay was 0.04 ng ml⁻¹. For chemogenetic studies, the average intra-assay coefficient of variation was 3.6% and the inter-assay coefficient of variation was 9.7%.

A commercially available mouse testosterone ELISA kit was used to measure plasma testosterone levels (DEV9911; Demeditec Diagnostics) in accordance with manufacturer's instructions. The ELISA sensitivity was $0.066\ ng\ ml^{-1}$ and the intra-assay coefficient of variation for testosterone was 9.09%.

Focal exposure with female bedding

The experiment was carried out in the laboratory of U.B. (University of Saarland School of Medicine, D-66421 Homburg, Germany). Two groups of GnRHR::IRES-Cre (GRIC)/eR26- τ GFP male mice were used, each comprising four animals: one group was exposed to the female-soiled bedding and urine for 30 min and euthanized 90 min later (to detect cFos activation); the other group was exposed to water for 30 min and euthanized 90 min later (controls). The female-soiled bedding used for the stimulus was composed of a mixture of soiled bedding and urine, collected from the cages of C57BL6/J estrous females.

Pheromonal stimulation

We tested the ability of urinary pheromones to activate GnRH-expressing neurons located in different areas of the brain. Urine presented to stimulate the animals and for the olfactory preference test was collected from sexually experienced males and from estrous females. Male and female (in estrous) urine was collected and stored at $-80\,^{\circ}\text{C}$ until the day of use. Soiled bedding from sexually experienced males and estrous females was also collected for pheromonal stimulation. Soiled bedding was then stored in a closed bag at $-20\,^{\circ}\text{C}$.

Behavioral assessment

Olfactory preference test. For all behavioral tests, the animal subjects were coded, and the investigator was blind to the genotype or treatment of each animal. The tests were conducted in the animals' home cages to minimize both manipulation and exposure to external stimuli. Tests were performed during the dark phase of the light cycle (>1 h after lights out). An olfactory habituation/dishabituation test was used to examine the animal's ability to discriminate distinct pheromone-containing urine samples (stud males versus estrous females). Pooled and undiluted urine samples collected from groups of male and estrous female mice were used for this test. Next, 50 µl of urine was delivered on a piece of filter paper placed within a petri dish (enabling direct contact with the source) positioned on opposite sides of the cage, equidistant from the cage walls. Naive male test mice were habituated for 30 min to the presence of the object (petri dish) containing a filter paper soaked in saline solution or urine from adult stud males or estrous females and then dishabituated by removing the objects and exposing the animals for 30 min to clean bedding. After the dishabituation period, the animals were then exposed to two urine sources from male and estrous females for 10 min and the time spent investigating the two urine sources was recorded and analyzed using the Behavioral Observation Research Interactive Software (BORIS; version 8.13) and EthoVision video tracking system (EthoVision XT 7.0, Noldus). The time the subject spent poking the nose on the filter paper containing the urine source was recorded. As standard practice in the field^{6,45,64}, a preference score was calculated by dividing the time spent investigating the female compartment minus the time spent investigating the male compartment by the total time spent investigating both compartments. A positive value of the preference score indicates a mate preference directed toward the stimulus female, whereas a negative value indicates a mate preference directed toward the stimulus male.

Sexual behavior test. All behavioral testing was initiated >1 h after onset of the dark cycle. All behavioral tests were videotaped and manually annotated using BORIS software.

Elevated plus maze test. The elevated plus maze test was used to assess the anxiety behavior of the mice. The equipment consisted of two open arms and two enclosed arms by 14.5-cm-high walls forming an elevated cross positioned 50 cm above the floor (36.5 × 6 cm). The mouse was placed in the middle of the maze and allowed to explore the maze for 10 min. A video tracking system (EthoVision XT 7.0, Noldus) recorded movements to calculate the percentage of time spent in the open arms, used as an index of anxiety behavior.

Spontaneous locomotor activity. Spontaneous locomotor activity was assessed in an open field test, using an infrared actimeter (Bioseb). The apparatus consisted of a square arena (45 × 45 cm) with a black polymethyl methacrylate floor and transparent 34-cm-high polymethyl methacrylate walls. Mice were placed in the center of the arena and allowed to explore freely for 10 min. Activity was recorded by two rows of infrared photocell sensors and processed with the Actitrack software (Bioseb).

Statistical analysis

All analyses were performed using Prism 9 (GraphPad). The normality of each group was determined by Shapiro–Wilk test. We did not assume equal variances. Statistically significant P values were considered when P < 0.05. No statistical methods were used to predetermine sample sizes, but our sample sizes are similar to those reported in previous publications 6,45,46,65,66 . Animals were randomized to experimental groups and investigators were blinded to group allocation during data collection and analyses. No samples or animals were excluded from the analysis.

For normal distribution, data were compared using unpaired two-sided Student's *t*-test and one-way and two-way ANOVA followed by Tukey's or Holm–Sidak's post hoc tests. For non-normally distributed values, Mann–Whitney *U* and Kruskal–Wallis tests were used. The Wilcoxon signed-rank test was used in all paired non-parametric analyses comparing before and after drug treatment during olfactory preference tests.

Inclusion and ethics statement

Postmortem human tissues used in our study were collected with ethics permissions obtained from the Regional and Institutional Committee of Science and Research Ethics of Semmelweis University (SE-TUKEB 251/2016), in accordance with the World Medical Association Declaration of Helsinki and the Hungarian Law (1997 CLIV and 18/1998/XII.27. EÜM Decree) in which the latter does not require prior written consent from the deceased person.

Reporting summary

Further information on research design is available in the Nature Portfolio Reporting Summary linked to this article.

Data availability

All data generated or analyzed in the current study are included in the article and its Extended Data. The raw snRNA-seq data conducted in this study have been deposited in Gene Expression Omnibus under accession code GSE268138. For snRNA-seq experiments, raw reads were aligned to Ensembl genome GRCm39 release 105_cr6.1.2. Source data are provided with this paper.

References

- 59. Mayer, C. et al. Timing and completion of puberty in female mice depend on estrogen receptor alpha-signaling in kisspeptin neurons. *Proc. Natl Acad. Sci. USA* **107**, 22693–22698 (2010).
- Zheng, G. X. et al. Massively parallel digital transcriptional profiling of single cells. *Nat. Commun.* 8, 14049 (2017).
- Imamura, F., Ito, A. & LaFever, B. J. Subpopulations of projection neurons in the olfactory bulb. Front. Neural Circuits 14, 561822 (2020).
- Tepe, B. et al. Single-cell RNA-seq of mouse olfactory bulb reveals cellular heterogeneity and activity-dependent molecular census of adult-born neurons. Cell Rep. 25, 2689–2703 (2018).
- 63. Steyn, F. J. et al. Development of a methodology for and assessment of pulsatile luteinizing hormone secretion in juvenile and adult male mice. *Endocrinology* **154**, 4939–4945 (2013).
- Brock, O., Bakker, J. & Baum, M. J. Assessment of urinary pheromone discrimination, partner preference, and mating behaviors in female mice. *Methods Mol. Biol.* 1068, 319–329 (2013).
- Chachlaki, K. et al. NOS1 mutations cause hypogonadotropic hypogonadism with sensory and cognitive deficits that can be reversed in infantile mice. Sci. Transl. Med. 14, eabh2369 (2022).
- 66. Silva, M. S. B. et al. Female sexual behavior is disrupted in a preclinical mouse model of PCOS via an attenuated hypothalamic nitric oxide pathway. *Proc. Natl Acad. Sci. USA* **26**, e2203503119 (2022).

Acknowledgements

We thank all staff of the Lille Neuroscience & Cognition research center for their constant assistance. We thank C. Laloux and Lille

In vivo Imaging and Functional Exploration platform (Univ. Lille, CNRS, Inserm, CHU Lille, Institut Pasteur of Lille, US41-UMS2014 PLBS, France) for technical support during behavioral assessment experiments. We also thank M. Tardivel and A. Bongiovanni (microscopy core facility; The BioImaging Center Lille, BICeL, US41-UMS2014 PLBS, France), N. Jouy (cytometry core facility, BICeL, US41-UMS2014 PLBS, France) and J. Devassine (Animal facility, BICeL, US41-UMS2014 PLBS, France) for expert technical assistance. This work was supported by the European Research Council under the European Union's Horizon 2020 Research and Innovation program (ERC-2016-CoG to P.G., grant agreement no. 725149/REPRODAMH), by the Agence Nationale de la Recherche (ANR-18-CE14-0017, ANR-19-CE16-0021-02 to P.G.) and INSERM-France (grant no. U1172 to P.G. and V.P.). Schematics and drawings were created with BioRender.com.

Author contributions

L.D., S.T. and M.S.B.S. designed and performed the study and were involved in all steps of the paper preparation. J.B. and A.G. performed the bioinformatic analyses. G.T. performed the whole-mount immunohistochemistry experiments. T.L. performed the electrophysiological experiments. A.L. performed the FACS isolation experiments. S.G. performed the RT-qPCR experiments. U.B. provided (GRIC)/eR26-τGFP and the Kiss1-IRES-Cre mouse lines and suggestions on the experiments, supervised the CRISPR genome editing experiments, and edited the paper. A.W. and V.W. designed and produced the AAV2/5-CAG-mCherry U6-Gnrhr gRNA. P.W. performed the stereotaxic injections for the in vivo CRISPR genome editing experiments and was involved in the analysis. E.H and G.R. provided human biological resources and edited the paper. F.L., G.N. and M.F. performed retrobeads tracing experiments and data analyses. S.Z. and S.B. designed and performed the in vivo calcium experiments and wrote the paper. P.P. contributed to experimental designs for the olfactory behavior experiments and edited the paper. S.C.S., M.B. and P.T.P. designed and performed snRNA-seq experiments and curated the data. S.M.S. supervised the bioinformatic analysis and edited the paper. S.R. and V.P. edited the paper. P.G. conceived this study, designed and managed the experimental studies, prepared the figures, and wrote the paper with input from all authors.

Competing interests

The authors declare no competing interests.

Additional information

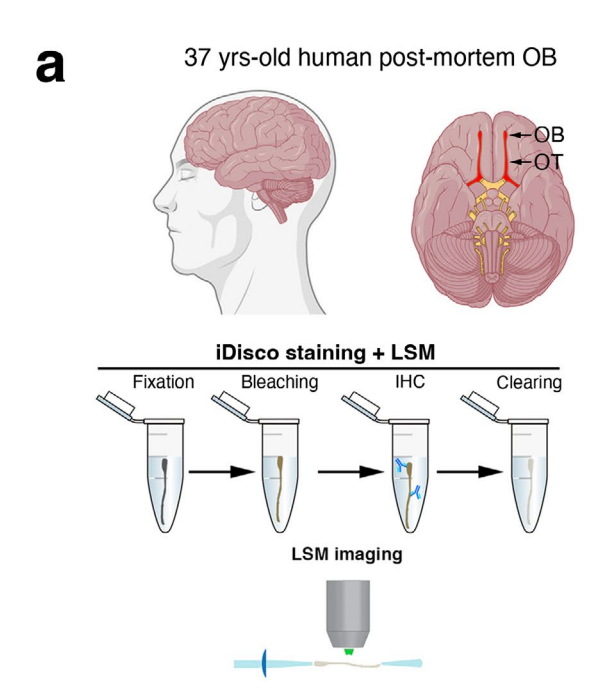
Extended data is available for this paper at https://doi.org/10.1038/s41593-024-01724-1.

Supplementary information The online version contains supplementary material available at https://doi.org/10.1038/s41593-024-01724-1.

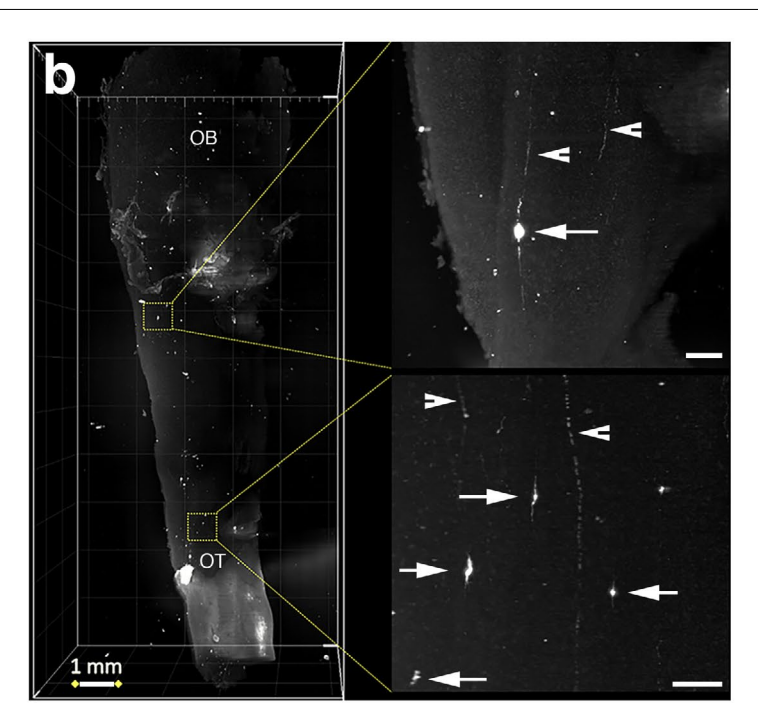
Correspondence and requests for materials should be addressed to Paolo Giacobini.

Peer review information *Nature Neuroscience* thanks Julie Bakker, Dayu Lin and the other, anonymous, reviewer(s) for their contribution to the peer review of this work.

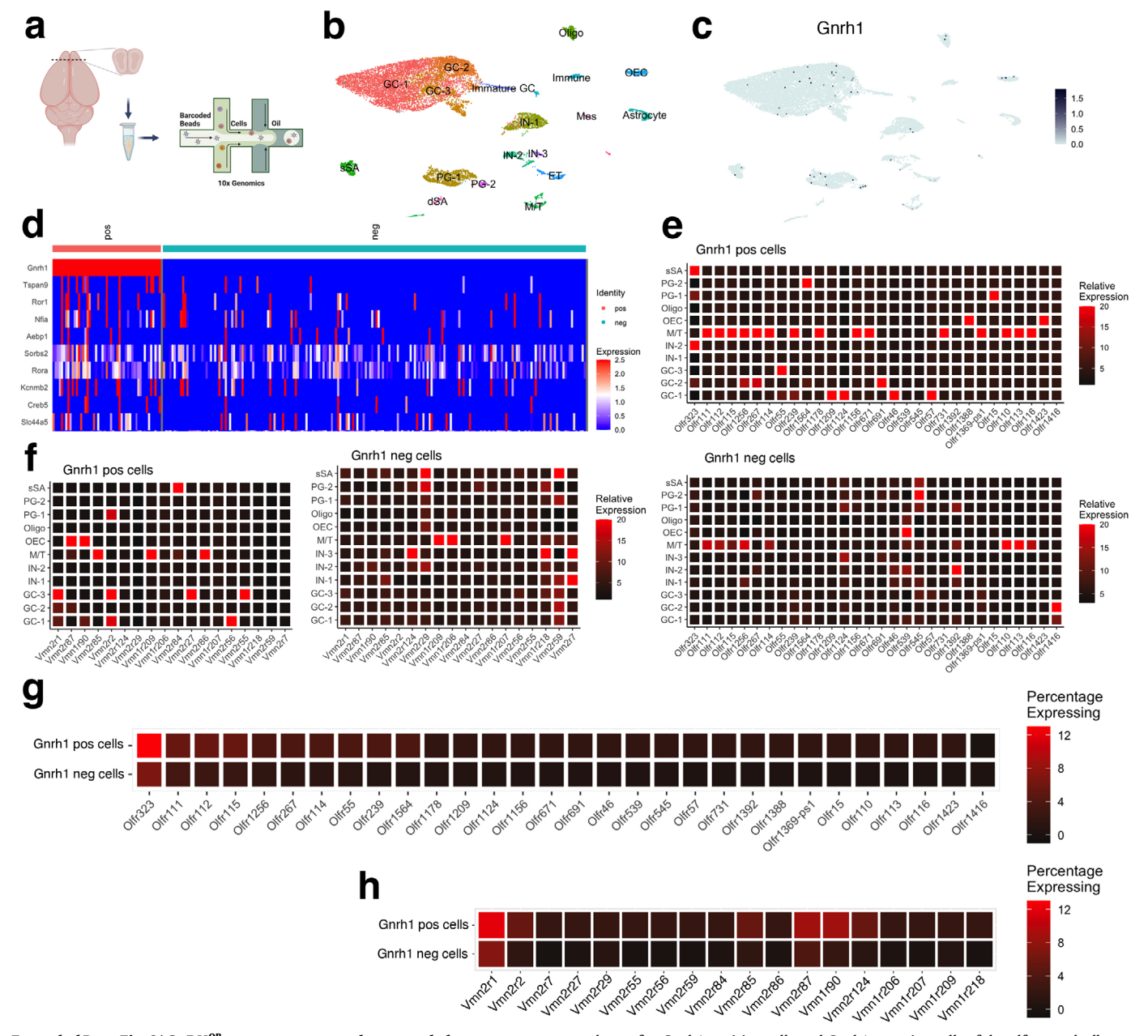
Reprints and permissions information is available at www.nature.com/reprints.



Extended Data Fig. 1 | **Distribution of GnRH neurons within the olfactory bulbs of humans. a**, Top: Lateral and inferior views of a human brain. The olfactory bulb (OB) and the olfactory tract (OT) are depicted in red. Bottom: schematic representation of solvent-based tissue clearing and light-sheet imaging protocol of the human post-mortem olfactory bulbs (OBs). **b**, iDisco+

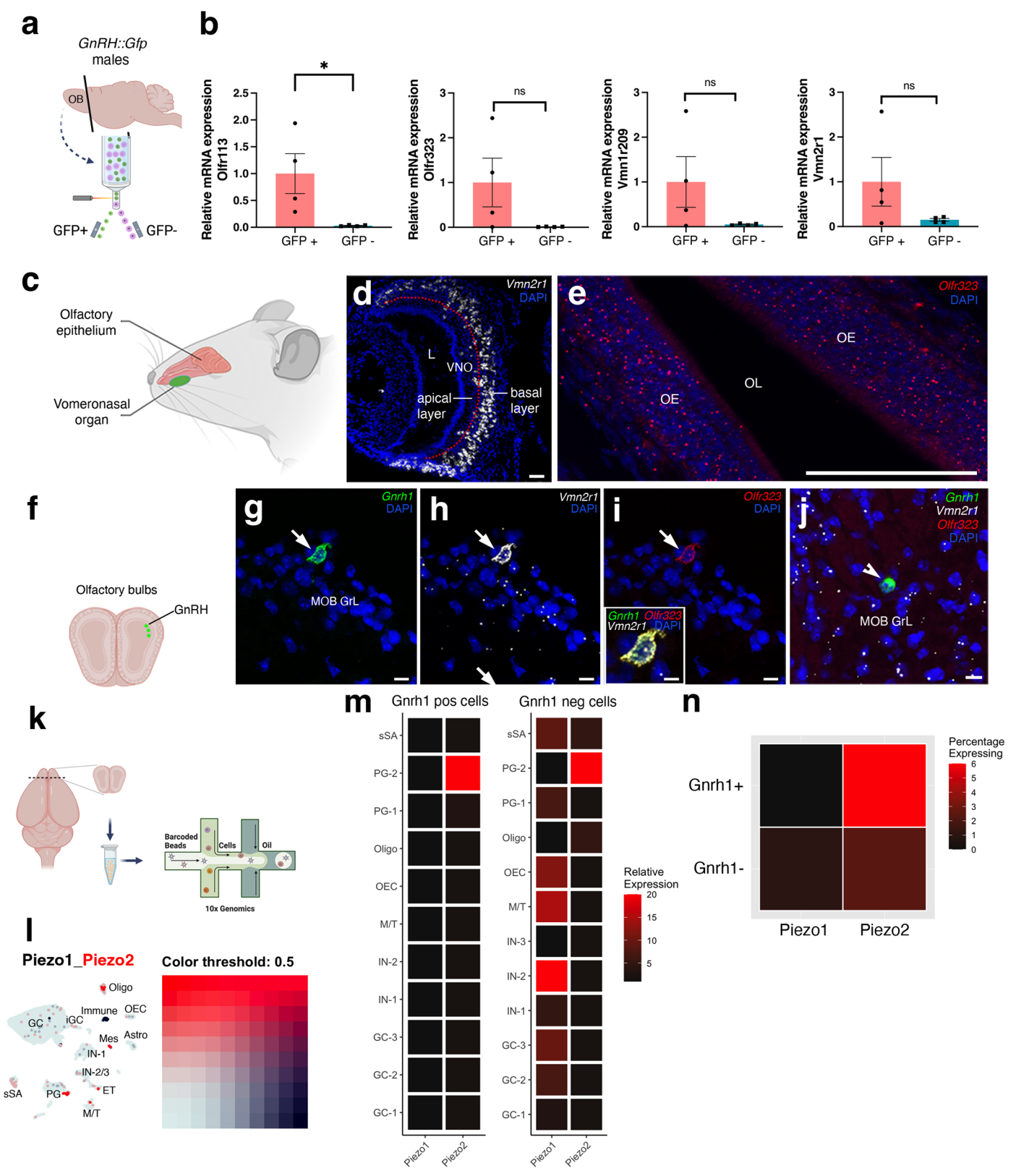


and light-sheet microscopy imaging showing the presence of GnRH neurons (arrows) and fibers (arrowheads) in the OB and OT of a 37-year-old postmortem brain (male). Representative pictures of n=3 postmortem brains of men and women. Scale bars: (**b**) left Fig. 1 mm, right upper figure 20 μ m, right lower figure 50 μ m.



Extended Data Fig. 2 | **GnRH**^{oB} **neurons express odorant and pheromone receptors. a**, Schematic representing single-nucleus RNA sequencing protocol. Two biological replicates were analyzed and each replicate comprised three olfactory bulbs (males, 18-week-old). **b**, UMAP visualization of the OB, colored by major cell types. **c**, UMAP visualization of *Gnrh1* expressing cells in the OB (black dots; other cell types in grey). **d**, Transcriptomic landscape of *Gnrh1*-positive cells compared with *Gnrh1*-negative cells in the OB. **e**, **f**, Heatmaps indicating the relative expression of olfactory and vomeronasal receptors within each neuronal

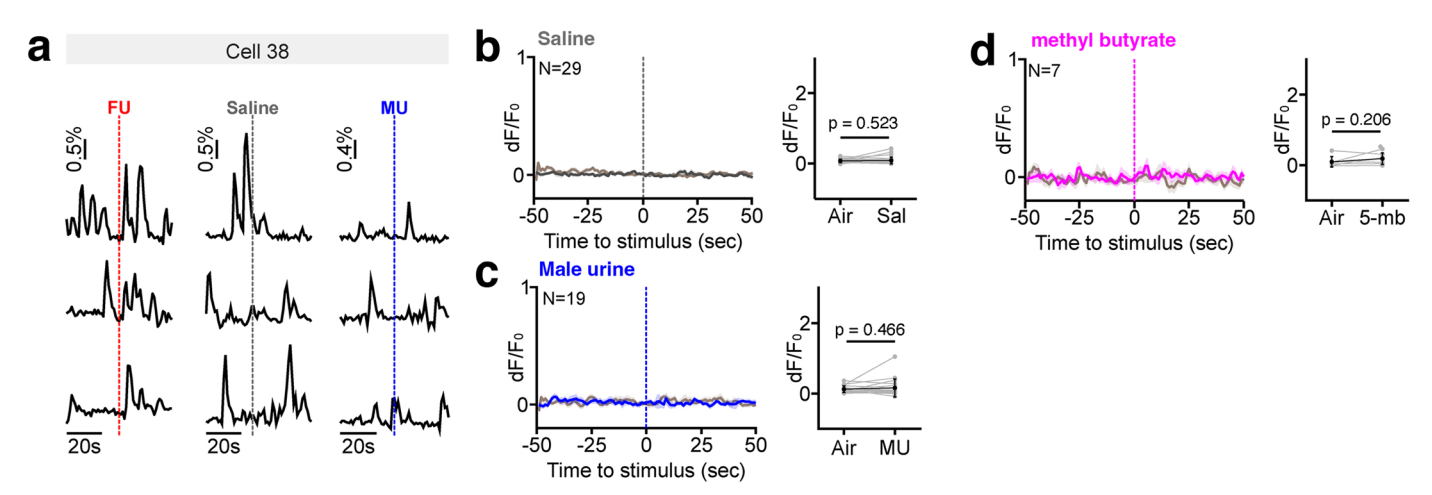
cluster for *Gnrh1*-positive cells and *Gnrh1*-negative cells of the olfactory bulb. **g**, Percentage expression profile of olfactory receptors in *Gnrh1*-positive cells and *Gnrh1*-negative cells of the olfactory bulb. **h**, Percentage expression profile of vomeronasal receptors in *Gnrh1*-positive cells and *Gnrh1*-negative cells of the olfactory bulb. Abbreviations: Oligo, Oligodendrocytes; PG, Periglomerular cells; GC, Granule cells; M/T, Mitral/Tufted cells; OEC, Olfactory ensheathing cells; IN, Inhibitory neurons; sSA, Superficial short axon cells; ET, endothelial cells; MES, mesenchymal cells; dSA, Deep short axon cells.



Extended Data Fig. 3 | See next page for caption.

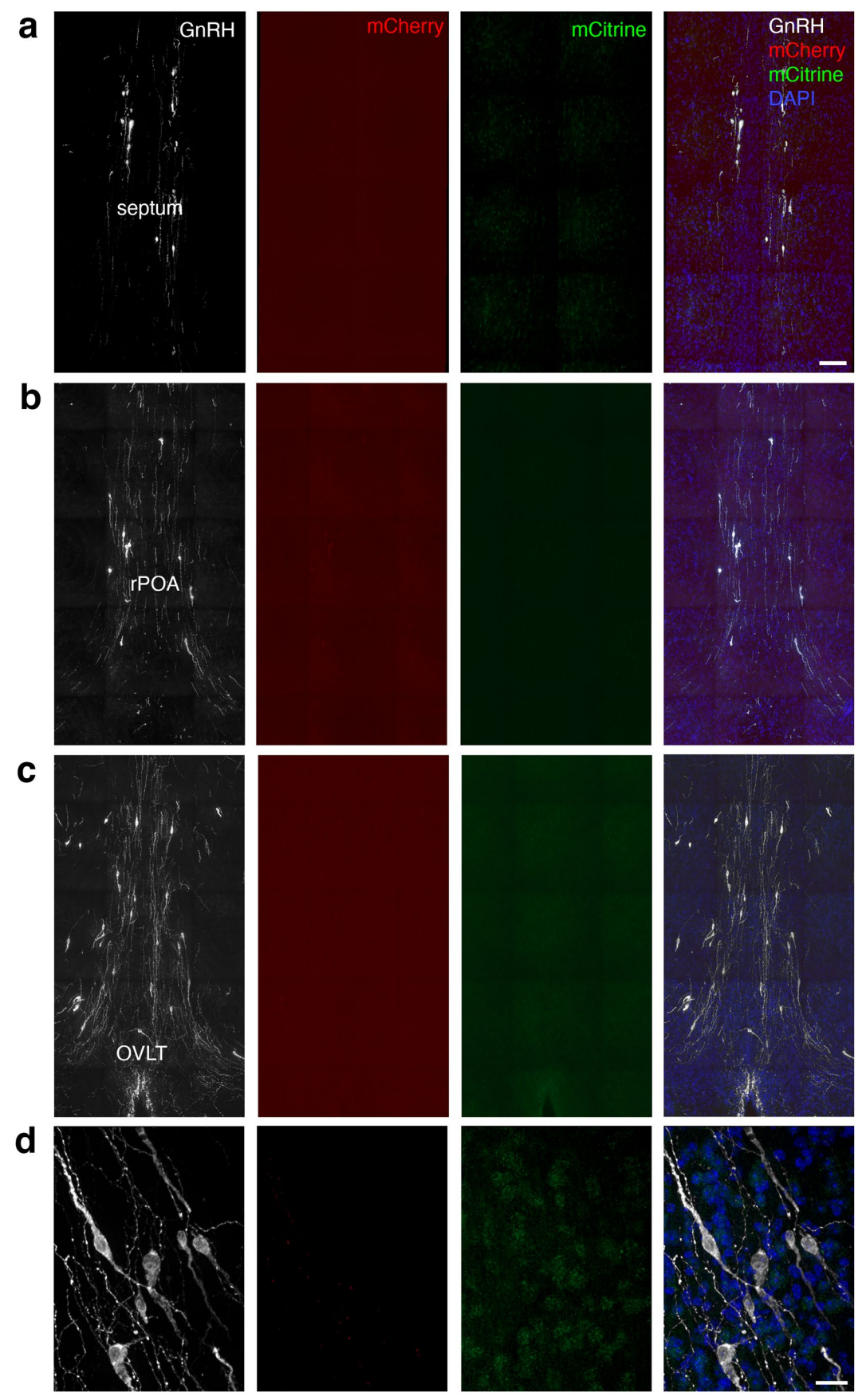
Extended Data Fig. 3 | **GnRH**^{oB} **neurons express olfactory/vomeronasal receptors and mechanosensitive ion channels. a**, Schematic strategy for sorting GnRH^{oB} and GnRH^{POA} cells from *Gnrh::Gfp* naïve male mice. **b**, mRNA expression level of *Olfr113*, *Olfr323*, *Vmn1r209*, *Vmn2r1* in GnRH-positive (GFP +) and GnRH-negative (GFP-) cells isolated from the OB. Values are mean \pm s.e.m (n = 4; 12-week-old males; *P = 0.0286; ns P > 0.05; two-sided paired Mann-Whitney U test). **c**, Schematic of the murine olfactory epithelium and vomeronasal organ. **d**, Representative coronal section of a VNO from an adult male mouse (P90) showing expression of *Vmn2r1* mRNA (white staining) by smFISH. The red dotted-line indicates the boundary between the basal and apical layer of the VNO. **e**, Representative coronal section of an OE from an adult male mouse (P90) showing expression of *Olfr323* mRNA (red) by smFISH. **f**, Schematic representation of the OB. GnRH cells located in the OB granular layer (GrL) are depicted in green. **g-i**, Representative coronal section of the OB from adult male

mice (P90) showing expression of *Gnrh1* (green), *Vmn2r1* (white) and *Olfr323* (red) in the MOB granular layer (MOB GrL). Arrows point to a *Gnrh1*-positive neuron co-expressing *Vmn2r1* and *Olfr323*, while the arrowhead in **j** point to a GnRH neuron which does not express *Vmn2r1* nor *Olfr323*. *n* = 3 mice used for the smFISH. Scale bars: **d**, 50 μm; **e**, 100 μm; **g**-**j**, 10 μm; inset in **i**, 5 μm. **k**, Schematic representing single-nucleus RNA sequencing protocol. **l**, UMAP visualization of the OB representing the distribution of *Piezo1* and *Piezo2* across the different cell clusters. **m**, Heatmaps indicating the relative expression of *Piezo1* and *Piezo2* within each neuronal cluster for *Gnrh1*-positive and *Gnrh1*-negative cells of the OB. **n**, Percentage expression profile of Piezo receptors in *Gnrh1*+ compared to *Gnrh1*- of the OB. Abbreviations: Oligo, Oligodendrocytes; PG, Periglomerular cells; GC, Granule cells; M/T, Mitral/Tufted cells; OEC, Olfactory ensheathing cells; IN, Inhibitory neurons; sSA, Superficial short axon cells; ET, endothelial cells; MES, mesenchymal cells; dSA, Deep short axon cells.



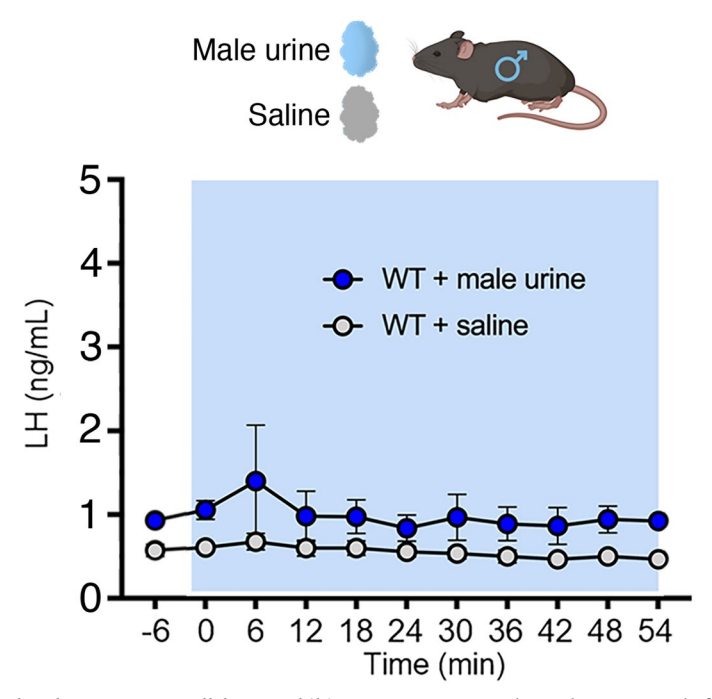
Extended Data Fig. 4 | **GnRH**^{oB} **neurons are preferentially activated by female urine. a**, Representative *in vivo* calcium-imaging responses of a cell to female urine (FU), saline (Sal) and male urine (MU). Three consecutive trials for each stimulus are represented. Dashed lines indicate stimulus onset. The displayed cell (cell ID = 38) was classified as a responsive cell to FU but not for Sal and MU. **b**, Quantification of cell responsiveness to Sal (n = 29 cells recorded from 13 mice; paired two-sided t test). Left: average fluorescent signal across all recorded

cells in response to Saline (dark gray) or fresh air (gray). Right: quantification of peak fluorescence in the 10 s after stimulus onset for Sal or Air. Gray dots and lines indicate single recorded cells. Black dots and line show the mean and the associated standard error (paired two-sided t test, n = 29 cells). \mathbf{c} , Same as in \mathbf{b} but for responses to MU (n = 19 cells recorded from 9 mice) (paired two-sided t test). \mathbf{d} , Same as in \mathbf{b} but for responses to methyl butyrate, n = 7 cells (paired two-sided t test). P values are shown in the figure.



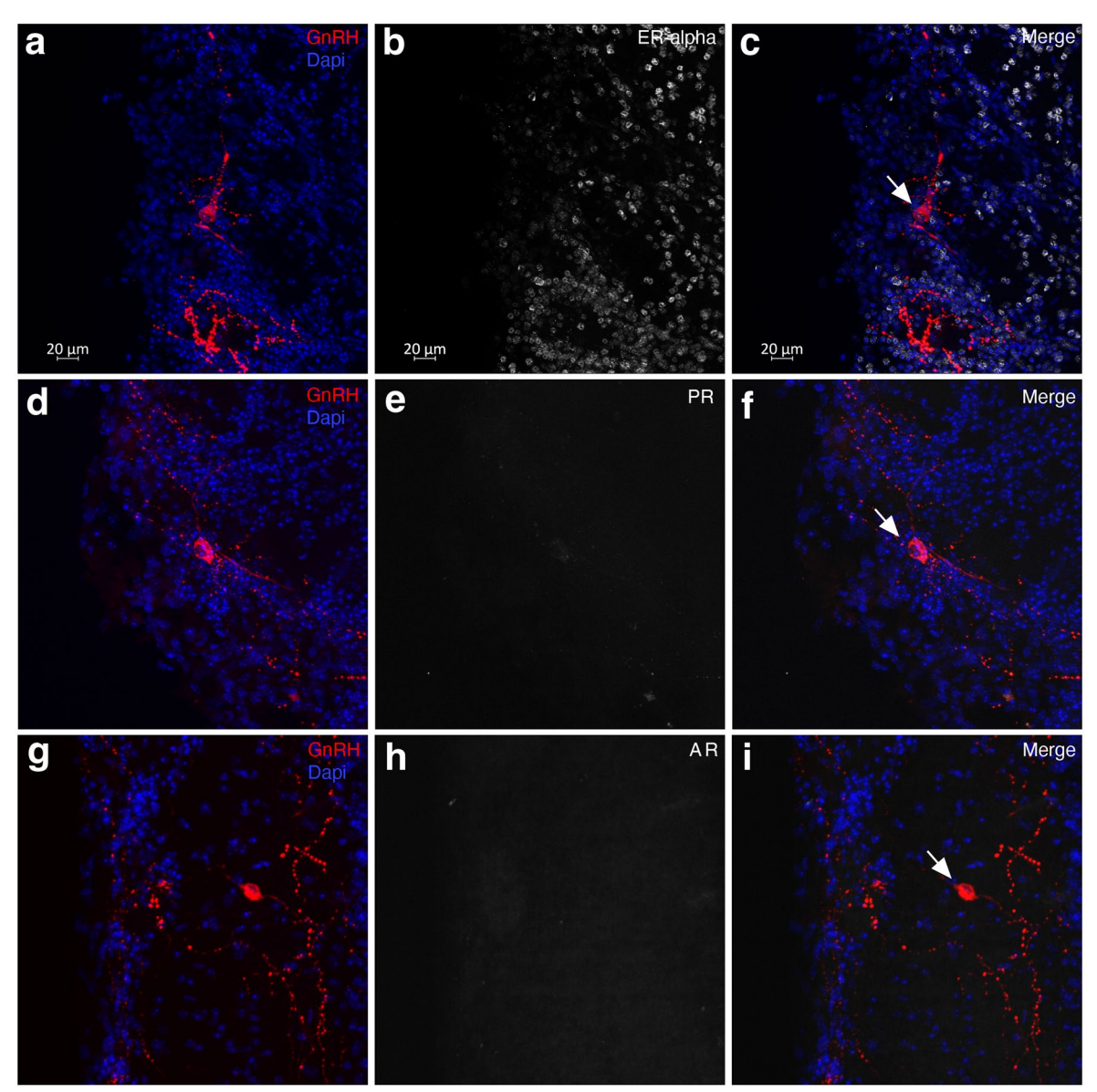
Extended Data Fig. 5 | Hypothalamic GnRH neurons are not infected by DREADDshM3Dq/hKORD viruses injected in the OB. a-d, Representative pictures showing immunostainings for GnRH, mCherry and mCitrine across the septal-

hypothalamic area, performed in three biological replicates. rPOA: rostral preoptic area; OVLT: organum vasculosum laminae terminalis. Scale bars: \mathbf{a} - \mathbf{c} , $100~\mu m$; \mathbf{d} , $20~\mu m$.

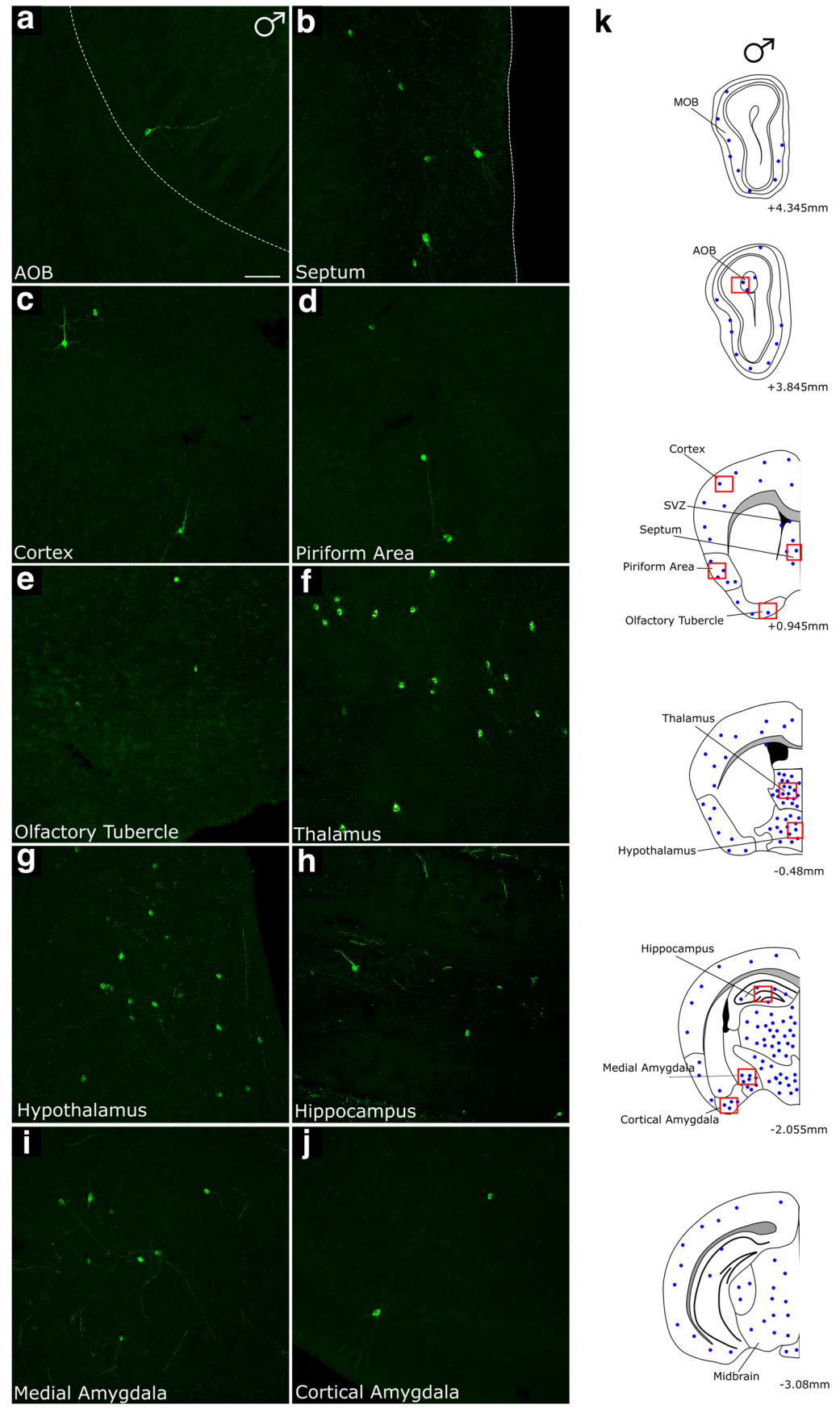


Extended Data Fig. 6 | Male mice exposed to the same-sex smell do not exhibit alterations in their levels of luteinizing hormone (LH). LH pulsatility in male mice (n = 6, 16-week-old) following the exposure to either male urine or saline.

 $\label{eq:micean} \mbox{Mice are exposed to male urine 1 min before T_0. Statistics by two-way ANOVA with Holm-Šídák's multiple-comparison test ($P > 0.05$). Values are represented as mean \pm s.e.m.$



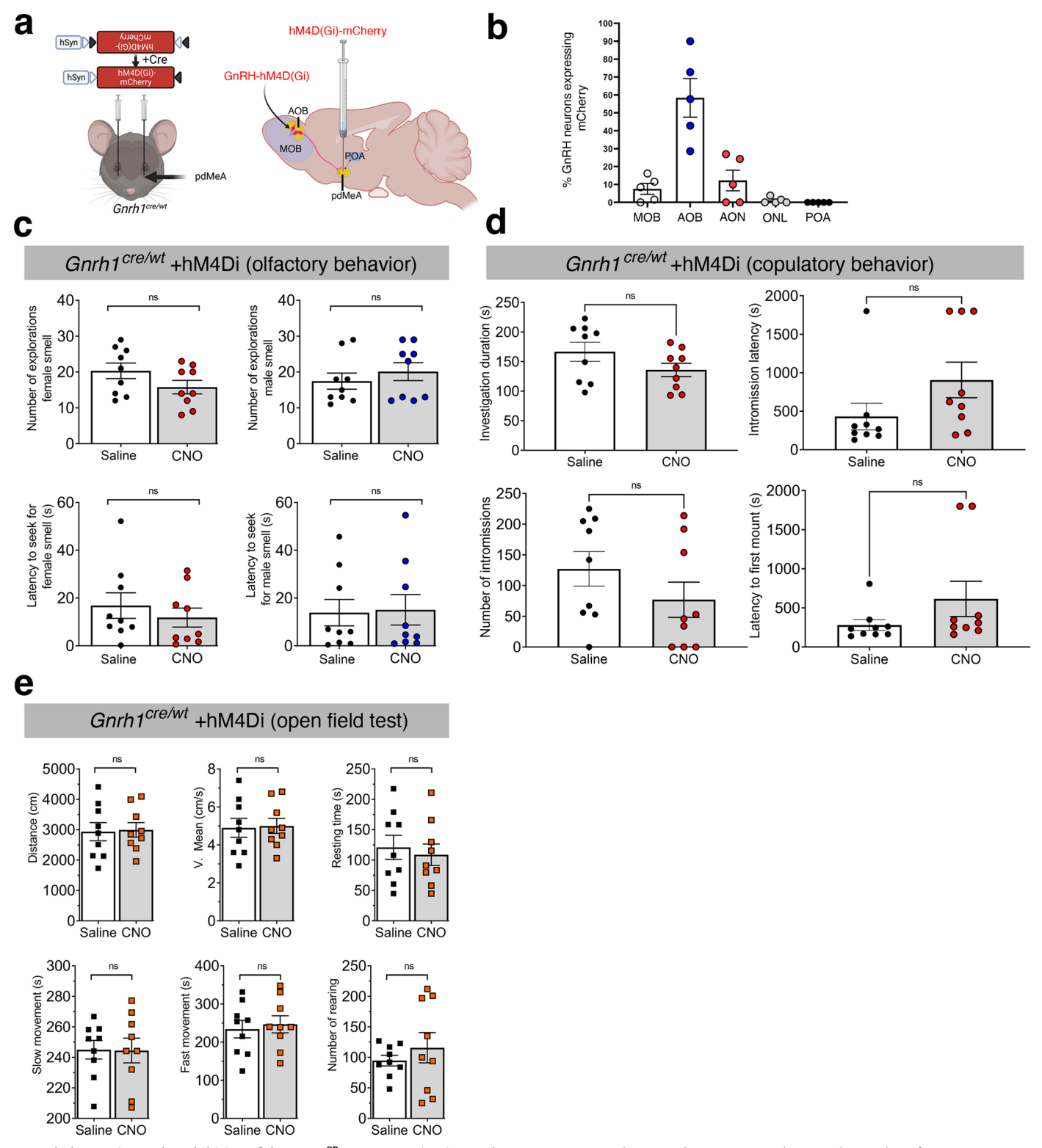
Extended Data Fig. 7 | **Sex-steroid receptor expression in the GnRH** on **eurons.** Representative coronal section of the OB from an adult male mouse (P90) showing expression of \mathbf{a} - \mathbf{c} , GnRH and ER α ; \mathbf{d} - \mathbf{f} , GnRH and PR; \mathbf{g} - \mathbf{i} , GnRH and AR by immunohistochemistry; n = 3 biological replicates. Scale bars: 20 μ m.



 $\textbf{Extended Data Fig. 8} \, | \, \textbf{See next page for caption.} \\$

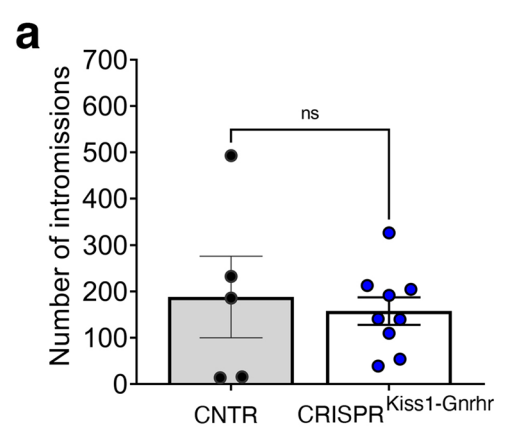
Extended Data Fig. 8 | **Distribution of GnRH receptor expressing cells in the mouse brain.** Coronal sections and GFP immunostaining (green) reveal the presence of *Gnrhr*-expressing cells along different areas of the male mouse's brain (twelve-week-old): **a**, AOB; **b**, septum; **c**, cortex; **d**, pririform area; **e**, olfactory tubercle; **f**, thalamus; **g**, hypothalamus; **h**, hippocampus; **i**, medial

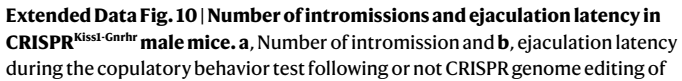
amygdala; j, cortical amygdala. k, Schematics showing the distribution of Gnrhr -expressing cells in male mice brains. Lower number indicates the distance from bregma. The experiments performed in at least three biological replicates. AOB: accessory olfactory bulbs; MOB: main olfactory bulbs; SVZ: subventricular zone. Scale bar: $50~\mu m$.

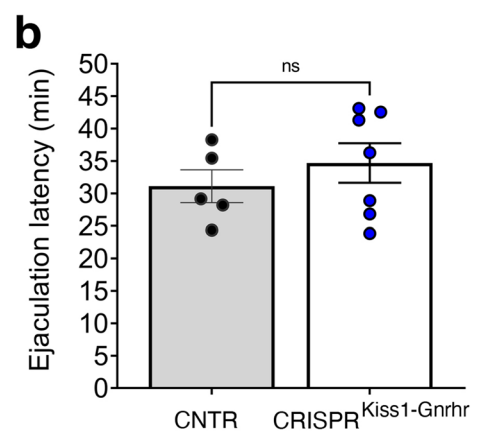


Extended Data Fig. 9 | The Inhibition of the GnRH OB neurons projecting to the medial amygdala does not modify the exploratory behavior or stress in male mice. a, Schematic representation of the bilateral AAV-hSyn-DIO-hM4D(Gi)-mCherry stereotaxic injection in the pdMeA. b, Percentage of GnRH neurons infected by the viral tracer in the OB and rPOA (n=5 male mice, age: P150). c, Number of explorations and latency to seek for female and male smells after CNO or saline injections (two-sided paired Wilcoxon signed rank test). d, Analysis of copulatory behavior after CNO or saline injections. The graphs represent the

investigation duration, the intromission latency, the number of intromissions and the latency to first mount (two-sided paired Mann-Whitney U test). **e**, Graphs showing the different parameters evaluated during the elevated plus maze test (EPM) and the open field test after the chemogenetic inhibition of GnRH^{OB} neurons projecting to the pdMeA (two-sided paired Mann-Whitney U test). Values in all graphs are represented as mean \pm s.e.m; n = 9, 12-24-week-old males; ns P > 0.05.







pdMeA^{Kiss1} neurons *in vivo* (n = 5 controls male mice; n = 9 CRISPR^{Kiss1-Garhr} male mice; 16-20-week-old males; ns P > 0.05; two-sided Mann-Whitney U test for both **a** and **b**). Values are represented as mean \pm s.e.m.

nature portfolio

Corresponding author(s):	Paolo Giacobini
Last updated by author(s):	2024/06/17

Reporting Summary

Nature Portfolio wishes to improve the reproducibility of the work that we publish. This form provides structure for consistency and transparency in reporting. For further information on Nature Portfolio policies, see our <u>Editorial Policies</u> and the <u>Editorial Policy Checklist</u>.

For all statistical analyses, confirm that the following items are present in the figure legend, table legend, main text, or Methods section.

\sim					
V	+-	٦ŧ	IC.	t١	CC
J	LC	コし	ıs	LΙ	CS

n/a	Confirmed
	$oxed{\boxtimes}$ The exact sample size (n) for each experimental group/condition, given as a discrete number and unit of measurement
	🔀 A statement on whether measurements were taken from distinct samples or whether the same sample was measured repeatedly
	The statistical test(s) used AND whether they are one- or two-sided Only common tests should be described solely by name; describe more complex techniques in the Methods section.
\boxtimes	A description of all covariates tested
	🔀 A description of any assumptions or corrections, such as tests of normality and adjustment for multiple comparisons
	A full description of the statistical parameters including central tendency (e.g. means) or other basic estimates (e.g. regression coefficient) AND variation (e.g. standard deviation) or associated estimates of uncertainty (e.g. confidence intervals)
	For null hypothesis testing, the test statistic (e.g. <i>F</i> , <i>t</i> , <i>r</i>) with confidence intervals, effect sizes, degrees of freedom and <i>P</i> value noted <i>Give P values as exact values whenever suitable.</i>
\boxtimes	For Bayesian analysis, information on the choice of priors and Markov chain Monte Carlo settings
\boxtimes	For hierarchical and complex designs, identification of the appropriate level for tests and full reporting of outcomes
\boxtimes	Estimates of effect sizes (e.g. Cohen's <i>d</i> , Pearson's <i>r</i>), indicating how they were calculated

Our web collection on statistics for biologists contains articles on many of the points above.

Software and code

Policy information about availability of computer code

Data collection

ApoTome and confocal images were taken using the Zen 2.3 (blue edition) software from Zeiss.

For two-photon functional imaging, Animals were placed under a standard laser scanning two-photon microscope (Nikon A1RMP) couple to a Chameleon Ultra II (Coherent Santa Clara, CA, λ exc = 920nm). The activity of GnRH positive neurons was monitored by imaging GCaMP fluorescence, collected via a 16x objective (Nikon CFI75 LWD 16xW NIR A.N.0,80 d.l. 3,0 mm). Signals were acquired by collecting temporal series (t-series) of images at an acquisition frame rate of 1.1-3 Hz at laser power ranging between 20 and 40 mW.

For stereotaxic surgeries for AAV injections, adult mice were anesthetized with 2% isoflurane and placed in a stereotaxic apparatus (Stoelting Co, Wood Dale, IL). For Patch-clamp recording, individual brain slices were placed in a submerged recording chamber (Warner Instruments) and continuously perfused at a rate of 3mL/min with oxygenated aCSF maintained at 32.8°C by a heater controller (TC-344C-Warner Instrument). GnRH neurons were visualized under x10 and x40 magnification using an upright fluorescence microscope with infrared differential interference contrast (DM-LFSA, Leica) and an ORCA-Frash4.0 digital CMOS camera (Hamamatsu). Recording pipettes were pulled from borosilicate glass capillaries (1.5 mm outer diameter, 1.12 mm inner diameter; World Precision Instruments) using a P1000 Flaming Brown puller (Sutter Instruments) and had a resistance of 6 M Ω . Whole-cell patch-clamp recordings were performed using a Multiclamp700B Amplifier, digitized with the Digidata 1322A interface and acquired with pClamp 10.2 software (Molecular Devices).

For FACS sorting experiments, a SONY SH800 Sorter Cytometer device using a 70 μm sorting chip was used.

3D Imaging was performed on the Ultramicroscope I (LaVision BioTec) equipped with a 1.1×/0.1NA and a 4×/0.3NA objectives and an Andor Neo 5.5 sCMOS camera. The light sheet was generated by a laser (wavelength 488nm, 568 nm or 647 nm, Coherent Sapphire Laser, LaVision BioTec) and two cylindrical lenses.

Data analysis

Statistical analyses were performed using Prism v9 (Graphpad Software, San Diego, CA). Gene expression data were analyzed using SDS 2.4.1 and Data Assist 3.0.1 software (Applied Biosystems). Electrophysiological recordings were analysed using the Clampfit 10.2 from pClamp software (Molecular Devices), FACS data were acquired and analyzed using the BD FACSDiva 8.0 (BD Biosciences) and Kaluza 2.0 (Beckman

Coulter) softwares. Images and figures were prepared using Adobe Photoshop 22.1.0 (Adobe Systems).

For single-cell RNA-seq analysis, reads were were processed with cell ranger (v.6.1.2) and aligned to Ensembl genome GRCm39 release 105_cr6.1.2. All cells with at least 200 detected genes and 500 UMI were retained. Datasets were further merged and analyzed with Seurat (v4.1.1) and cells with mitochondrial genes greater than 5% were discarded. Read counts were normalized by a scaling factor of 10,000 followed by log transformation. The data was then scaled and centered using the ScaleData function with default parameters. A principal component analysis was performed and all dimensions where the percent change in variation against the next subsequent principal component was greater than 0.1% were used to construct a nearest neighbor graph using the FindNeighbors function. Cells were clustered with a resolution of 0.2 and visualized by Uniform Manifold Approximation and Projection (UMAP). Clusters were manually annotated using FindAllMarkers functions to determine each cluster's significant marker genes. Markers were used to annotate clusters by matching them to known features of olfactory bulb populations. Go term analysis was performed using enrichGO for all subontologies. All visualizations were created using the Seurat package with modifications performed using ggplot2 (v.3.3.6).

Behavioral analysis was performed with Behavioral Observation Research Interactive Software (BORIS) (version 8.13) and Ethovision video tracking system (Ethovision XT 7.0, Noldus, Wageningen, Netherlands).

Two-photon data analysis:Temporal series recorded by two-photon imaging were first imported into the open-source ImageJ/Fiji software 71 and pre-processed in order to extract the fluorescence signal. A region of interest (ROI) was drawn following the cell profile and the average fluorescence intensity in the defined region was evaluated for each frame. The temporal profile of cell fluorescence was extracted for all trials from each recorded cell and analysed using Matlab software (TheMathWorks, R2021B).

All behavior tests were videotaped and manually annotated using BORIS software. For 3D-imaging, ImspectorPro v5.1.363 software (LaVision BioTec) was used for image acquisition: the z-step between each image was fixed at 4 µm, and for tile imaging the overlap was set to 10%. The resulting sequences of tiff files were processed with Imaris Converter and Imaris Stitcher (Oxford Instruments), and Imaris (Oxford Instruments), all v9.8, for visualization and analysis.

For cell counting, GnRH neurons were visualized using an Axio Imager Z2 ApoTome microscope equipped with a motorized stage (Zeiss, Germany) and an ORCA-Flash 4.0 V2 camera (Hamamatsu, Japan) driven by the Zen 2.3 blue edition imaging software (Zeiss).

For manuscripts utilizing custom algorithms or software that are central to the research but not yet described in published literature, software must be made available to editors and reviewers. We strongly encourage code deposition in a community repository (e.g. GitHub). See the Nature Portfolio <u>guidelines for submitting code & software</u> for further information.

Data

Policy information about availability of data

All manuscripts must include a data availability statement. This statement should provide the following information, where applicable:

- Accession codes, unique identifiers, or web links for publicly available datasets
- A description of any restrictions on data availability
- For clinical datasets or third party data, please ensure that the statement adheres to our policy

All data generated or analyzed in the current study are included in this published article and its Extended Data Figures. The raw snRNA-seq data conducted in this study have been deposited in Gene Expression Omnibus (GEO) under accession code GSE268138. For single-nucleus RNAseq experiments, raw reads were aligned to Ensembl genome GRCm39 release 105_cr6.1.2. Source data are provided with this paper.

Research involving human participants, their data, or biological material

Policy information about studies with <u>human participants or human data</u>. See also policy information about <u>sex, gender (identity/presentation)</u>, <u>and sexual orientation</u> and <u>race</u>, <u>ethnicity and racism</u>.

Reporting on sex and gender	The olfactory bulbs were dissected from the brain of three post-mortem individuals (37 y-old male; 64-y-old male; 77-y-old female).
Reporting on race, ethnicity, or other socially relevant groupings	N/A
Population characteristics	The olfactory bulbs were dissected from the brain of three individuals (37 y-old male; 64-y-old male; 77-y-old female) who had no neurological or endocrine disorders in their patient history.
Recruitment	N/A. Post-mortem tissues.
Ethics oversight	Ethic permissions were obtained from the Regional and Institutional Committee of Science and Research Ethics of Semmelweis University (SE-TUKEB 251/2016), in accordance with the Hungarian Law (1997 CLIV and 18/1998/XII.27. 723 EÜM Decree/) and the World Medical Association Declaration of Helsinki.

Note that full information on the approval of the study protocol must also be provided in the manuscript.

Hiel	ld-s	pecifi	c re	por	tıng

<u> </u>	<u> </u>	[*]
Please select the one below th	at is the best fit for y	your research. If you are not sure, read the appropriate sections before making your selection.
Life sciences	Behavioural & soc	cial sciences

Life sciences study design

All studies must disclose on these points even when the disclosure is negative.

Sample size

No statistical methods were used to pre-determine sample sizes but our sample sizes are similar to those reported in previous publications (PMID: 36048943; PMID: 36197968; PMID: 35867816; PMID: 29374161; PMID: 37572660). In accordance with ethics guidelines, we made an effort to use the fewest number of animals to achieve statistical significance without compromising outcomes. Sample sizes are provided in the main text, methods section and figure legends.

Data exclusions

No samples or animals were excluded from the analysis.

Replication

The number of biological replicates is indicated in the figure legends.

Randomization

Animals were randomized to experimental groups.

Blinding

Investigators were blinded to group allocation during data collection and analyses.

Behavioural & social sciences study design

All studies must disclose on these points even when the disclosure is negative.

Study description

Briefly describe the study type including whether data are quantitative, qualitative, or mixed-methods (e.g. qualitative cross-sectional, quantitative experimental, mixed-methods case study).

Research sample

State the research sample (e.g. Harvard university undergraduates, villagers in rural India) and provide relevant demographic information (e.g. age, sex) and indicate whether the sample is representative. Provide a rationale for the study sample chosen. For studies involving existing datasets, please describe the dataset and source.

Sampling strategy

Describe the sampling procedure (e.g. random, snowball, stratified, convenience). Describe the statistical methods that were used to predetermine sample size OR if no sample-size calculation was performed, describe how sample sizes were chosen and provide a rationale for why these sample sizes are sufficient. For qualitative data, please indicate whether data saturation was considered, and what criteria were used to decide that no further sampling was needed.

Data collection

Provide details about the data collection procedure, including the instruments or devices used to record the data (e.g. pen and paper, computer, eye tracker, video or audio equipment) whether anyone was present besides the participant(s) and the researcher, and whether the researcher was blind to experimental condition and/or the study hypothesis during data collection.

Timing

Indicate the start and stop dates of data collection. If there is a gap between collection periods, state the dates for each sample cohort.

Data exclusions

If no data were excluded from the analyses, state so OR if data were excluded, provide the exact number of exclusions and the rationale behind them, indicating whether exclusion criteria were pre-established.

Non-participation

State how many participants dropped out/declined participation and the reason(s) given OR provide response rate OR state that no participants dropped out/declined participation.

Randomization

If participants were not allocated into experimental groups, state so OR describe how participants were allocated to groups, and if allocation was not random, describe how covariates were controlled.

Ecological, evolutionary & environmental sciences study design

All studies must disclose on these points even when the disclosure is negative.

Study description

Briefly describe the study. For quantitative data include treatment factors and interactions, design structure (e.g. factorial, nested, hierarchical), nature and number of experimental units and replicates.

Research sample

Describe the research sample (e.g. a group of tagged Passer domesticus, all Stenocereus thurberi within Organ Pipe Cactus National Monument), and provide a rationale for the sample choice. When relevant, describe the organism taxa, source, sex, age range and any manipulations. State what population the sample is meant to represent when applicable. For studies involving existing datasets, describe the data and its source.

Sampling strategy

Note the sampling procedure. Describe the statistical methods that were used to predetermine sample size OR if no sample-size calculation was performed, describe how sample sizes were chosen and provide a rationale for why these sample sizes are sufficient.

Data collection

Describe the data collection procedure, including who recorded the data and how.

Timing and spatial scale

Indicate the start and stop dates of data collection, noting the frequency and periodicity of sampling and providing a rationale for

ς.
ō
⋾
N
C
Ņ
u
u

Timing and spatial scale	these choices. If there is a gap between collection periods, state the dates for each sample cohort. Specify the spatial scale from which the data are taken
Data exclusions	If no data were excluded from the analyses, state so OR if data were excluded, describe the exclusions and the rationale behind them, indicating whether exclusion criteria were pre-established.
Reproducibility	Describe the measures taken to verify the reproducibility of experimental findings. For each experiment, note whether any attempts to repeat the experiment failed OR state that all attempts to repeat the experiment were successful.
Randomization	Describe how samples/organisms/participants were allocated into groups. If allocation was not random, describe how covariates were controlled. If this is not relevant to your study, explain why.
Blinding Did the study involve field	Describe the extent of blinding used during data acquisition and analysis. If blinding was not possible, describe why OR explain why blinding was not relevant to your study. Describe the extent of blinding used during data acquisition and analysis. If blinding was not possible, describe why OR explain why blinding was not relevant to your study. Describe the extent of blinding used during data acquisition and analysis. If blinding was not possible, describe why OR explain why blinding was not relevant to your study. Describe the extent of blinding used during data acquisition and analysis. If blinding was not possible, describe why OR explain why blinding was not relevant to your study.
Did the study involve field work, collec	blinding was not relevant to your study. d work? Yes No tion and transport
Did the study involve field work, collec	d work? Yes No
Did the study involve field in	blinding was not relevant to your study. d work? Yes No tion and transport
Did the study involve field	blinding was not relevant to your study. d work? Yes No tion and transport Describe the study conditions for field work, providing relevant parameters (e.g. temperature, rainfall).

Mathods

We require information from authors about some types of materials, experimental systems and methods used in many studies. Here, indicate whether each material, system or method listed is relevant to your study. If you are not sure if a list item applies to your research, read the appropriate section before selecting a response.

Waterials & experimental systems		TVICTIOUS	
n/a	Involved in the study	n/a	Involved in the study
	Antibodies	\boxtimes	ChIP-seq
\boxtimes	Eukaryotic cell lines		Flow cytometry
\boxtimes	Palaeontology and archaeology	\boxtimes	MRI-based neuroimaging
	Animals and other organisms		
	Clinical data		
	Dual use research of concern		
\boxtimes	Plants		

Antibodies

Antibodies used

Materials & experimental systems

We used the following primary antibodies: anti-GnRH (Rat #EH1044; dilution 1:10000; produced by Dr Erik Hrabovszky: Laboratory of Reproductive Neurobiology, Institute of Experimental Medicine, Budapest, Hungary); anti-GFP (Chicken, dilution 1:5000, Ayes Lab GFP-1020, lot #GFP3717982); anti-RFP (rabbit, dilution 1:1000, Rockland 600-401-379, lot #46510); anti-GnRH (rabbit polyclonal antibody; dilution 1:2000; Proteintech 26950-1-AP, lot #49588); anti-cFos (mouse; dilution 1:500; Genetex GTX 60996, lot #822002386), anti-ERα (rabbit polyclonal; dilution 1:1000; Millipore 06-935, lot #3586856); anti-AR (rabbit; dilution 1:500; Millipore 06-680, lot #3811357); anti-PR (rabbit; dilution 1:500; Sigma SAB4502184, lot #210558).

Secondary antibodies were used as follow: Donkey anti-rabbit Alexa Fluor 488 (Invitrogen A21206, lot #2668665); Donkey anti-rabbit Alexa Fluor 568 (Invitrogen A10042, lot #2540901); Donkey anti-Chicken Alexa Fluor 488 (Jackson ImmunoResearch 703-545-155, lot #1649925); Donkey anti-rat Alexa Fluor 488 (Invitrogen A21208, lot #1979698); Donkey anti-rat Alexa Fluor 594 (Invitrogen A21209, lot #2400917); Donkey anti-rat Alexa Fluor 647 (Invitrogen A78947, lot #2497480) diluted 1:500. For whole-mount immunolabeling the following secondary antibodies were used: Goat anti-Rabbit AlexaFluor 488, Invitrogen A11008, lot #2284594; Goat anti-Chicken AlexaFluor 568, Invitrogen A11041, lot #1383072; Goat anti-Rat AlexaFluor 647, Invitrogen A21247, lot #2089926; dilution 1:1000.

Validation

These primary antibodies were validated in mouse tissues or cells using IF/IHC with the expected intracellular localization and patterns of the expected cell types. The anti-GnRH antibody (Rat anti-GnRH #EH1044; produced by Dr Erik Hrabovszky: Laboratory of Endocrine Neurobiology, Institute of Experimental Medicine, Budapest, Hungary) was previously validated (PMID: 26388735) in mouse and humans hypothalamic sections. The anti-GFP (Aves Lab GFP-1020): validated in mouse brain sections for

immunohistochemistry (PMID: 38016471; PMID: 38012403; PMID: 37996531). Anti-RFP (Rockland 600-401-379): validated by vendor and PMID: 37898094, PMID: 36843592. Anti-GnRH (Proteintech; 26950-1-AP): KD/KO validated by vendor and PMID: 31263453. Anti-cFos (Genetex GTX 60996): validated by vendor znd PMID: 36712055. Anti-ERα (Millipore 06-935): validated by vendor and PMID: 25157819, PMID: 20133455. Anti-AR (Millipore 06-680): validated by vendor and PMID: 25864123, PMID: 24875621. Anti-PR (Sigma-Aldrich, SAB4502184): validated by vendor and in PMID: 35867816.

Secondary antibody specificity were validated by the secondary antibody only negative control in IF.

			- 11	
\vdash \sqcup \sqcup	'ar\	otic c	ווםי	IIndc
Lur	(ai v	/Utile l	CII	\cdots

Policy information about <u>cell lines</u>	s and Sex and Gender in Research
Cell line source(s)	no eukaryotic cell lines were used in this study
Authentication	n/a
Mycoplasma contamination	n/a
Commonly misidentified lines (See <u>ICLAC</u> register)	n/a

Palaeontology and Archaeology

Specimen provenance

Provide provenance information for specimens and describe permits that were obtained for the work (including the name of the issuing authority, the date of issue, and any identifying information). Permits should encompass collection and, where applicable, export.

Specimen deposition

Indicate where the specimens have been deposited to permit free access by other researchers.

Dating methods

If new dates are provided, describe how they were obtained (e.g. collection, storage, sample pretreatment and measurement), where they were obtained (i.e. lab name), the calibration program and the protocol for quality assurance OR state that no new dates are provided.

Tick this box to confirm that the raw and calibrated dates are available in the paper or in Supplementary Information.

Ethics oversight

Identify the organization(s) that approved or provided guidance on the study protocol, OR state that no ethical approval or guidance was required and explain why not.

Note that full information on the approval of the study protocol must also be provided in the manuscript.

Animals and other research organisms

Policy information about <u>studies involving animals</u>; <u>ARRIVE guidelines</u> recommended for reporting animal research, and <u>Sex and Gender in Research</u>

Laboratory animals

Mouse_ mus musculus; strain: C57BL/6J. Mice were housed in a temperature (21-22 °C) and humidity-controlled environment (30-60 %), with 12 h: 12 h light:dark cycle and ad libitum access to food and water. They were housed in individually ventilated cages, with a maximum of 6 mice per cage. Males and females were used for studies evaluating the number of GnRH-OB neurons. For all the other experiments, only males were used. Mice were analysed at between 12-24 weeks of age.

Tg(Gnrh1::cre)1Dlc mice, Gnrh::gfp mice, GnRHR::IRES-Cre (GRIC)/eR26-Tau-GFPand the Kiss1-IRES-Cre59 mouse lines were generous gifts of Dr. Catherine Dulac (Howard Hughes Medical Institute, Cambridge MA) and Dr Ulrich Boehm (University of Saarland School of Medicine, D-66421 Homburg, Germany). R26-CAG-LSL-Cas9-P2A-GFP were purchased from Jackson (strain number 026175).

Wild animals

None.

Reporting on sex

Most findings regarding behavioral and genomic analysis only apply to male mice. For neuroanatomical descriptions of the number of OB GnRH neurons in mice, we used both male and female mice.

Field-collected samples

None.

Ethics oversight

Animal studies were approved by the Institutional Ethics Committees for the Care and Use of Experimental Animals of the University of Lille and the French Ministry of National Education, Higher Education and Research (APAFIS#2617- 2015110517317420 v5 and APAFIS#13387- 2017122712209790 v9), the Universities of Turin and Homburg and by the National Council on Animal Care of the Italian Ministry of Health (authorization # 813/2018-PR) and the Department for Environment and Consumer Protection - Veterinary Section, Cologne, North Rhine-Westphalia, Germany. All experiments were performed in accordance with the guidelines for animal use specified by the European Union Council Directive of September 22, 2010 (2010/63/EU).

Note that full information on the approval of the study protocol must also be provided in the manuscript.

Clinical data			
Policy information about <u>cl</u> All manuscripts should comply	inical studies with the ICMJE guidelines for publication of clinical research and a completed CONSORT checklist must be included with all submissions.		
Clinical trial registration	Provide the trial registration number from ClinicalTrials.gov or an equivalent agency.		
Study protocol	Note where the full trial protocol can be accessed OR if not available, explain why.		
Data collection Describe the settings and locales of data collection, noting the time periods of recruitment and data collection.			
Outcomes Describe how you pre-defined primary and secondary outcome measures and how you assessed these measures.			
Dual use research	n of concern		
	ual use research of concern		
Hazards			
Could the accidental, del	iberate or reckless misuse of agents or technologies generated in the work, or the application of information presented a threat to:		
No Yes			
Public health			
National security			
Crops and/or lives	tock		
Ecosystems Any other significa	ant area		
Z Z Any other signmen			
Experiments of concer	rn		
Does the work involve ar	ny of these experiments of concern:		
No Yes			
	to render a vaccine ineffective		
	to therapeutically useful antibiotics or antiviral agents		
	ence of a pathogen or render a nonpathogen virulent Sibility of a pathogen		
Alter the host rang			
	diagnostic/detection modalities		
	nization of a biological agent or toxin		
Any other potentia	ally harmful combination of experiments and agents		
Plants			
Seed stocks	no seed stocks were used in this study		
Novel plant genotypes	n/a		
Authentication	n/a		
ChIP-seq			
Data deposition			
Confirm that both raw and final processed data have been deposited in a public database such as GEO.			
Confirm that you hav	e deposited or provided access to graph files (e.g. BED files) for the called peaks.		

For "Initial submission" or "Revised version" documents, provide reviewer access links. For your "Final submission" document,

Data access links

May remain private before publication. provide a link to the deposited data.

Provide a list of all files available in the database submission.

Genome browser session (e.g. UCSC)

Provide a link to an anonymized genome browser session for "Initial submission" and "Revised version" documents only, to enable peer review. Write "no longer applicable" for "Final submission" documents.

Methodology

Replicates Describe the experimental replicates, specifying number, type and replicate agreement.

Sequencing depth Describe the sequencing depth for each experiment, providing the total number of reads, uniquely mapped reads, length of reads and

whether they were paired- or single-end.

Describe the antibodies used for the ChIP-seq experiments; as applicable, provide supplier name, catalog number, clone name, and Antibodies

lot number

Peak calling parameters Specify the command line program and parameters used for read mapping and peak calling, including the ChIP, control and index files

Data quality Describe the methods used to ensure data quality in full detail, including how many peaks are at FDR 5% and above 5-fold enrichment.

Software Describe the software used to collect and analyze the ChIP-seq data. For custom code that has been deposited into a community repository, provide accession details.

Flow Cytometry

Plots

Confirm that:

The axis labels state the marker and fluorochrome used (e.g. CD4-FITC).

The axis scales are clearly visible. Include numbers along axes only for bottom left plot of group (a 'group' is an analysis of identical markers).

All plots are contour plots with outliers or pseudocolor plots.

A numerical value for number of cells or percentage (with statistics) is provided.

Methodology

Instrument

Sample preparation The olfactory bulbs and preoptic regions of Gnrh::gfp transgenic mice were microdissected and enzymatically dissociated using a Papain Dissociation System (Worthington, Lakewood, NJ) to obtain single-cell suspensions.

FACS was performed using a SONY SH800 Sorter Cytometer device

Software BD FACSDiva 8.0 (BD Biosciences) software for acquisition and sorting, Kaluza 2.0 (Beckman Coulter) software for analysis.

Cell population abundance A total of 174 ± 20 (range, 44 - 700) GFP-positive cells were sorted per animal.

The sort decision was based on measurements of GFP fluorescence (excitation: 488 nm, 50 mW; detection: GFP bandpass Gating strategy 530/30 nm, autofluorescence bandpass 695/40 nm) by comparing cell suspensions from the OB and the preoptic region of

Gnrh::gfp animals.

Tick this box to confirm that a figure exemplifying the gating strategy is provided in the Supplementary Information.

Magnetic resonance imaging

Experimental design

Indicate task or resting state; event-related or block design. Design type

Specify the number of blocks, trials or experimental units per session and/or subject, and specify the length of each trial Design specifications or block (if trials are blocked) and interval between trials.

Behavioral performance measures State number and/or type of variables recorded (e.g. correct button press, response time) and what statistics were used to establish that the subjects were performing the task as expected (e.g. mean, range, and/or standard deviation across

Acquisition			
Imaging type(s)	Specify: fu	unctional, structural, diffusion, perfusion.	
Field strength	Specify in	Tesla	
		e pulse sequence type (gradient echo, spin echo, etc.), imaging type (EPI, spiral, etc.), field of view, matrix size, ness, orientation and TE/TR/flip angle.	
Area of acquisition	State whe	ther a whole brain scan was used OR define the area of acquisition, describing how the region was determined.	
Diffusion MRI Used	☐ Not u	ised	
Preprocessing			
1 0	Provide detail on software version and revision number and on specific parameters (model/functions, brain extraction, segmentation, smoothing kernel size, etc.).		
	If data were normalized/standardized, describe the approach(es): specify linear or non-linear and define image types used for transformation OR indicate that data were not normalized and explain rationale for lack of normalization.		
	Describe the template used for normalization/transformation, specifying subject space or group standardized space (e.g. original Talairach, MNI305, ICBM152) OR indicate that the data were not normalized.		
	Describe your procedure(s) for artifact and structured noise removal, specifying motion parameters, tissue signals and physiological signals (heart rate, respiration).		
Volume censoring	Define your software and/or method and criteria for volume censoring, and state the extent of such censoring.		
Statistical modeling & inferen	ice		
71	Specify type (mass univariate, multivariate, RSA, predictive, etc.) and describe essential details of the model at the first and second levels (e.g. fixed, random or mixed effects; drift or auto-correlation).		
. ,	Define precise effect in terms of the task or stimulus conditions instead of psychological concepts and indicate whether ANOVA or factorial designs were used.		
Specify type of analysis: Whole brain ROI-based Both			
Statistic type for inference Specify voxel-wise or cluster-wise and report all relevant parameters for cluster-wise methods.			
(See Eklund et al. 2016)			
Correction	Describe the type of correction and how it is obtained for multiple comparisons (e.g. FWE, FDR, permutation or Monte Carlo).		
Models & analysis			
n/a Involved in the study Functional and/or effective of Graph analysis Multivariate modeling or pre	,	is	
Functional and/or effective connectivity		Report the measures of dependence used and the model details (e.g. Pearson correlation, partial correlation, mutual information).	
Graph analysis		Report the dependent variable and connectivity measure, specifying weighted graph or binarized graph, subject- or group-level, and the global and/or node summaries used (e.g. clustering coefficient, efficiency, etc.).	
Multivariate modeling and predict	tive analysis	Specify independent variables, features extraction and dimension reduction, model, training and evaluation	

Sis Specify independent variables, features extraction and dimension reduction, model, training and evaluation metrics.